SURFACE ENHANCED RAMAN SCATTERING FROM Au AND Ag NANOPARTICLE COATED MAGNETIC MICROSPHERES

A THESIS

SUBMITTED TO THE DEPARTMENT OF CHEMISTRY

AND THE INSTITUTE OF ENGINEERING AND SCIENCES

OF BILKENT UNIVERSITY

IN PARTIAL FULFILLMENT OF THE REQUIREMENTS

FOR THE DEGREE

OF MASTER OF SCIENCE

BY

HACI OSMAN GÜVENÇ

JULY 2008

I certify that I have read this thesis and that in my opinion is it is fully adequate, in scope and quality, as a thesis of the degree of Master in Science

……..

Dr. Gülay Ertaş (Principal Advisor)

I certify that I have read this thesis and that in my opinion is it is fully adequate, in scope and quality, as a thesis of the degree of Master in Science

……..

Prof. Dr. Osman Yavuz Ataman

I certify that I have read this thesis and that in my opinion is it is fully adequate, in scope and quality, as a thesis of the degree of Master in Science

……..

Prof. Dr. Şefik Süzer

I certify that I have read this thesis and that in my opinion is it is fully adequate, in scope and quality, as a thesis of the degree of Master in Science

……..

Prof. Dr. Atilla Aydınlı

I certify that I have read this thesis and that in my opinion is it is fully adequate, in scope and quality, as a thesis of the degree of Master in Science

……..

Assist. Prof. Dr. Emrah Özensoy

Approved for the Institute of Engineering and Sciences

……..

Prof. Dr. Mehmet Baray

Director of Institute of Engineering and Science

ABSTRACT

SURFACE ENHANCED RAMAN SCATTERING FROM Au AND Ag NANOPARTICLE COATED MAGNETIC MICROSPHERES

HACI OSMAN GÜVENÇ

M.S. in Chemistry

Supervisor: Dr. Gülay Ertaş

July, 2008

A novel SERS substrate was prepared by coating Au or Ag nanoparticles onto magnetic microspheres prepared by a modified suspension polymerization method. The micron-sized magnetic microspheres were prepared in two steps: In the first step, inorganic core which consisted of oleic acid coated magnetic magnetite nanoparticles were prepared by co-precipitation method. The second step was the encapsulation of oleic acid coated magnetite nanoparticles by a modified suspension polymerization method. Magnetic microspheres were modified with amine functional groups in order to immobilize Au or Ag nanoparticles onto magnetic microspheres via amine groups of magnetic microspheres, however, a high background signal was obtained in Raman measurements due to the amine groups. Alternatively, Au or Ag nanoparticles were coated directly onto magnetic microspheres by hydroxylamine and sodium borohydrate reduction methods for Au nanoparticle coating and sodium borohydrate for Ag nanoparticle coating. For the first time, Au and Ag nanoparticle coated magnetic microspheres were prepared and used as SERS substrate successfully. The

magnetic microspheres were characterized by Scanning Electron Microscopy (SEM), Fourier Transform Infrared Spectroscopy (FTIR), Energy dispersive X-Ray spectroscopy (EDX) attached to SEM, Raman spectroscopy and X-Ray Diffraction (XRD). The average size of magnetic microspheres is measured to be 22 μm from their SEM images. EDX analysis demonstrated that magnetic microspheres were coated with Au or Ag nanoparticles. Moreover, commercially available amine functionalized magnetic microspheres were immobilized with Au nanoparticles and its SERS activity was significantly than the Au nanoparticle coated magnetic microspheres prepared in this study. Enhancement factors for Au and Ag nanoparticle coated magnetic microspheres were calculated to be ca. 10^5 and 10^7, respectively, however, in case of Au nanoparticle immobilized Spherotech magnetic microspheres, enhancement factor was only $2x10^2$ using Rhodamine 6G as SERS probe. Interactions of aspartic acid with Ag and Au nanoparticles were followed by Raman spectroscopy at various pH values. pH dependent interactions of aspartic acid with Au and Ag metals were followed depending on pH for the first time. Protonation or deprotonation of amine or carboxyl groups on aspartic acid depending on pH of the solution affects the interacting functional groups with metal nanoparticles and increase in the signal of the corresponding group was measured. It is found that aspartic acid interacts through amine and carboxyl groups with Ag surface at low pH values and via only carboxyl groups at higher pH values. However, aspartic acid interacts with Au surface through amine and carboxyl groups at all pH values under investigation.

ÖZET

MANYETİK PARÇACIKLAR ÜZERİNE KAPLANMIŞ Au ve Ag NANOPARÇACIKLARINDAN YÜZEY GÜÇLENDİRİLMİŞ RAMAN SAÇILMASI

HACI OSMAN GÜVENÇ

Kimya Yüksek Lisans Tezi

Danışman: Dr. Gülay Ertaş

Temmuz, 2008

Au ve Ag nanoparçacıkların manyetik mikroparçacıklar üzerine kaplanması ile yeni bir SERS alttaşı bu çalışmada önerilmektedir. Mikron boyuttaki manyetik parçacıklar iki basamakta hazırlanmıştır: İlk basamak, inorganik çekirdeği oluşturan oleik asit kaplı demir oksit nanoparçacıklarının birlikte çökelme yöntemi ile hazırlanmasıdır. İkinci basamak ise, süspansiyon polymerizasyon yöntemi ile oleik asit kaplı manyetik demir oksit nanoparçacıklarının varlığında, manyetik mikroparçacıkların hazırlanması ve son basamakta bu mikroparçacıkların Au veya Ag nanoparçacıkları ile kaplanmasıdır. Manyetik mikroparçacıkların, nanoparçacıklarla kaplanması için diğer seçenek, nanoparçacıkların amin fonksiyonel grupları içeren manyetik parçacıklar üzerine sabitleştirilmesidir. Ancak bu durumda amin gruplarından dolayı Raman ölçümlerinde yüksek zemin sinyali görülmüştür. Bu yönteme alternatif olarak, Au veya Ag nanoparçacıkları manyetik mikroparçacıklar üzerine doğrudan olarak farklı indirgenme yöntemleri ile kaplanmıştır. Au nanoparçacık kaplaması için hidroksilamin ve sodyum borohidrür, Ag nanoparçacık

kaplanması için sodyum borohidrür indirgeme yöntemleri kullanılmıştır. Literatürde ilk kez, Au veya Ag nanoparçacık kaplı manyetik mikroparçacıkları hazırlanmış ve SERS subsratı olarak kullanılabilirliği gösterilmiştir. Manyetik mikroparçacıklar SEM, FTIR spektroskopisi, EDX, Raman spektroskopisi ve XRD ile karakterize edilmiştir. SEM görüntülerinden, manyetik parçacıkların ortalama boyutu 22 μm olark ölçülmüştür. EDX analizleri sonucunda manyetik parçacıkların Au ve Ag nanoparçacıkları ile kaplandıkları gösterilmiştir. Buna ek olarak, amin fonksiyonel grupları içeren Spherotech marka manyetik mikroparçacıklar Au nanoparçacıkları ile kaplanmış ve SERS aktivitesi bu çalışmada hazırlanan Au nanoparçacık kaplı manyetik mikroparçacıklarının aktivitesinde çok daha düşük bulunmuştur. Au ve Ag nanoparçacık kaplı manyetik parçacıklar için Raman sinyallerinde 10^5 and 10^7 kat artışlar ölçülürken, Au nanoparçacık kaplı Spherotech manyetik mikroparçacıklarda artış $2x10^2$ olarak bulunmuştur.

Aspartik asitin, farklı pH değerlerinde Au ve Ag nanoparçacıkları ile etkileşimleri Raman spektroskopisi ile ilk kez detaylı olarak takip edilmiştir. Aspartik asitin Au ve Ag nanoparçacıkları ile etkileşimi pH'nın fonksiyonu olarak takip edilmiştir. Buna ek olarak, aspartik asitin SERS sinyalleri ilk defa rapor edilmektedir. Aspartik asit farklı pH değerlerinde farklı formlarda bulunmakta ve bu farklı formlarda olması fonksiyonel gruplarının, amin ve karboksil, metal yüzey ile olan etkileşimini değiştirmekte ve SER spektrumlarında da metal yüzey ile etkileşen grubun sinyallerinde artış ortaya çıkmaktadır. Bu deneyler ışığında, aspartik asitin amin ve karboksil groupları ile düşük pH değerlerinde, karboksil grupları ile yüksek pH değerlerinde Ag yüzeyi ile etkileştiği sonucu ortaya çıkmıştır. Aspartik asit, Au yüzeyi ile incelenen pH değerlerinde amin ve karboksil grupları ile etkileşmektedir.

ACKNOWLEDGEMENTS

This short, but comprehensive scientific survey more than for achieving my master thesis is an enjoyable period of my life, and an impressive preface of my academic carrier. The most probable reason this is the great interaction with my supervisor, Dr. Gülay Ertaş, for during this period. I am aware of the privilege to work with my supervisor, and so I have my deepest gradititude for her.

I would also like to express my deepest thanks to Prof. Dr. Şefik Süzer.

Thanks to previous and current Süzer-lab members; Can Pınar Cönger, Hikmet Sezen, İlknur Kaya-Tunç, Eda Özkaraoğlu, Hatice Elmas Başbuğ, and Derya Şenocak.

I would like to express my appreciation to my dear friends for their moral support without any remuneration; Altuğ Poyraz, Halil İbrahim Okur, Cemal Albayrak, Murat Altunbulak, Mustafa Fatih Genişel, Sündüs Erbaş, Tufan Duman, Osman Beyaztaş and Tuğrul Sarıarslan. Special thanks are also due to Ethem Anber, Emine Yiğit, and Hüsnü İçer.

I always feel myself indebted to Bilkent University and Chemistry Department for providing highly equipped education and research opportunity.

Finally, I want to express my deepest gratitude to my family especially my little sister Fatma Nur and my best friends Ahmet Gökhan Çelik, Yusuf Tamer, Abdussamed Köşker for 12 years.

TABLE OF CONTENTS

LIST OF FIGURES

LIST OF TABLES

CHAPTER 1

1. INTRODUCTION

Laser spectroscopic methods are currently employed in a broad range of applications in pure and applied sciences, including physical, chemical, and biological sciences. One of the aims of the molecular spectroscopy is to identify the characteristic vibrations of molecules under different chemical and physical environment. Spectroscopic techniques such as Diffuse Reflectance Spectroscopy, FTIR Spectroscopy, Fluorescence Spectroscopy, FTIR, Auger Electron Spectroscopy (AES), X-Ray Photoelectron Spectroscopy (XPS), and Electron Energy Loss Spectroscopy (EELS) provide information on the identification of chemical composition, determination of molecular structure and intermolecular interactions. Among them Raman spectroscopy has the advantage over transmission FTIR spectroscopy in terms of analyzing aqueous samples. However, water is a weak Raman scatterer, Raman is more immune to interference from interference by water. On the other hand, since water absorbs in FTIR measurements, aqueous samples cannot be analyzed via simple transmission FTIR methods. When compared with some surface techniques, Raman spectroscopy involves a non-destructive operation that can provide information from the surface of samples down to a few micrometers, whereas AES and XPS have the sensitivity only up to 10 nm of the materials. Similarly, the sensitivity of EELS for surface structures is lower than the sensitivity of Raman Spectroscopy. Although having high sensitivity to monolayer adsorbates, photoelectron spectroscopy techniques such as AES and XPS suffer from the requirement of ultra-high-vacuum (UHV) condition and they can not be applied to

detect the interfacial process between solid and liquid phases. Furthermore, since glass is transparent to Raman scattered light, it is easy to analyze samples on glass surfaces or in glass cells. In spite of the advantages mentioned above, the major drawback of the Raman spectroscopy is its low scattering efficiency. Raman scattering cross section lies in 10^{-29} - 10^{-32} cm^2 (for comparison, a good fluorescence cross section is 10^{-16} cm^2)[1-3]. Both resonance enhanced and/or surface enhanced Raman scattering are the preferred method to overcome this low sensitivity problem.

1.1 Raman Scattering and Surface Enhancement

1.1.1 Raman Scattering

In 1928, the Indian physicist C.V Raman discovered that when light was scattered from the molecules, scattering process results two types of scattered light; one of which had the same energy as the incident light and the second one, small fraction of scattered light had different energy of when the molecules were responsible for the scattering. Raman was awarded 1931 Nobel Prize in physics for this discovery.

Two types of scattering processes, elastic and inelastic scattering are observed when light is scattered from a molecule: In elastic scattering process, the scattered photons have the same energy (wavelength) as the incident ones. These elastically scattered photons are called as Rayleigh scattering photons. However, a small number of photons are scattered inelastically having different energy than the incident photons. Inelastical scattering process is called Raman scattering or Raman effect. In

order to obtain the Raman effect, the molecule should be excited from the ground state to a virtual energy state, and then relax into an excited vibration state, which generates Stokes Raman scattering. However, the molecule can stay in an elevated vibrational energy state, in this case the Raman scattering is then called anti-Stokes Raman scattering. Stokes scattering occurs at lower energy than the Rayleigh scattering, and anti-Stokes radiation has greater energy, while both Stokes and anti-Stokes are equally displaced from the Rayleigh feature. Usually, Stokes scattering is followed in Raman Spectroscopy since anti-Stokes scattering is less intense. Raman scattering via this virtual state can be thought as the polarization of the molecules electron cloud. The electric field of the incident light will force the electron cloud surrounding the molecule to oscillate with illumination. The oscillating electrons will then radiate an optical field which is identical to that of the incident light. The electron cloud is symmetrically distributed around a single atom and thus the re-radiated light is equally probable in any in-plane direction and will be in the same frequency as the incident light, this is called Rayleigh scattering. It can be assumed that at a finite temperature the atoms will oscillate with some frequency. The electron cloud surrounding the molecule will oscillate at the frequency of the incident light, but the absolute shape of the cloud will change at the frequency of the molecular vibrations. This oscillation in the shape of the electron cloud will subsequently change the optical field generated. A Fourier analysis of the scattered light will contain frequency components equal to the incident light, as well as other frequencies both higher and lower than the incident light. In addition, if the molecule is not vibrating, at any given moment in time the electron cloud will form a dipole moment across the atoms. Different atoms will feel a different field and so a different force will be applied to each atom. This is sufficient to induce a vibrational mode within the

molecule and so induce Raman scattering. The probability of inducing the transition is small as the molecular field is oscillating faster as compared to the atomic motion, and so will effectively average to zero.[4]This gives some intuition about why Raman scattering is weak. The energy difference between the incident and scattered light is called Raman shift and is calculated in wavenumbers through equation (1):

$$\Delta E = \frac{1}{\lambda_{incident}} - \frac{1}{\lambda_{scattered}} \quad (1)$$

in which **ΔE** is Raman shift in wavenumbers, $\lambda_{incident}$ is the wavelength of incident light in nm and $\lambda_{scattered}$ is the wavelength of scattered light in nm.

1.1.2 Surface Enhanced Raman Scattering (SERS)

Efficient Raman scattering from pyridine molecules adsorbed on silver electrode surfaces was first observed by Fleischmann et al.[5] in 1974. Fleischmann et al. observed that the Raman signal on a roughened silver electrode was 10^5-10^6 times stronger compared to the bulk pyridine. Jeanmaire et al.[6] and Creighton et al.[7] independently reported similar results on roughened silver electrode. Jeanmaire et al.[6] proposed an electric field enhancement mechanism whereas Creighton et al.[7] suggested that the observed enhancement is due to interaction of molecular electronic states of molecule with the metal surface. The effect was later called Surface Enhanced Raman Scattering.

The discovery of SERS has opened a promising way to overcome the traditionally low sensitivity problem in Raman spectroscopy. It does not only improves the surface sensitivity which makes Raman spectroscopy a more potent

detection tool in various applications, but also generates a stimulus for the study of the interfacial processes involving enhanced optical scattering from adsorbates on metal surfaces. It is a breakthrough that the employment of surface enhancement has solved the low intensity problem of Raman scattering and made it possible to work as a more satisfying surface technique.

1.1.3 Mechanisms of SERS

What mechanism causes the enhancement of Raman spectra of molecules located near a metal? This issue has recently been discussed in many theoretical and experimental works and reviews.[1, 8-11] Unfortunately, a large number of publications consider only certain SERS properties; however, no theory explaining the full range of experiments accompanying this effect is yet known. All of the theories proposed can be divided into two mechanisms. One is the *electromagnetic enhancement* in which the enhancement is caused by the surface plasmon resonance generated on the roughened metal surface; the other is the *chemical enhancement* which involves changes to the adsorbate electronic states due to chemisorption of the analyte.[12] It is believed that chemical enhancement is responsible from electronic transitions between the adsorbate and metal surface. There is still a degree of uncertainty regarding the level of enhancement from each mechanism.[10] This uncertainty comes from a difficulty of the SERS experiments since samples are random in nature; it is difficult to quantify where the SERS signal comes from. What is more, returning to the same point at a later stage may give a different result. With this uncertainty in results, it is hard to prove if any one is more correct, so both will be discussed separately in this thesis.

Electromagnetic Mechanism (EM)

When discussing the EM mechanism, we have to mention the localized surface plasmon resonance (LSPR) which is responsible for it. Surface plasmon is defined as the collective excitation of the electron gas of a metal confined to the near surface. Localized surface plasmon resonance is the excitation of surface plasmons by incident light at nanometer-sized metallic structures. Once the wavelength of the incident light is close to the LSPR of metallic surface, the molecules adsorbed or close to the surface yield a large electromagnetic field which is responsible for the enhancement in the Raman signal. Electromagnetic mechanism is a result of an enhanced electromagnetic field produced at the metal surface.[8]

It is possible to explain the SERS as a five step process. In the first step, light is incident on a surface at a certain angle and can excite a surface plasmon. Second, the large electric field of the plasmon will polarize molecules bound to the surface, creating large effective dipole moments within them. Third, if a molecule now changes its vibrational state then, the molecular polarisation will be altered. Forth, this change in polarisation subsequently affects the emitted plasmon, leading to a new plasmon surface field. Finally the surface plasmon can couple into an outgoing Raman scattered photon.[1, 8-10] The EM does not depend on the nature of specific molecule-metal interactions on the surface, nor on their adsoption properties and are characterized by distances considerably exceeding the atomic size. Therefore, where the EM is operative, the SERS spectra are not different from the Raman spectra of free molecules.[1, 8]

Chemical Mechanism (CM)

The EM mechanism can not account for all the enhanced phenomena observed in SERS experiments. There are a number of cases where this model simply does not work and a different approach is required. For instance, Arenas et al.[13] analyzed SERS spectra of pyrazine on silver surface and obtained some transitions and vibrations, which could not be explained by EM. Jiang et al.[14] studied the SERS spectra of crystal-violet molecules adsorbed on gold surface and obtained a peak corresponding to π-π^* electronic excitation of the adsorbed molecule that could be explained by another mechanism than EM. Campion et al.[15] reported SERS spectrum of pyrometillic anhydride on smooth copper surface and observed an enhancement which was attributed to another SERS mechanism. The proposed mechanism is the chemical mechanim (CM) which is due to a charge transfer between the metal and the adsorbed molecules.[10, 16] Since it requires direct contact between molecule and the metal substrate, the chemical enhancement factor is often considered to be around one or two orders of magnitude. This enhancement factor combines with the electromagnetic enhancement through a multiplication, so while much smaller would potentially be observable experimentally. A number of sources have been postulated to be responsible for the chemical enhancement by Kenipp et al.[1] and Otto et al.[17] however, experimental proof is hard to come by.

According to the chemical theories, the polarizability of the molecule-metal system should be studied under conditions of adsorption, since Raman scattering from an isolated molecule is a result of the modulation of the electronic polarizability of the molecule. Consequently, new excited states will appear due to the possibility of charge transfer and local changes in the electron charge density near the surface

because of chemical bonding or tunneling of electrons from the metal to the molecule. Chemical mechanisms exist when the distance between the molecule and the metal is in the order of the atomic size. The chemical nature of the molecules and the adsorption sites of the surface are the major factors determining Raman scattering enhancement. The observed SERS spectra can differ significantly from the corresponding Raman spectra of non-adsorbed molecules.[18]

1.1.4 Substrates for SERS

The molecules adsorbed on metal surfaces turned out to have large Raman cross-section under certain conditions. The magnitude of the Raman scattering cross section enhancement depends on the chemical nature of the adsorbed molecules, the type of metal surface and its structure. The greatest enhancement occurs on Ag, Au and Cu; the metal surface must be rough and have specific adsorption sites. Various SERS substrates have been studied: 1) systems of metal particles in suspensions and colloids which are small by comparison with the wavelength of the incident light such as Au nanoparticles,[19-24] Ag nanoparticles,[23, 25-27] 2) electrodes, where the surfaces become SERS active after a specific oxidation-reduction cycle has occurred in the electrochemical cell,[28-31] 3) SERS-active metal surfaces with controllable roughness prepared by lithographic techniques.[32-35]

Colloidal nanoparticles (such as Au and Ag) have been studied as SERS substrates, since they are easily prepared and show reasonable surface enhancement factors. For many SERS studies the chemical reduction of metal ions is commonly used in the preparation of metal colloids in the solution phase. Metal colloids due to simplicity of their preparation and the possible control of particle size and shape, have

been used most frequently to produce SERS active media in solutions. However, a major disadvantage is their tendency to aggregate spontaneously upon addition of analytes. This often leads to poor reproducibility of the SERS spectra. Affixation of colloidal nanoparticles onto solid surfaces such as glass slides[32, 36, 37] and silica[38-4040] are some means of addressing this problem. To our knowledge the use of magnetic microspheres as SERS substrate has been shown only in one study[41] so far in which the immobilization of gold nanoparticles onto amine-modified magnetic microparticles was demonstrated to detect naphthalene in aqueous solutions.

Thus, controlled particle deposition onto solid substrate seems like one of the most promising and simplest methods of forming a SERS substrate. Development of stable substrates with larger optical enhancement remains to be one of the most important challenges for SERS experiments.

1.1.5 Applications of SERS Techniques

SERS has important applications in many areas of chemistry, including chemical analysis, [25,26] catalysis[26,34] and biological systems[43-46] for characterizing proteins, enzymes at interfaces since SERS enhancement effect results in preferential enhancement of vibrational modes of molecules that are close to the metal surface. Therefore, SERS can be used to determine functional groups of the adsorbed species, that are responsible for the interaction with the surface and the conformation of adsorbate on the surface.[20]

The interaction of amino acids with surfaces is an important oppurtunity for developing and examining biological systems in which SERS is used as the analyzing tool. Moreover, SERS studies of amino acids adsorbed on a metal surface yield basic

and guiding information for SERS studies of biopolymers adsorbed on metal surfaces. SERS of aspartic acid on Ag colloids,[25, 26] on electrochemically prepared Ag surface,[29] and SERS of lysine and glycine on electrochemically prepared Ag surface[29], Ag colloids[24, 27, 42, 43], Au colloids[19, 44] have been reported. Podstawka et al. [42, 44] have reported SER spectra of amino acids and their homodipeptides on both Ag and Au colloids. Furthermore, Stewart et al. [28] studied the SERS of heteropeptides of di- and tripeptides on electrochemically prepared Ag surface, whereas Podstawka et al.[45] reported SERS of heterodipeptides containing methionine on Ag colloids. In a similar study, Herne et al.[27] reported SERS of tripeptides on colloidal Ag. Moreover, SERS of γ-aminobutyric acid on colloidal Ag[46] and homologous series of α,ω- amino acids on colloidal Ag and Au[20] have been reported. Dou et al. [19] obtained SERS of lysine and its oligomers and polymers on Au colloids and stated that SERS of lysine polymer having chain length greater than 5 were not obtained since polypeptide did not adsorb on Au colloid due to steric hindrance of the peptide backbone.

1.2 Magnetic Microparticles

Magnetic microparticles are micrometer-sized particles, which are used in a various fields of science like biosciences and biotechnology for cell and protein separation[47-52], in medicine as drug carriers[53-57] and in industry for metal recovery and industrial wastewater treatment to adsorb metal ions.[54, 58-61] The magnetic microparticles typically consist of a nanometer scaled inorganic magnetic core e.g. iron, nickel and/or cobalt and a polymeric shell such as methacrylates,[62-68] methyl methacrylate, glycidyl methacrylate, 2-hydroxyethyl methacrylate, poly (ethylene glycol)[69, 70] and poly styrene.[48, 71, 72]

The inorganic core provides magnetic properties, whereas the polymer shell stabilizes the magnetic microspheres in solution, protects from aggregation and provides variety of functional groups that can be used for many applications. The advantages of using magnetic microspheres as a support in a polymer shell can be summarized below:

1) They can be collected in solution and separated from the solution by a n external magnet,
2) Magnetic supports are easily adaptable to automation by modification with different functional groups
3) They are more resistant to acidic and basic solutions than magnetic iron nanoparticles.

As mentioned above, magnetic microparticles consist of magnetic core that is surrounded by a polymer shell. Magnetite (Fe_3O_4) nanoparticles in the core are prepared by co-precipitation of ferrous (Fe(II)) and ferric (Fe(III)) salts by using a strong base like NaOH or NH_3; this technique was first applied by Massart and has been also known as the Massart method.[73] There are various studies on the synthesis of magnetite nanoparticles for different applications.[63, 74-79] A surfactant, mostly oleic acid, is used in order to stabilize the magnetite nanoparticles in solution by preventing agglomeration of the particles. Moreover, surfactant provides the dispersion of nanoparticles in hydrophobic media and helps in forming a polymer shell that surrounds the magnetic core.

The polymer shell of the magnetic microparticles are prepared by suspension polymerization,[49, 71, 80] emulsion polymerization,[69, 81] or dispersion polymerization.[62, 64, 82] Suspension polymerization yields microparticles in size range of 50 μm to 2 mm, whereas dispersion polymerization has 0.5 μm to 10 μm and emulsion polymerization

yields smaller microparticles up to 1 μm.[83] Of these methods, suspension polymerization is the simplest one and more suitable for production of magnetic polymer microspheres with higher saturation of magnetization.[48, 63, 65, 84]

In suspension polymerization, the organic phase containing an initiator and monomers is dispersed in aqueous phase containing a stabilizer to form droplets by agitation. The presence of both continued agitation and a suitable stabilizer have a stabilizing effect on the formed droplets in aqueous phase. Moreover, the stabilizer prevents the coalescence and breakage of droplets. The size of the particle depends on the droplet size that is stabilized in aqueous phase and is expected to be in the same size of the initially formed monomer droplets. The most important issue to control the size of the particles is formation of stable droplets during polymerization.[83] However, in suspension polymerization, it is difficult to control the particle size and size morphology of final particles, since the exact mechanisms of breakage and coalescence/aggregation of the polymerizing drops which depend on the physical properties of the continuous and dispersed phases as well as on the flow and mixing conditions in the reactor are generally not very well understood. There are still theoretical and experimental studies going on analysis of flow patterns and mixing mechanisms in agitated vessels for the formation of stable droplets for uniform size distribution.[85, 86]

2. AIM OF THIS STUDY

The aims of this thesis can be divided into two categories: the preparation of SERS substrate composed of colloidal Au or Ag coated on magnetic microspheres and the comparison of aspartic acid interaction with colloidal Au and Ag using Raman spectroscopy as a tool.

In the first part of this study, magnetic microspheres are prepared in two steps with a narrow size distribution by suspension polymerization in the presence of oleic acid coated magnetite nanoparticles. Oleic acid capped magnetite nanoparticles and magnetic microspheres are characterized by FTIR, XRD, Raman Spectroscopy, SEM and EDX as well. Later on, Au and Ag nanoparticles as SERS substrates are coated on magnetic microspheres by different reduction processes and their SERS properties after Rhodamine 6G adsorption are discussed.

In the second part of this study, we mainly focus on the interaction of aspartic acid with colloidal Au and Ag surfaces at various pH values with 532 and 632 nm lasers as excitation sources in Raman Spectrometer. The interaction of aspartic acid with colloidal Au and Ag are followed by Raman spectroscopy.

3. EXPERIMENTAL

3.1 Materials

$HAuCl_4.3H_2O$, Ethylene diamine (EDA), NH_3, $NaBH_4$, CuCl, NaOH, HCl, poly(vinyl alcohol) (PVA) were purchased from Sigma-Aldrich, Oleic acid, Dimethyl formamide (DMF), methyl methacrylate (MMA), divinyl benzene(DVB), benzoyl peroxide(BPO), $FeCl_3.6H_2O$ were purchased from Merck, $FeCl_2.4H_2O$, aspartic acid, $NH_2OH.HCl$ and $AgNO_3$ were purchased from Fluka. MMA and DVB were purified to remove the inhibitors as explained in Section 3.3.2.

3.2. Instrumentation

The FTIR spectra were recorded using a Bruker Tensor 27 FTIR spectrometer. Each spectrum was obtained by averaging 512 interferograms with a resolution of 2 cm^{-1}. The transmission spectrum was taken for a film of pure liquid oleic acid spreaded over a KBr pellet. A ZnSe crystal attachment together with deuterated L-alanine doped triglycene sulphate (DLATGS) detector were used to record the attenuated total reflection (ATR) spectra of a film of oleic acid capped iron oxide nanoparticles and a pellet of magnetic microspheres.

The X-Ray diffraction (XRD) patterns were collected on a Rigaku Miniflex diffractometer using a high power Cu-K_α source operating at 30kV/15mA. The XRD patterns were collected in the 10-70 2θ range with a scan rate of 0.5θ/min.

Raman spectra were recorded on a Jobin Yvon LABRAM Raman spectrometer. The spectrometer is equipped with a HeNe laser operated at 20 mW with a wavelength 632.8 nm and 532.1 nm diode laser operated at 50 mW power with a CCD camera. In this thesis, unless otherwise specified, HeNe laser was used as the source for Raman measurements. The signal collected was transmitted into a 600 g/mm grating with a resolution of 3 cm^{-1}. The Raman spectra were collected by manually placing the 10x lens near the desired point of the sample on silicon wafer and all the spectra were calibrated according to the silicon peak at 522 cm^{-1}. Raman signals from Au/Ag coated microspheres were obtained by focusing on one microsphere to obtain the best signals.

The image of magnetic microspheres were recorded with a Zeiss Evo40 Scanning Electron Microscope (SEM) with LaB_6 filament at 5 kV. Energy dispersive X-Ray (EDX) measurements were done with Bruker AXS detector attached to the Zeiss SEM.

UV-Vis spectra of Au and Ag nanoparticles were recorded with a Cary 5E UV-Vis-NIR spectrometer and OceanOptics HR4000 UV-VIS spectrometer.

3.3 SERS Substrate: Colloidal Nanoparticle Coated Magnetic Microspheres

In this study, Au or Ag nanoparticle coated magnetic microspheres were synthesized in a three step process: (1) preparation of oleic acid coated magnetic iron oxide nanoparticles by co-precipitation method; (2) encapsulation of the magnetite

nanoparticles into PMMA-DVB polymer by a modified suspension polymerization method; (3) coating the microspheres with Au or Ag nanoparticles.

3.3.1 Preparation of Magnetic Iron Oxide Nanoparticles

Magnetic iron oxide nanoparticles were prepared by co-precipitation of Fe(II) and Fe(III) salts in the presence of NH_3 according to the following equation (2):[73]

$$Fe^{2+} + 2Fe^{3+} + 8OH^- \rightarrow Fe_3O_4 + 4H_2O \quad (2)$$

In co-precipitation reaction, 4.7 g of $FeCl_2.4H_2O$ and 1.72 g of $FeCl_3.6H_2O$ were dissolved in 160 ml water and heated to 90°C; 6.0 ml of 25 % (v/v) NH_3 solution was added and then, 4.0 ml of oleic acid was added after the color of the solution turned into black from brown. After heating the solution 15 minutes, the gel like oleic acid coated iron oxide nanoparticles were formed. Magnetic iron oxide nanoparticles were collected by magnetic decantation and washed with water and ethanol for the removal of unreacted oleic acid and followed by checking for FTIR signal of free oleic acid.

3.3.2 Preparation of Polymer Coating of Magnetite Nanoparticles by Suspension Polymerization Method

In this study, encapsulation of oleic acid coated magnetite nanoparticles with a polymer was realized by a suspension polymerization method with some modifications used in a conventional suspension polymerization. In a suspension polymerization, two phases are present: organic and aqueous phases. Organic phase

consists of monomer, cross-linker, initiator and oleic acid coated iron oxide nanoparticles, whereas aqueous phase consists of the stabilizer. Monomer, methyl methacrylate (MMA), was washed in aqueous solution of 1.0 M sodium hydroxide in a separatory funnel. After draining of the heavier layer of the organic phase, rinsing in water was repeated till the organic layer remained clear. In order to remove the remaining water, organic layer was dried with anhydrous sodium sulfate for 1 h and then, the monomer was distilled under nitrogen gas, using copper(I)chloride as a stabilizer. Divinyl benzene was washed with 5.0 % (w/v) sodium hydroxide solution and deionized water and dried with anhydrous sodium sulfate.

In the reaction vessel, 19.0 ml of MMA, 1.0 ml of divinyl benzene (DVB), 1.0 g of oleic acid coated magnetite nanoparticles and 0.8 g of benzoyl peroxide (BPO) were mixed together in a shaker for 15 minutes to disperse the oleic acid coated magnetite nanoparticles in monomer. This organic phase was mixed with the 100 ml of aqueous phase including 5.0 g of polyvinyl alcohol (PVA). The mixture was heated to 40°C stirring vigorously in a water bath and after an hour the temperature was increased to 60°C. After an hour the temperature was increased to 70°C in ten minutes. After 4 hours at 70°C spherical shaped magnetic particles were obtained. The particles were washed with deionized water and ethanol for removal of unreacted reactants and collected by magnetic decantation.

Table 1. Preparative conditions of magnetic microspheres by suspension polymerization method.

Organic Phase	**Amount**
Oleic acid coated magnetite nanoparticles (g)	1.0
Methyl methacrylate (ml)	19.0
Divinyl benzene (ml)	1.0
Benzoyl peroxide (g)	0.8
Aqueous Phase	
Water (ml)	100
PVA (g)	5.0
Temperature (ºC)	40 (1 h), 60 (1h) 70 (3 h)

3.3.3 Coating Magnetic Microspheres with Au or Ag Nanoparticles

3.2.3.1 Amine Modification of Magnetic Microspheres Prepared by Suspension Polymerization

First, magnetic microspheres were washed twice with 10 mL of dimethyl formamide (DMF) and then, 0.3 g of magnetic microspheres were dispersed in a mixture of 10 ml of DMF and 10 ml of ethylene diamine (EDA). The mixture was agitated gently at 110°C for 12 hours in a reflux system. After the reaction was over, magnetic microspheres were separated by magnetic decantation and washed with water and ethanol to remove residual EDA.

3.3.3.2 Coating Magnetic Microspheres with Au Nanoparticles

To coat magnetic microspheres with Au nanoparticles by ***citrate reduction method***; 0.2 g of magnetic microspheres was dispersed in 100 ml of $2.5x10^{-4}$ M $AuCl_4^-$ solution and to this solution, 5.0 ml of 1.0 % (w/v) sodium citrate was added and then, mixed for 15 minutes. Magnetic microspheres were collected by magnetic decantation and washed with deionized water.

For coating magnetic microspheres with Au nanoparticles by ***hydroxylamine reduction, a "seeding" method***[87]; 0.2 g of magnetic microspheres were kept in 120 ml of $1.0x10^{-4}$ M, $3.0x10^{-4}$ M or $5.0x10^{-4}$ M $AuCl_4^-$ for 1 hour. Afterwards, 5.0 ml of $1.0x10^{-3}$ M NH_2OH was added dropwise. After 10 minutes, 5.0 ml of 0.1 % (w/v) $AuCl_4^-$ ($2.5x10^{-3}$ M) solution was added. The stirring process was stopped in 10 minutes. The microspheres were collected by magnetic decantation and washed with water.

In order to coat magnetic microspheres with Au nanoparticles by ***sodium borohydrate reduction method***; 0.2 g of magnetic microspheres were dispersed in 100 ml of $1.0x10^{-3}$ M $AuCl_4^-$ solution. Two different residing period were used for adsorbing $AuCl_4^-$ ions on magnetic microspheres, namely1 hour and 24 hours. Different concentrations of $AuCl_4^-$ and $NaBH_4$ were tested as displayed in Table 2 to find the optimum parameters for the best coating of Au nanoparticles.

Table 2. Preparative conditions for coating magnetic microspheres with Au nanoparticles prepared by $NaBH_4$ reduction method.

	$HAuCl_4$, M	**$NaBH_4$, M**	**Residing Period, h**
Set 1	$1.0x10^{-3}$	$2.0x10^{-3}$	1
Set 2	$1.0x10^{-3}$	$2.0x10^{-3}$	24
Set 3	$5.0x10^{-3}$	$2.0x10^{-3}$	24
Set 4	$5.0x10^{-3}$	$4.0x10^{-3}$	24
Set 5	$5.0x10^{-3}$	$1.0x10^{-3}$	24

3.3.3.3 Coating Magnetic Microspheres with Ag Nanoparticles

In order to coat magnetic microspheres with Ag nanoparticles, $NaBH_4$ reduction method was used. Five sets of experiments were carried out by dispersing 0.2 g of magnetic microspheres in the different concentrations of $AgNO_3$ and $NaBH_4$ as shown in Table 3.

Table 3. Preparative conditions for coating magnetic microspheres with Ag nanoparticles prepared by $NaBH_4$ reduction method.

	$AgNO_3$, M	**$NaBH_4$, M**	**Standing Period, h**
Set 1	$1.0x10^{-3}$	$2.0x10^{-3}$	1
Set 2	$1.0x10^{-3}$	$2.0x10^{-3}$	24
Set 3	$5.0x10^{-3}$	$2.0x10^{-3}$	24
Set 4	$5.0x10^{-3}$	$4.0x10^{-3}$	24
Set 5	$5.0x10^{-3}$	$1.0x10^{-3}$	24

3.3.4 Immobilization of Au Nanoparticles onto Amine Functionalized Spherotech Magnetic Microspheres

Amine functionalized magnetic microspheres, 8 μm in diameter were purchased from Spherotech company. Au nanoparticles were prepared by Turkevich method which was explained in Section 3.5. 100 ml of Au nanoparticles were concentrated by centrifugation to a final volume 5.0 ml. 1.0 ml of concentrated Au nanoparticles was mixed with 0.25 μl amine functionalized microspheres and then, shaken for 2 h. Magnetic microspheres were separated by magnetic decantation and washed with deionized water and ethanol for removal of free Au nanoparticles in solution.

The SERS activities were tested with Rhodamine 6G (R6G) molecule which is a commonly used SERS probe.[88-91] The structural formula of R6G is displayed in Fig. 1.

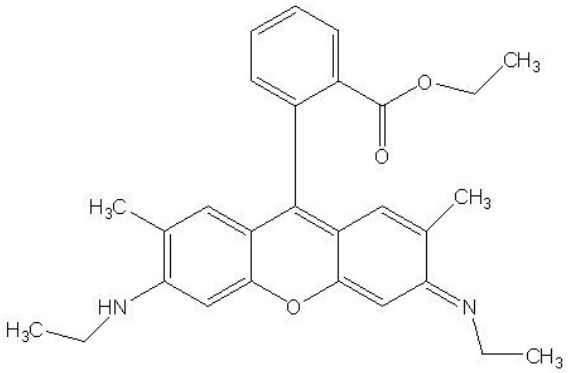

Figure 1. Structural formula of R6G.

3.4 Preparation of Ag Nanoparticles

Ag nanoparticles were prepared by $NaBH_4$ reduction method that was described by Singha et al.[92] 60 ml of $2.0x10^{-3}$ M $NaBH_4$ were cooled to 5°C in an ice bath and then, 20 ml of $1.0x10^{-3}$ M $AgNO_3$ solution were added dropwise in 20 minutes to the vigorously stirring $NaBH_4$ solution and the color of the resulting solution was yellow. Ag nanoparticles were kept for 24 h at room temperature for stabilization. The synthesized Ag nanoparticles had the maximum absorption at around 395 nm.

3.5 Preparation of Au Nanoparticles

Two methods were used to prepare Au nanoparticles. One of them was citrate capped Au nanoparticles prepared by Turkevich method described by Brown et al.[87] In this method, 100 ml of $2.5x10^{-4}$ M $HAuCl_4$ was heated to boiling and afterwards, 5.0 ml of 1.0 % (w/v) sodium citrate solution was added to boiling solution. The color of the solution was turned from black to red-wine in 5 minutes. The solution was kept at boiling temperature for 15 minutes more. The synthesized Ag nanoparticles had the maximum absorption at around 521 nm.

In the second method, Au nanoparticles were prepared by $NaBH_4$ reduction method same as Ag nanoparticles prepared by $NaBH_4$ reduction method described in section 3.4.[19] 60 ml of $1.0x10^{-3}$M $NaBH_4$ solution was cooled to 5°C in ice bath and 20 ml of $1.0x10^{-3}$M $HAuCl_4$ solution was added dropwise in 20 minutes to the vigorously stirred $NaBH_4$ solution and the color of the resulting solution was red-

wine. Au nanoparticles were kept for 24 h at room temperature for stabilization and their maximum absorption was measured at around 515 nm.

4. RESULTS AND DISCUSSION

4.1 SERS Substrate: Au or Ag Nanoparticle Coated Magnetic Microspheres

A three-step process was adapted in order to obtain Au or Ag nanoparticle coated magnetic micospheres as shown in Fig. 2. In the first step, hydrophobized magnetite nanoparticles with a diameter of about 5 nm were synthesized in a classical co-precipitation procedure.[73] In a second step, the magnetite nanoparticles were encapsulated with a monomer by a suspension polymerization process and after polymerization, polymer magnetite loaded particles were obtained. In a third step, Au or Ag nanoparticles were coated onto magnetic microspheres either by soaking them in solutions of $AuCl_4^-$ or Ag^+ and sodium borohydride, hydroxylamine or citrate as a reducing agents or immobilization of Au or Ag nanoparticles onto amine functionalized magnetic microspheres. The first step has already been well known in the literature.[59, 75-77, 93, 94] It is the scope of this study to develop the second and the third steps of the synthesis route and our future direction is to use the Au or Ag nanoparticle coated magnetic microspheres as SERS substrates.

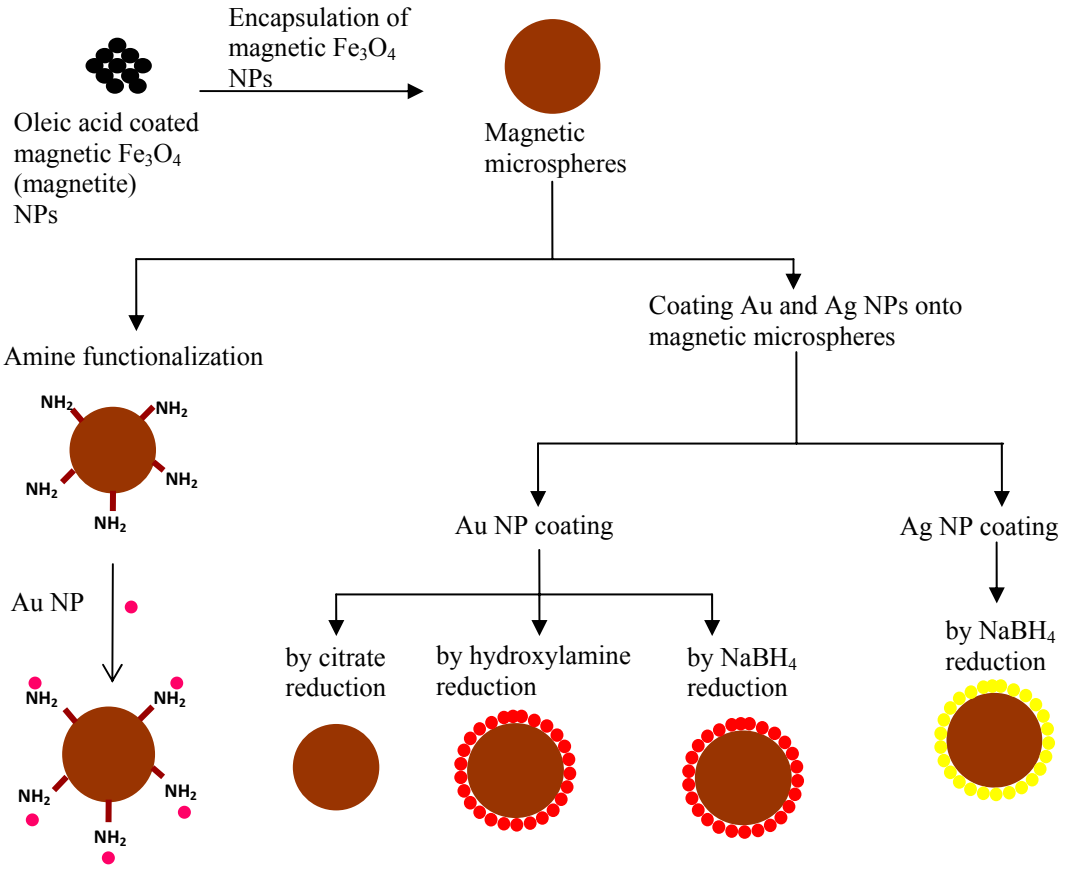

Figure 2. Schematics of the steps for the preparation of Au or Ag nanoparticle (NP) coated magnetic microspheres.

4.1.1 Oleic Acid Coated Magnetic Iron Oxide Nanoparticles

Magnetic iron oxide nanoparticles were prepared by slow addition of ammonia at 90°C to aqueous solution of ferrous chloride and aqueous solution of ferric chloride and then, oleic acid was coated on the surface of magnetic iron oxide nanoparticles. Fig. 3 is the XRD pattern of the nanoparticles which is identical to pure magnetite.[75, 94, 95] Magnetite type iron oxide (Fe_3O_4) consists of two different oxidation states of iron, Fe(II) and Fe (III) in the form of FeO and Fe_2O_3, respectively. The crystallite size of particles was calculated by Scherrer's equation from the most intense XRD line in the pattern. Scherrer's formula is given as [96]:

$$D_p = \frac{0.94\lambda}{\beta_{1/2}\cos\Theta} \quad (3)$$

where Dp is the crystalline size, λ is source wavelength and $\beta_{1/2}$is peak full with half maximum (FWHM) at the diffraction angle at θ. By using the Scherrer's formula above with respect to XRD line at 35.5, the average crystalline size of magnetite nanoparticles as calculated as ***21 nm.***

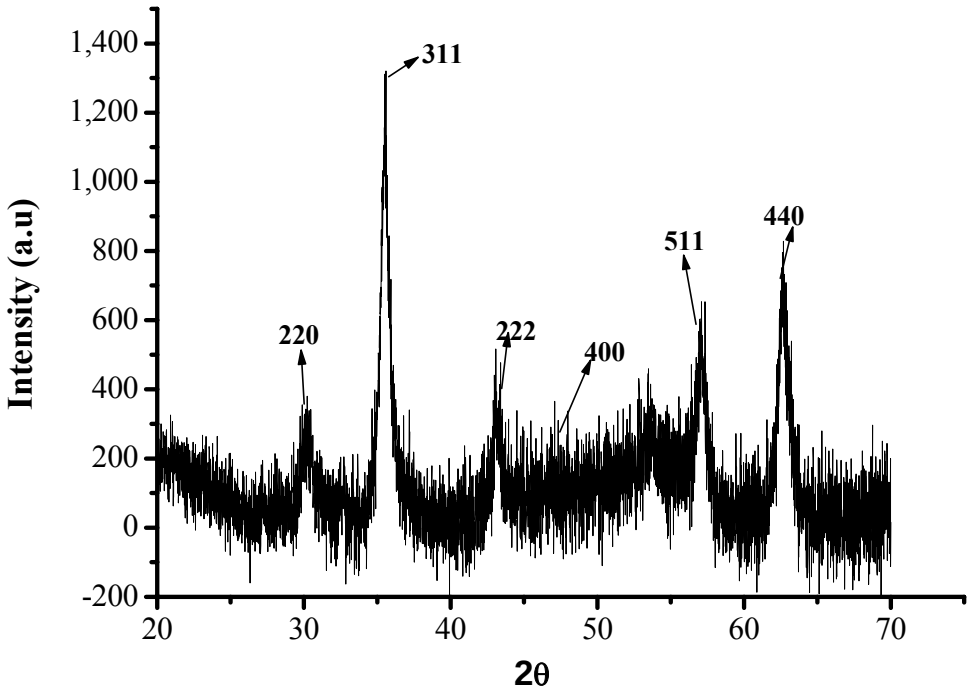

Figure 3. XRD pattern of oleic acid coated magnetic Fe_3O_4 nanoparticles.

The coated oleic acid makes the magnetite nanoparticles hydrophobic and thus prevents their coagulation. These hydrophobized magnetite nanoparticles could be easily dispersed in the monomer in the polymerization step. In order to confirm the

coating of the magnetite surface with oleic acid, FTIR spectra of the oleic acid coated magnetite and pure oleic acid were measured (see Fig. 4). FTIR spectrum of pure oleic acid is shown in Fig. 4a and the assignments of oleic acid peaks are given in Table 4. Two sharp peaks at 2925 and 2854 cm^{-1} were assigned as asymmetric and symmetric stretching modes of CH_2, respectively. The peak at 1710 cm^{-1} was attributed to C=O stretching and the peak at 1288 cm^{-1} exhibited the presence of C-O stretching. The O-H out-of-plane bending bands appeared at 937 cm^{-1}. [97] The spectrum of oleic acid coated magnetite nanoparticles is also displayed in Fig. 4b. The asymmetric and symmetric stretching of CH_2 in pure oleic acid shifted from 2925 and 2854 cm^{-1} to 2914 and 2848 cm^{-1} on the surface of magnetite nanoparticles, respectively. It is also observed that, C=O stretching peak of carboxyl group at 1710 cm^{-1} in the spectrum of pure oleic acid was not observed anymore in the spectrum of oleic acid coated magnetite nanoparticles. Additionally, two new peaks at 1520 and 1418 cm^{-1} are the characteristics of the asymmetric and symmetric stretching of COO^-. This result indicated that oleic acid is chemisorbed onto the magnetite nanoparticles as a carboxylate. The type of interaction between carboxylate group of oleic acid and the Fe atom can be monodentate, bridging (bidentate), chelating (bidentate) and ionic depending on the wavenumber difference between the asymmetric and symmetric stretching of COO^-.[97] The largest wavenumber difference (Δ) which is 200-320 cm^{-1} corresponding to monodentate interaction, whereas Δ is between 140-190 cm^{-1} for bridging bidentate and the smallest Δ‹110 $cm^{-1}$for chelating bidentate. In this study, the difference was 102 cm^{-1} indicating that the carboxylate groups of ***oleic acid binds to the iron atoms chelating bidentate.***

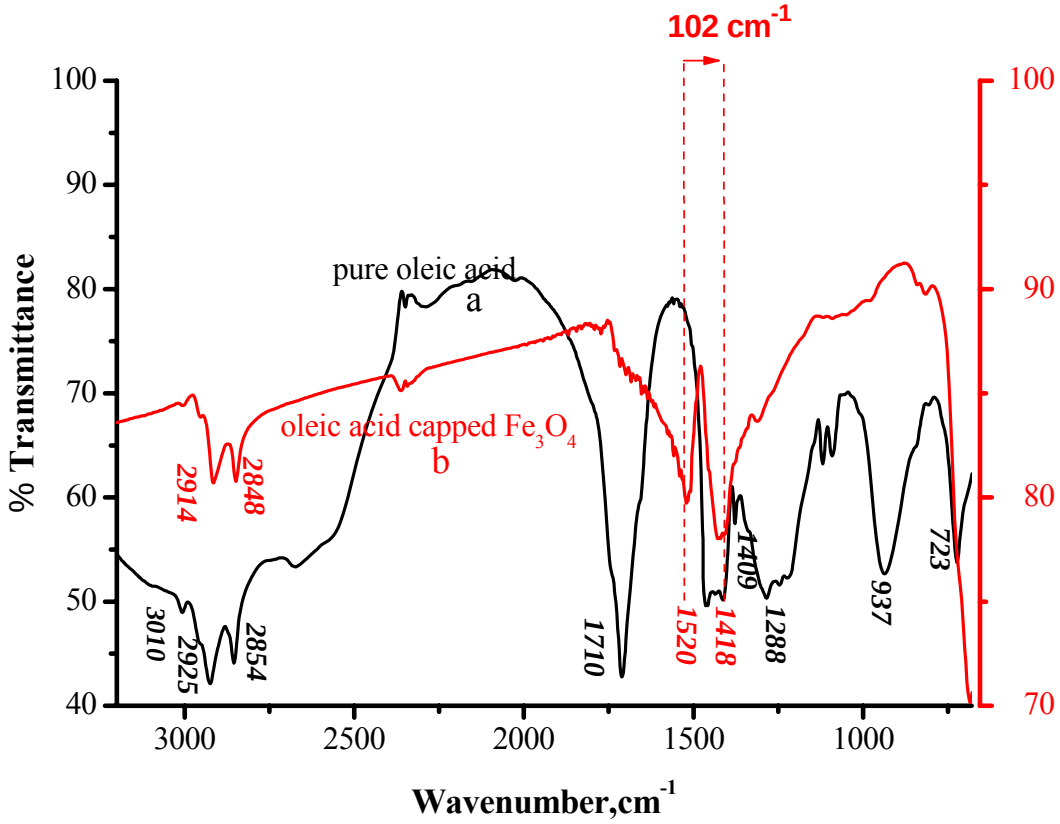

Figure 4. FTIR spectra obtained from **a)** pure oleic acid and **b)** oleic acid coated magnetite nanoparticles.

Table 4. FTIR peak assignments of pure oleic acid.

FTIR Band (cm^{-1})	**Assignments**
723	CH_2 rocking
937	O-H out-of-plane bending
1288	C-O stretching
1409	CH_3 umbrella
1466	O-H in-plane bending
1710	C=O stretching
2848	asymmetric CH_2 stretch
2914	symmetric CH_2 stretch
3010	C-H stretch in C=C-H

4.1.2 Encapsulation of the Magnetite Nanoparticles in PMMA-DVB

Magnetic microspheres were prepared by a suspension polymerization method in the presence of oleic acid coated magnetite nanoparticles. In suspension polymerization, which is in fact a kind of precipitation polymerization, two phases are present; aqueous and organic phase. In organic phase, MMA was used as a functional monomer, BPO was the hydrophobic initiator and DVB was the cross-linker. Since oleic acid is hydrophobic, oleic acid coated magnetite nanoparticles are dispersed easily in hydrophobic monomer MMA, cross-linker DVB and hydrophobic initiator BPO to form a uniform organic phase. Conventional suspension polymerization processes produce polymer particles larger than about 5 μm, and mostly between about 10 and 300 μm, and particle sizes even larger with a broad size distribution, the control of which is one of the important issues in suspension polymerization. The particle size and particle size distribution are controlled by polymerization temperature, the amount of magnetite nanoparticles, stirring rate, the ratio of reactants and the type of suspension agent (stabilizer). In our study, PVA was used as a stabilizer in the aqueous solution to stabilize the droplets. The stabilizer usually provides sites for nucleation of droplets and also provides colloidal stability for the growing droplets as a result of their adsorption at the droplet–water interfaces. In the present work, PVA was used to decrease the hydrophilicity of the MMA surface or increase the charge density of the MMA surface to increase the repulsive force between microspheres. Therefore, increasing PVA concentration in the aqueous solution increases the viscosity of the medium and allow more PVA molecules to be

diffused and adsorbed at the droplet–water interfaces. Thus, in this study a larger amount of PVA (20 % w/w of monomers) was used to obtain stable droplets. Typical values used in conventional polymerization is around 1% PVA. The magnetite is a strong inhibitor by adsorbing free radicals during polymerization, so it seems to slow down the polymerization rate. Consequently, a larger amount of initiator BPO which also decreases the nucleation period of particles[65, 67] was added (4 % w/w of monomers) in the present work than that of conventional suspension polymerization (typically 0.1-1.0 % of monomer) and also the smaller amount of oleic acid coated magnetite nanoparticles (1.0 g) were used. The reaction temperature was increased at a controlled rate from 40 ºC to 70 ºC. On the other hand, in conventional suspension polymerization, the reaction is carried out at 70 ºC. It is found that by keeping at lower temperature gives the advantage to forming uniform monomer droplets with high magnetic content. During residing period, the size of droplets gets smaller with diffusion of monomer into aqueous phase.[65, 67] The detailed recipe was shown in Table 1.

The microspheres exhibited a strong magnetization in the presence of a magnetic field. They presented a good magnetic response, being easily attracted by a magnet as is shown in Fig. 5.

a)  b) 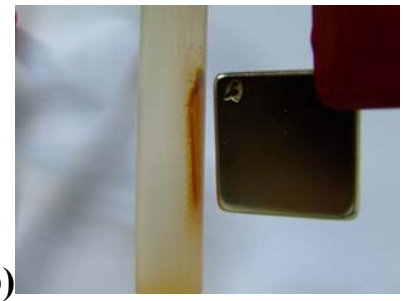

Figure 5. The magnetic property of the product is demonstrated by attracting a cluster of magnetic particles to a magnet. **a)** Magnetic microspheres in water and then, **b)** being attracted by a magnet.

The XRD pattern of the oleic acid coated magnetite nanoparticles and the magnetic microsphere are shown in Fig. 6. There is no change in the XRD pattern after encapsulation of magnetite nanoparticles in the polymer matrix. Therefore, we can conclude that the magnetite nanoparticles are dispersed in the polymer matrix and this further explains that magnetic property of microparticles were still present. The results shown in Fig. 6 also reveal that magnetite nanoparticles dispersed in the polymer matrix are high purity magnetite nanoparticles.

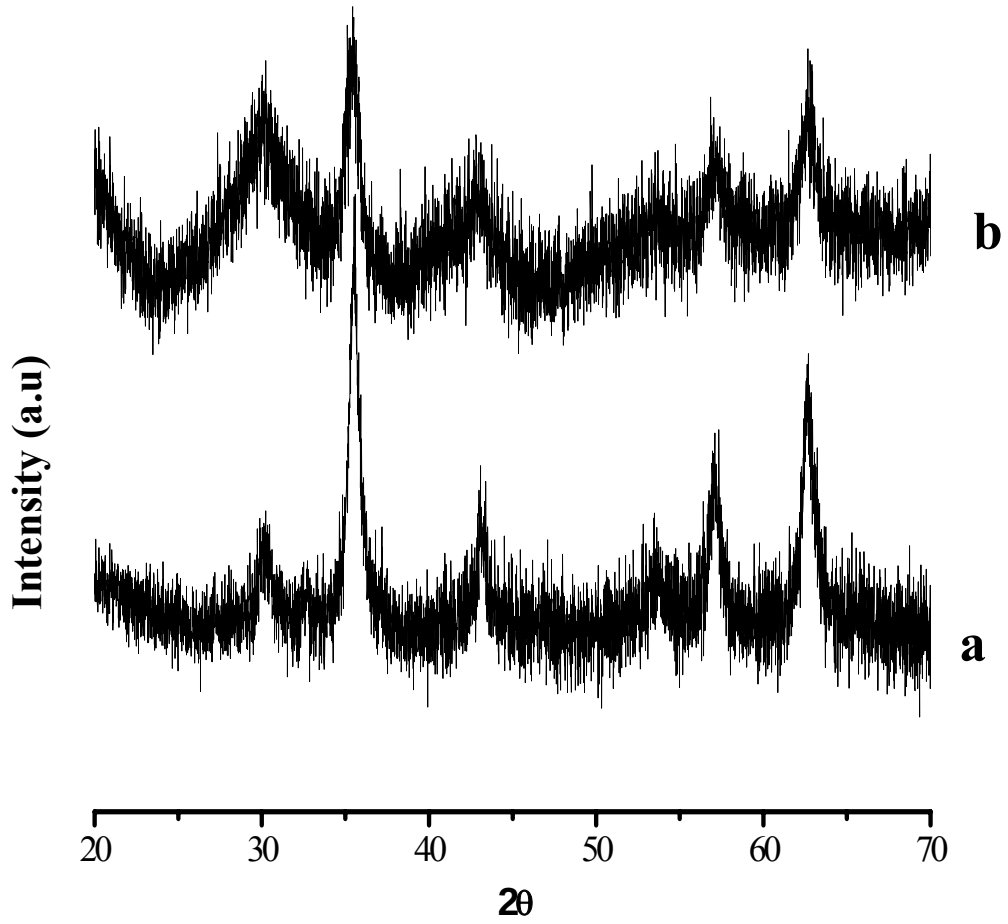

Figure 6. XRD pattern of **a)** oleic acid coated magnetite nanoparticles and **b)** magnetic microspheres (background subtracted)

Fig. 7 shows the morphology of magnetic microspheres prepared by suspension polymerization. However, due to charging of the microspheres; the images are not clearly visible. However, the shapes of microspheres were mostly spherical and as an example of the particles without charging is shown as an inset of Fig 7. The size of microspheres ranged from 18 to 30 μm with a mean diameter of 22 μm. The particle size distribution from SEM images is shown in Fig. 8. The histogram was drawn from total of 100 individual microspheres from three different regions of

microspheres. The average size was determined to be approximately 22 μm. Size distribution of microparticles are usually classified as monodisperse, nearly monodisperse or poly disperse by using poly dispersity index (PDI) value.[98, 99] PDI is calculated by using the following equation:

$$PDI = \frac{D_w}{D_n} \tag{4}$$

where D_w is the weight-average-diameter and D_n is number-average diameter and are given as: [98, 99]

$$D_w = \frac{\sum N_i D_i^4}{\sum N_i D_i^3} \tag{5}$$

$$D_n = \frac{\sum N_i D_i}{\sum N_i} \tag{6}$$

in which N_i and D_i correspond to the values of number of particles at that given diameter and diameter of the particles. For the calculation of PDI values ranging from 1.00 to 1.10 are regarded as monodisperse distributions of particle, ranging from 1.10 to 1.20 regarded as nearly monodisperse distribution. For the set of particles in Fig. 8, PDI value is calculated as ***1.16*** which indicates that magnetic microspheres synthesized in this study are ***nearly monodisperse.***

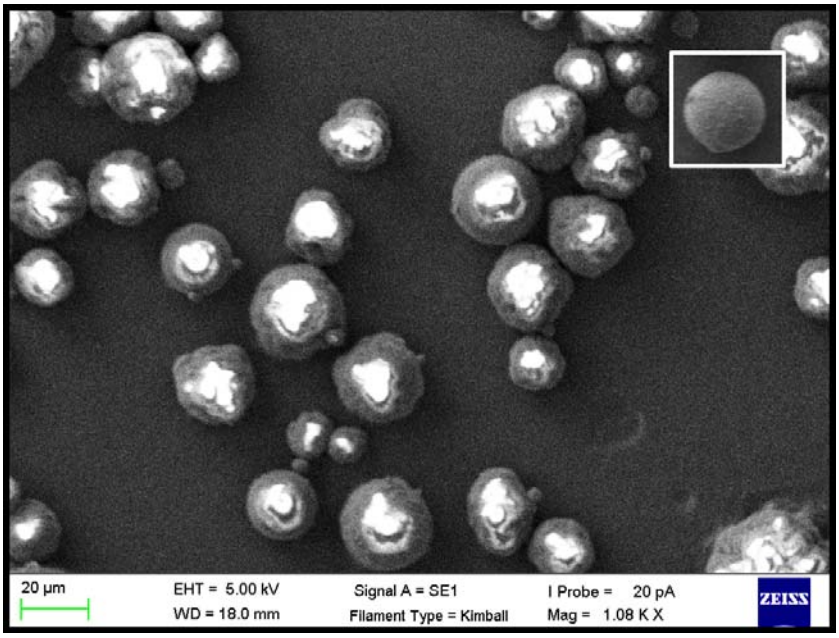

Figure 7. SEM image of magnetic microspheres. Inset image shows one of the microspheres without charging

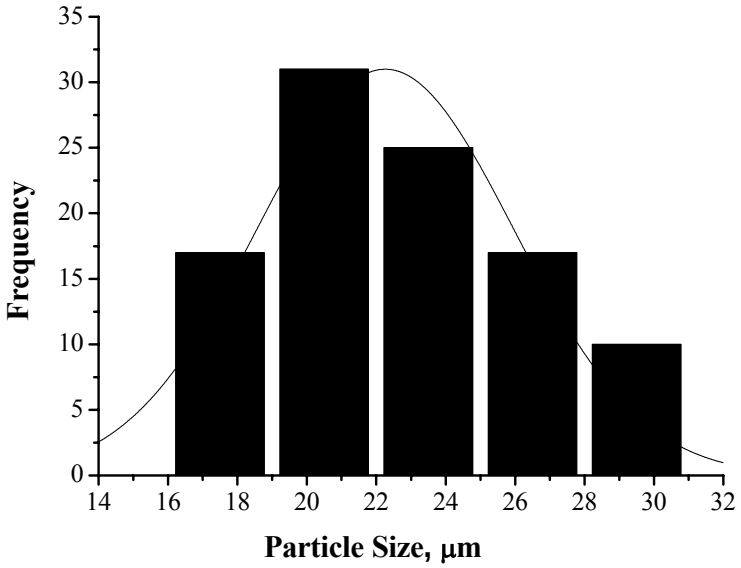

Figure 8. Size distribution curve of magnetic microspheres from SEM images.

4.1.3 Capping Magnetic Microspheres with Au or Ag Nanoparticles

4.1.3.1 Immobilization of Nanoparticles on Amine-Modified Magnetic Microspheres

The surface of magnetic microspheres synthesized using suspension polymerization were modified with amine functional groups due to high affinity of amine groups for colloidal nanoparticles.[41] To understand whether the magnetic microspheres are indeed modified with amine functional groups through the reaction in equation 7, ATR-IR spectra of magnetic microspheres before and after amine functionalization were recorded as shown in Fig. 9. In amine functionalization $–OCH_3$ groups in PMMA was replaced with $–NH(C_2H_6)NH_2$ groups as illustrated in equation 7. In the ATR-IR spectrum of magnetic microparticles the intense peak at 1724 cm^{-1} was attributed to C=O of the poly(methyl methacrylate) and the peaks at 1385 cm^{-1} and 1144 cm^{-1} exhibited the presence of $–OCH_3$ and C-O-C bands. In addition, 1240 cm^{-1} was obtained from O-C bands. The peak at 2998 cm^{-1} was assigned to aromatic C-H vibrations of DVB, whereas the peaks at 2853 cm^{-1} and 2843 cm^{-1} were ascribed to asymmetric and symmetric vibrations of C-H bands. On the other hand, in the spectrum of amine modified magnetic microspheres, signal for C=O stretching peak at 1724 cm^{-1} was insignificant and two new peaks appeared at 1658 cm^{-1} and 1526 cm^{-1} which were attributed to amide I and amide II bands due to ethylene diamine bonding to PMMA microparticles. Amide I band refers to the combination of C=O stretching, C-N stretching and N-H in plane bending, while amide II band is combination of C-N stretching and N-H in plane bending.[100]

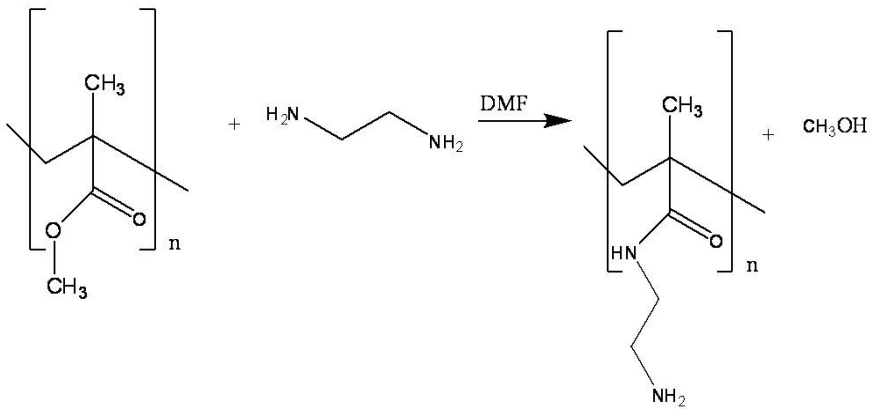

(7)

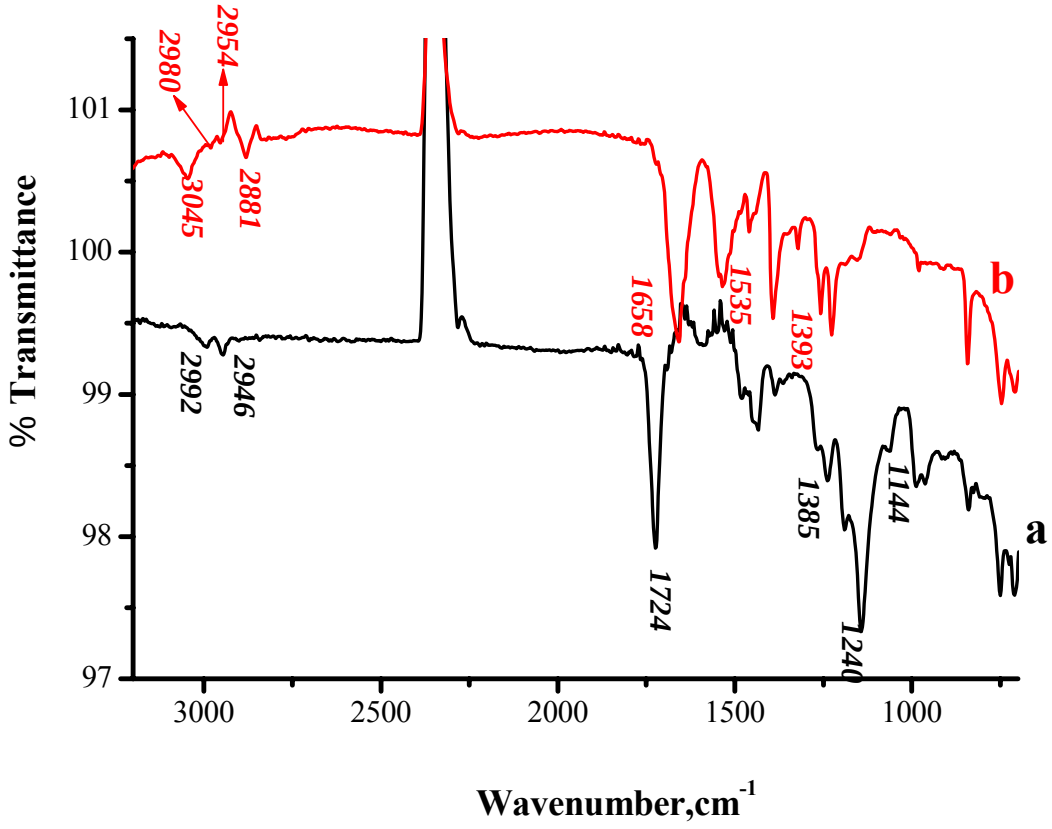

Figure 9. ATR-IR spectra of **a)** magnetic microspheres and **b)** amine functionalized magnetic microspheres.

Raman spectra of magnetic microspheres before and after amine modification were recorded as depicted in Fig. 10. Raman spectrum of magnetic microspheres before amine modification shows the typical Raman bands of PMMA[101, 102] which are summarized in Table 5. In the spectrum of magnetic microspheres after amine modification, a high background was measured as shown Fig. 10b. This high background is assumed to originate from EDA where its Raman spectrum alone has also a high background. These amine functionalized microparticles can be used for support for biomedical applications; however, it is not possible to use them as SERS substrate after coating with nanoparticles due to the presence of high background measured which can mask the SERS spectrum of analyte molecules for further applications. In order to modify magnetic microspheres with amine functional groups, different ammination reagents were tried such as APS, dimethyl amine, triethyl amine and ammonia. However, amine modification was not achieved with any of these reagents.

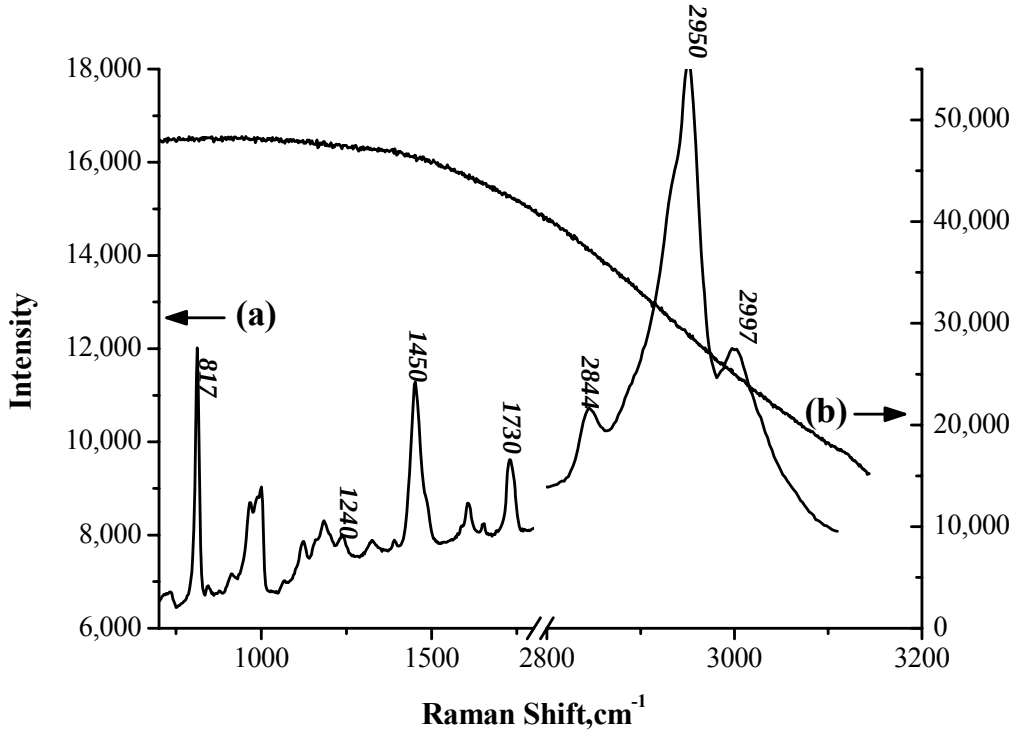

Figure 100. Raman spectra of **a)** magnetic microspheres and **b)** amine modified magnetic microspheres. Integration time was 20 s for spectrum (a) and 1 second for spectrum (b).

Table 5. Selected Raman bands of magnetic microspheres and their assignments.

Raman Shift (cm^{-1})	**Assignments**
817	CH_2 stretching
1240	C–COO stretching
1460	C–H deformation of α-CH
1730	C=O stretching of C–COO
2884	Combination band involving O–CH_3
2920	C–H symmetric stretching of O–CH_3 with C–H symmetric stretching of α-CH_3 and CH_2 anti-symmetric stretching
2997	C–H anti-symmetric stretching of O–CH_3

4.1.3.2 Coating Magnetic Microspheres with Au or Ag Nanoparticles

In this section, we will describe and assees the various methods of coatings with Au and Ag nanoparticles onto magnetic microspheres and their potential to be used as SERS substrates using R6G as analyte molecule which is commonly used as a SERS probe in the literature.

4.1.3.2.1 Coating Magnetic Microspheres with Au Nanoparticles

Coating Magnetic Microspheres with Au Nanoparticles Prepared by Turkevich Method

Turkevich method[103] is the commonly used method to synthesize the citrate capped Au nanoparticles. In this method, gold nanoparticles are produced in a liquid by reduction of chloroauric acid. After dissolving chloroauric acid, the solution is heated until boiling under vigorous stirring while a reducing agent is added. This causes $AuCl_4^-$ ions to be reduced to neutral gold atoms. As more and more of these gold atoms form, the solution becomes supersaturated and gold gradually starts to precipitate in the form of sub-nanometer particles. The rest of the gold atoms that form, stick to the existing particles and if the solution is stirred vigorously enough, the particles achieved fairly uniform in size. In the present study, this method is adapted to coat magnetic microspheres with Au nanoparticles. Magnetic microspheres were

added to gold solution, and the rest of the procedure was the same as in the synthesis of Au nanoparticles except the reaction was carried out at room temperature not to destroy the surface of the particles. However, the EDX elemental map images and SER spectrum showed that the formation of Au nanoparticles on the surface of the particles was not successful due to the lack of a significant number of nuclei on the surface of the magnetic microparticles to deposit and reduce gold ions onto the surface of the particle or the unsuccessful oxidation of citrate into acetone dicarboxylic which is responsible for the reduction of gold ions into atoms.

Coating Magnetic Microspheres with Au Nanoparticles Prepared by Hydroxylamine Reduction Method

The synthetic route of Au nanoparticles involves the preparation of small gold seeds, followed by dropwise addition of $AuCl_4^-$u solution to the growth solution for further particle growth. In the growth solution, hydroxylamine hydrochloride is used as a mild reducing agent while gold seeds serve as nucleation centres which provide the nuclei for subsequent growth of large gold nanoparticles. This same procedure is optimized to coat the surface of the magnetic microparticles. Magnetic microparticles were soaked in various concentrations of $AuCl_4^-$solutions and the rest of the procedure was followed in order to form Au nanoparticles on the surface of the microspheres. Fig. 11 displays EDX elemental plots of magnetic microspheres taken after coating with different concentrations of $AuCl_4^-$. As shown in Fig. 11, the Au nanoparticle distribution on the surface of microspheres is more uniform with the increase of $AuCl_4^-$concentration from $1.0x10^{-3}$ M to $3.0x10^{-3}$ M however; increasing the concentration further makes the coating even worse. This is probably due to the lack

of the amount of hydroxylamine to reduce all $AuCl_4^-$ ions on the surface of magnetic microspheres. Moreover, the coating with $1.0x10^{-3}$ M $AuCl_4^-$ concentration was repeated twice, the coating is better compared to coating the surface once with $1.0x10^{-3}$ M $AuCl_4^-$ as shown in Fig. 11d.

Au nanoparticle coated magnetic microspheres at various $AuCl_4^-$ concentrations were evaluated for their SERS activity using $5.0x10^{-7}$ M R6G as shown in Fig. 11. Raman signals from Au/Ag coated microspheres were obtained by focusing on only one microsphere in 100 μl of $5.0x10^{-7}$ M R6G solution. The data also confirm the successful coating of Au nanoparticles on the surface of the microspheres. SERS signals with varying intensities were measured for different coatings and the highest SERS signals were measured from the microspheres coated with $3.0x10^{-3}$ M $AuCl_4^-$ concentration compatible with SEM images.

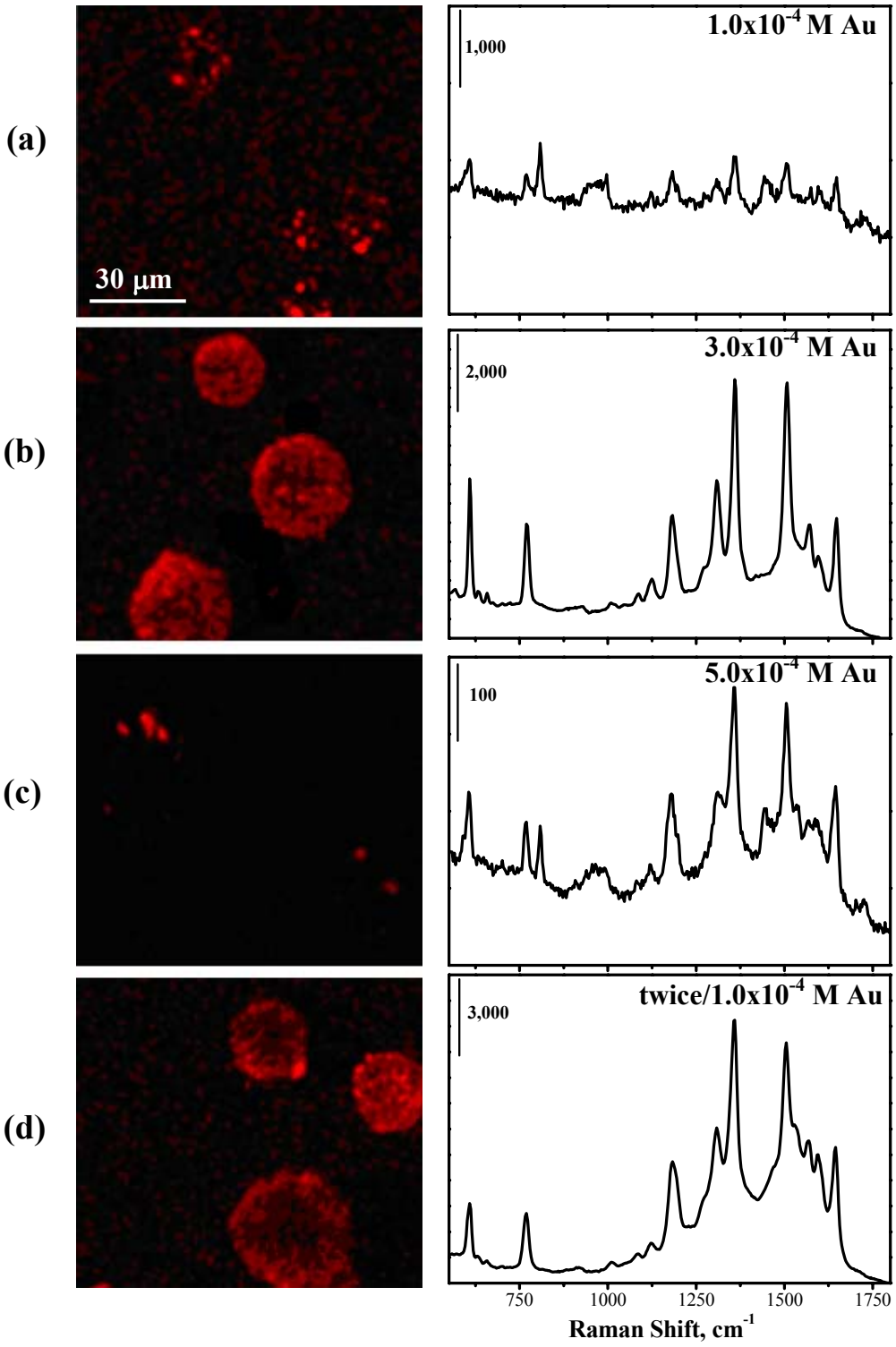

Figure 11. EDX elemental plot for Au on Au nanoparticle coated magnetic microspheres prepared by the reduction of $AuCl_4^-$ with $1.0x10^{-3}$ M hydroxylamine at various $AuCl_4^-$ concentrations on which the SER spectra of $5.0x10^{-7}$ M R6G were also shown next to each EDX plot. Red color shows gold spots. $AuCl_4^-$ and magnetic

microspheres were mixed for 24 h in each experiment except for (a) (1 hr). Integration time was 1 s for each SER spectra.

The chemical composition of the Au nanoparticle coated magnetic microspheres was investigated using an EDX spectrometer attached to Zeiss SEM. The EDX spectrum (Fig. 12) shows the presence of gold on the surface of two microspheres analyzed.

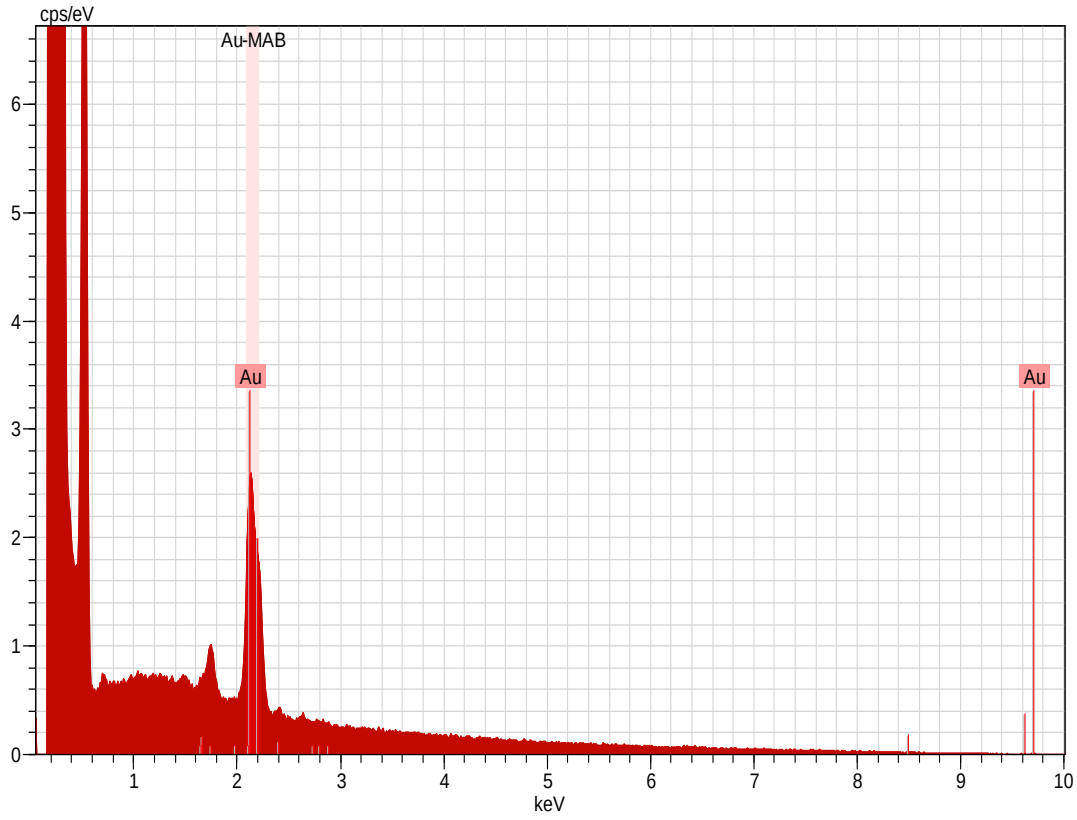

Figure 12. EDX spectrum of Au nanoparticle coated magnetic microspheres.

The stability of the coating is followed for a period of 11 months. The Au coating is stable for a period of 11 months with no degradation as seen from the EDX elemental plot for Au. (Fig. 13)

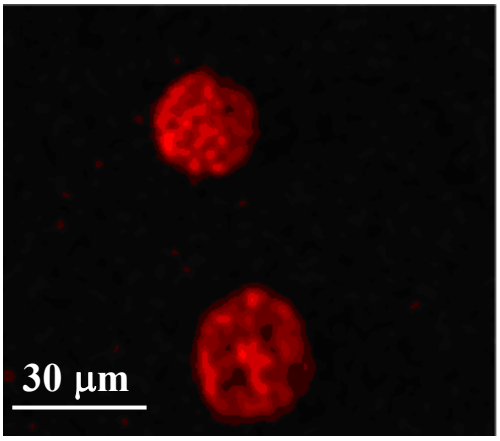

Figure 13. EDX elemental plot for Au after 11 months correspond to Fig. 11b from the same set of microspheres. Au nanoparticle coated magnetic microspheres in deionized water for 11 months with no degradation.

The Raman spectrum of free R6G molecules, magnetic microspheres, magnetic microspheres in R6G solution, Au nanoparticle coated magnetic microspheres and Au nanoparticle coated magnetic microspheres in R6G solution are shown in Fig. 14. In order to compare the intensities of each sample, the Raman signal measurements were carried out only from one microsphere. As can be seen from Fig. 14, blank signals from magnetic microspheres alone or coated with Au nanoparticles are negligible as compared to SERS signals from R6G molecules. The observed Raman bands with their assignments are summarized in Table 6.[88, 104]

In addition to signal enhancement, SERS can also greatly reduce the problems of fluorescence interferences often observed in Raman spectroscopy by effective adsorption of the analyte to the metal surface. The R6G molecule itself fluorescence and this causes a high background in the Raman spectrum however, when we adsorb R6G onto Au nanoparticle coated magnetic microspheres background signal decreases. This is a result of the ability of SERS to quench fluorescence in combination with the large signal enhancement means that we can produce high quality Raman spectra at low concentrations in the range of parts per billion.

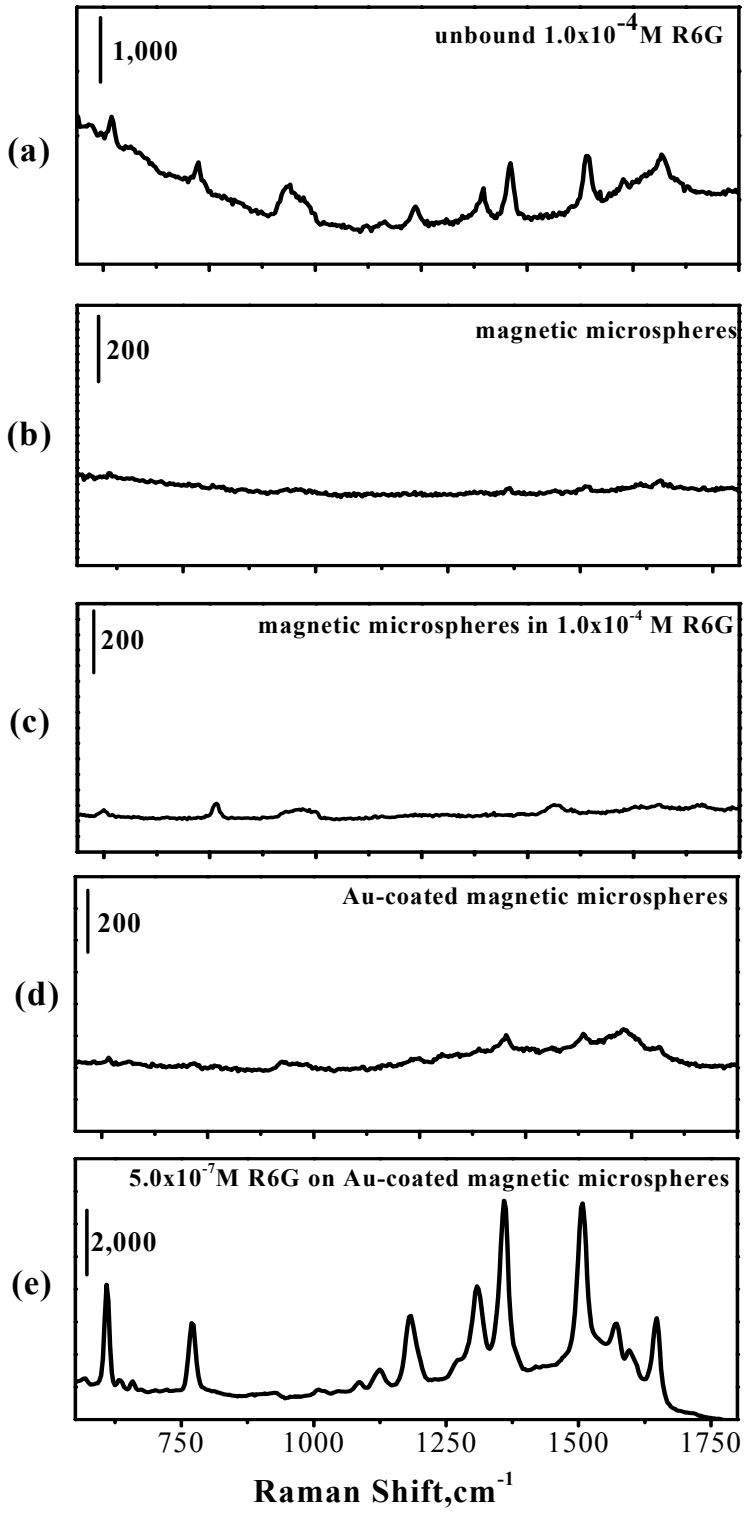

Figure 144. Raman spectrum of **a)** 1.0×10^{-4}M R6G, **b)** magnetic microspheres in deionized water, **c)** magnetic microspheres in 1.0×10^{-4}M R6G, **d)** Au coated magnetic microspheres and SER spectrum of **e)** 5.0×10^{-7} M R6G on Au nanoparticle coated magnetic microspheres. Integration time was 100 s for spectrum (a) and for others were 1 s.

Table 6. Selected observed bands in Raman spectrum of R6G with their assignments.

Raman Bands (cm^{-1})	**Assignment**
615	CCC in-plane deformation
778	CH in-plane deformation
1189	CH in-plane deformation
1316	CC stretching + CN stretching
1368	CC stretching + CN stretching
1511	CC stretching
1574	CC stretching
1650	CC stretching

It should be noted that there are no frequency shifts between the SER spectra of R6G molecules on the surface of Au nanoparticle coated magnetic microspheres and Raman spectrum of the non-adsorbed R6G molecules as seen from Fig 14. This observation proves that the enhancement in Raman signal is mostly due to electromagnetic mechanism which does not depend on the nature of molecule-metal interactions on the surface.[1, 8, 104]

Reliable determination of the SERS enhancement factor is an important step in SERS experiments, but it is full of experimental difficulties. First of all, the exact number of molecules contributing to SERS is not known exactly and there seems to be no hope to have this information. However, even if this were known, not all of the molecules are SERS active. Because the SERS cross section depends on surface topology, the presence of active sites etc. Besides, the proper evaluation of the quantity of adsorbed substance is also a complicated problem to deal with. Only a few

attempts have been made using radiochemical methods.[105] The amount of adsorbate can be evaluated relative to the equilibrium concentration of the free substance, but only a rough estimation is achieved. Therefore, SERS enhancement factors were calculated by comparing the intensity of the appropriate R6G molecule peak measured in the SERS experiments to the corresponding peak measured from liquid R6G. When the peak height are normalized for acquisition time under the same collection conditions, the SERS enhancement factor (EF) is given by:[106-108]

$$EF = \frac{I_{SERS} C_{bulk}}{I_{bulk} C_{SERS}} \tag{8}$$

where I_{SERS} is the height of the peak in SERS, C_{SERS} is the concentration of the analyte in SERS measurement, I_{bulk} is height of the peak in Raman scattering, C_{bulk} is the concentration of the analyte in Raman measurement. Using this equation, the enhancement factors have been calculated with respect to peaks at 614, 776 and 1364 cm^{-1} as $1.7x10^5$, $3.6x10^5$, $2.1x10^5$, respectively.

SER spectra from $5.0x10^{-7}$ M R6G molecule on the surface of different microspheres are shown in Fig. 15. The relative standard deviations (RSD %) for three measurements are around 10 % for the three peaks at 614, 776 and 1364 cm^{-1}.

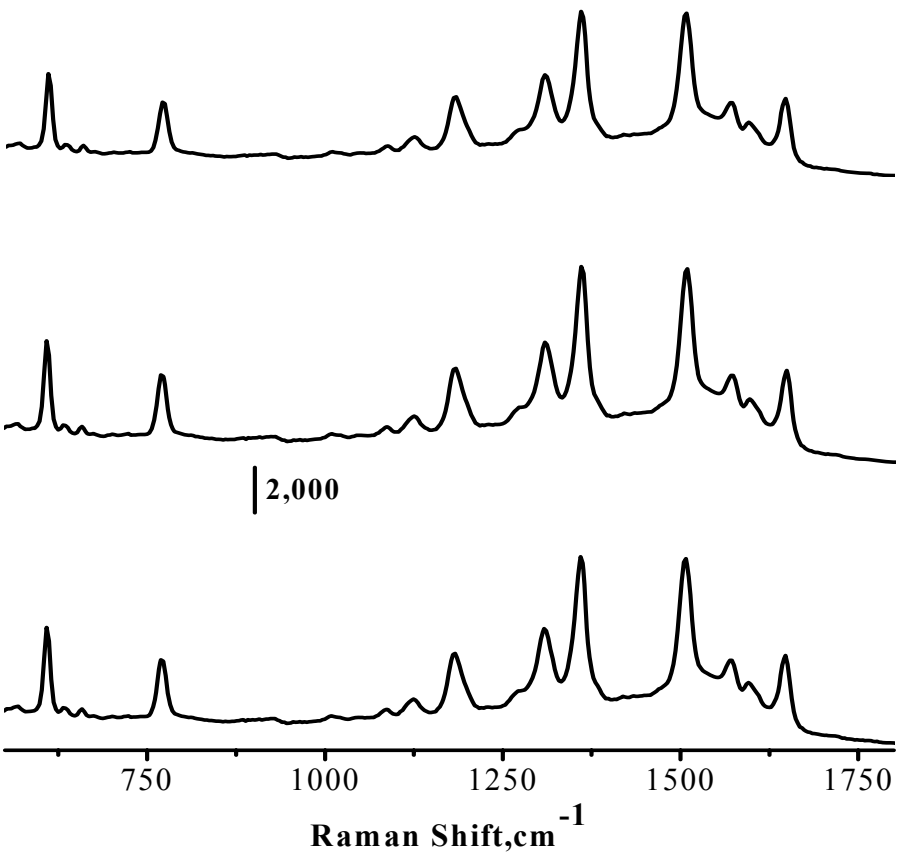

Figure 15. SER spectra of three replicates of 5.0×10^{-7} M R6G on different Au nanoparticle coated magnetic microspheres. Integration time was 1 s.

Coating Magnetic Microspheres with Au Nanoparticles Prepared by $NaBH_4$ Reduction Method

Magnetic microspheres were mixed with various $AuCl_4^-$ aqueous solutions at room temperature for 24 h to adsorb all $AuCl_4^-$ ions in the solution onto the surface of magnetic microspheres and then, various concentrations of $NaBH_4$ were used to reduce $AuCl_4^-$ to Au. As magnetic microspheres were kept longer in $AuCl_4^-$ solution, more $AuCl_4^-$ ions were adsorbed on microspheres which yielded better Au nanoparticle coating on the surface as seen in Figure 16a and 16b, 1 and 24 h residing periods, respectively. Fig.16 displays EDX elemental plots for Au on magnetic microspheres which were taken after coating the surface of the microspheres with different concentrations of $AuCl_4^-$ and $NaBH_4$. As shown in Fig.16, the Au nanoparticle distribution on the particles is more with the increase of residing period from 1 to 24 h (Fig. 16a and 16b). The increase of $AuCl_4^-$ concentration from $1.0x10^{-3}$ M to $5.0x10^{-3}$ M by keeping the $NaBH_4$ concentration constant yielded worse coating with a decrease in SERS signals as shown in Fig. 16b and 16c. This is due to the lack of $NaBH_4$ concentration to reduce $AuCl_4^-$ ions, since further decreasing the $NaBH_4$ concentration by 50% makes the coating even worse as shown in Fig 16e. Therefore, the $NaBH_4$ concentration was increased to $4.0x10^{-3}$ M and the coating becomes more uniform at $5.0x10^{-3}$ M $AuCl_4^-$ concentration as shown in Fig. 16d. Two coatings as shown in Fig. 16b and 16d showed similar since their SERS signals since their SERS activities were almost equal to each other.

EDX spectrum of two microspheres was taken and shown in Fig. 17 which also depicts the presence of Au on the microspheres.

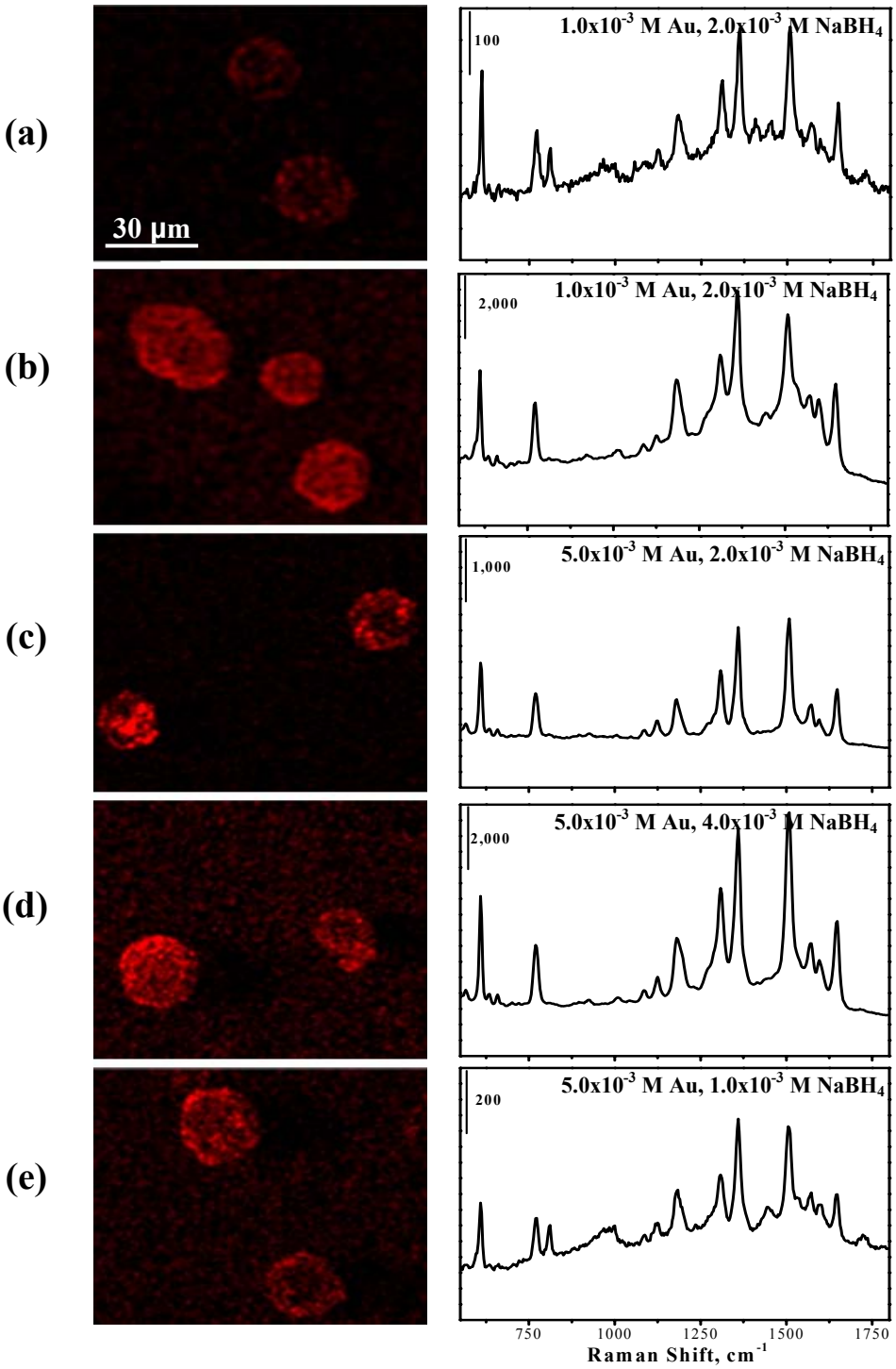

Figure 16. EDX elemental plot for Au on Au nanoparticle coated magnetic microspheres prepared by the reduction of $AuCl_4^-$ with $NaBH_4$ at various $AuCl_4^-$ and $NaBH_4$ concentrations on which the SER spectra of $5.0x10^{-7}$ M R6G were also shown next to each EDX plot. Red color shows gold spots. $AuCl_4^-$ and magnetic microspheres were mixed for 24 h in each experiment except for a (1 hr). Integration time was 1 s for each SER spectra.

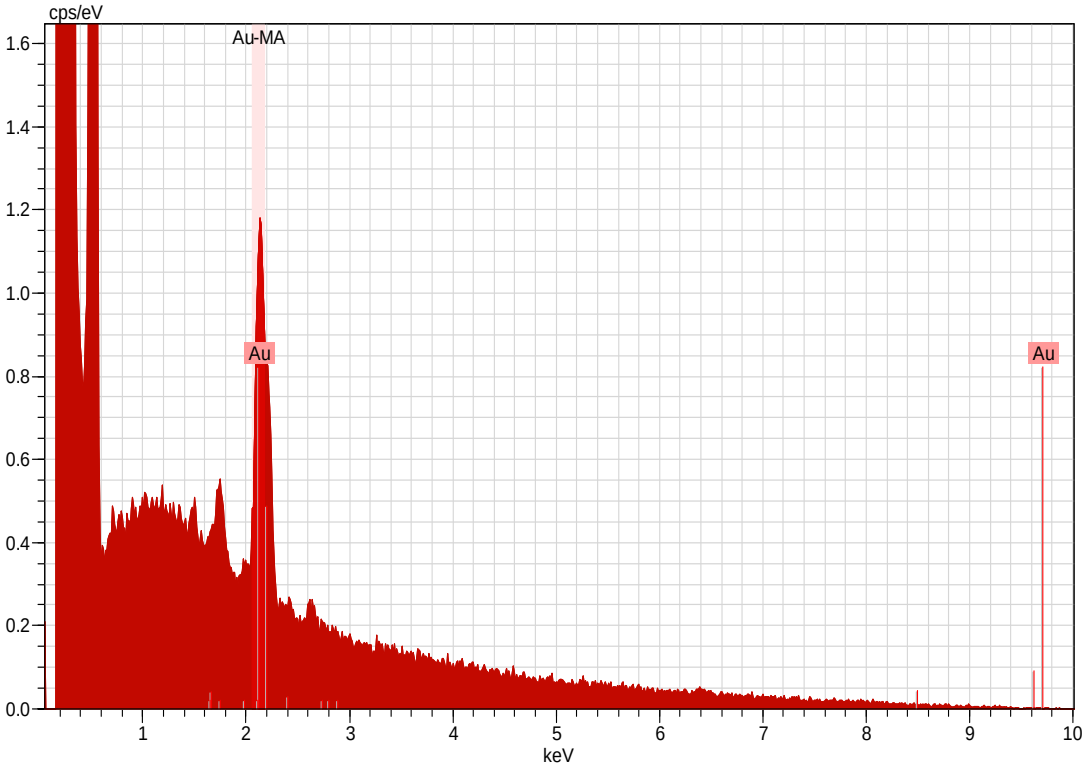

Figure 17. EDX spectrum of Au nanoparticle coated magnetic microspheres.

Fig. 18 shows the Raman spectrum of free R6G molecules, magnetic microspheres, magnetic microspheres in R6G solution, Au nanoparticle coated magnetic microspheres and Au nanoparticle coated magnetic microspheres in R6G solution. As can be seen from Fig. 18, the blank signals from magnetic microspheres alone or coated with Au nanoparticles are negligible compared to SERS signals from R6G molecules on the surface of Au nanoparticle coated magnetic microspheres using $NaBH_4$ reduction method.

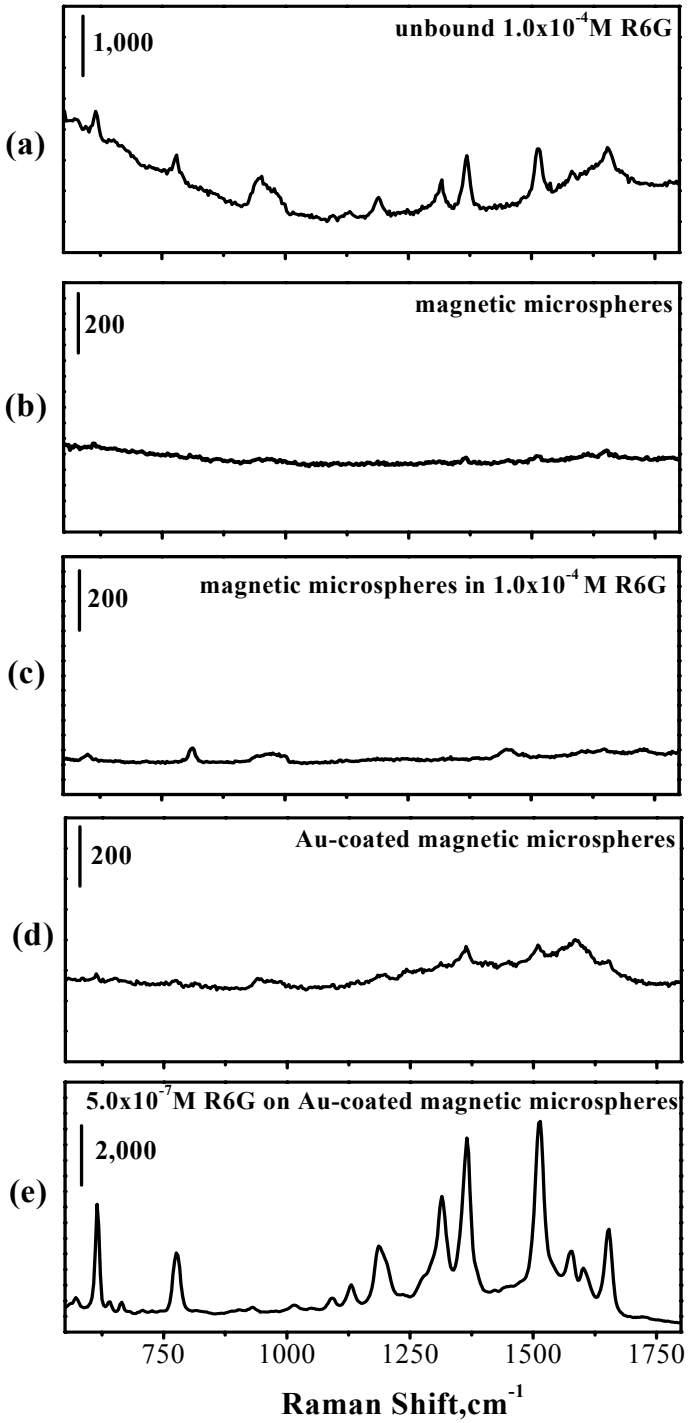

Figure 18. Raman spectrum of **a)** 1.0×10^{-4}M R6G, **b)** magnetic microspheres in deionized water, **c)** magnetic microspheres in 1.0×10^{-4}M R6G, **d)** Au coated magnetic microspheres SER spectrum of **e)** 5.0×10^{-7}M R6G on Au nanoparticle coated magnetic microspheres. Integration time was 100 sec for spectrum (a) and for others were 1 sec.

SER spectra of $5.0x10^{-7}$ M R6G on the surface of three different Au nanoparticle coated magnetic microspheres were shown in Fig. 19. The relative standard deviations (RSD%) of peak heights for three measurements were around 10 %. The enhancement factors for these peaks were calculated using equation 3 as $1.1x10^{5}$, $2.7x10^{5}$ and $1.5x10^{5}$ for the three peaks at 614, 776 and 1364 cm^{-1}, respectively.

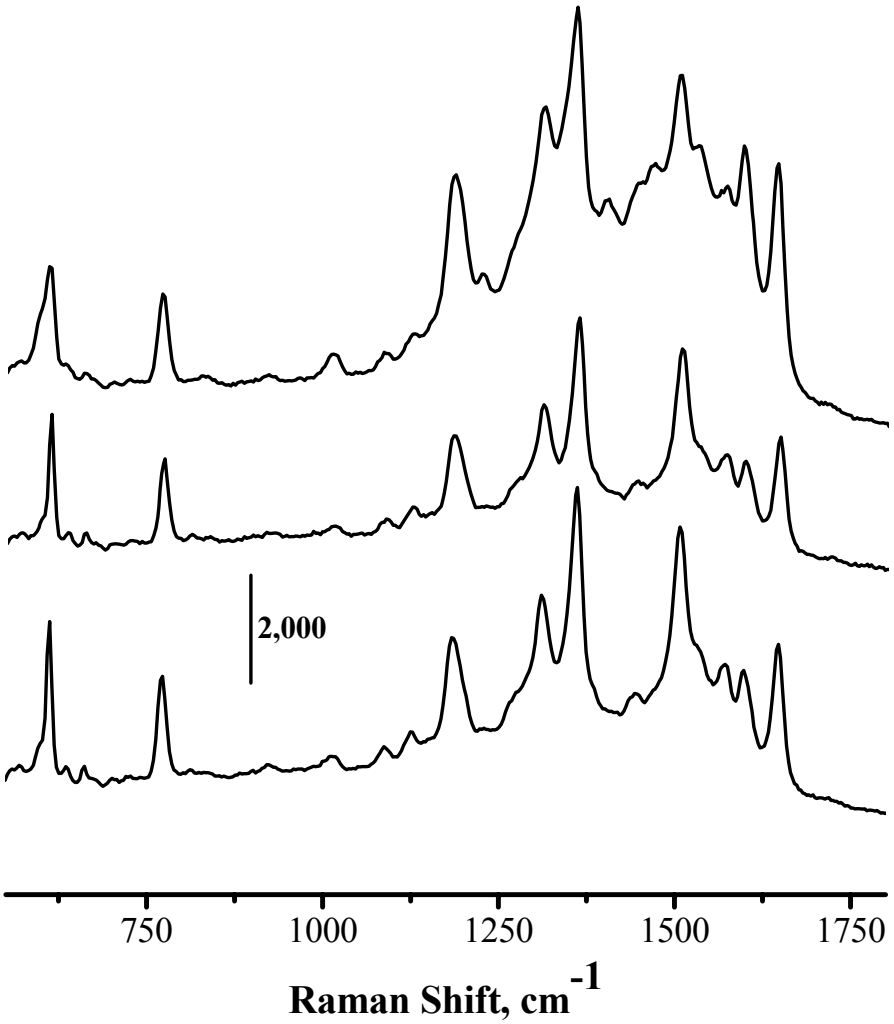

Figure 19. SER spectra of three replicates of $5.0x10^{-7}$ M R6G on different Au nanoparticle coated magnetic microspheres. Integration time was 1 sec.

Raman spectrum of liquid R6G and SER spectra of R6G on Au nanoparticle coated magnetic microspheres and R6G in Au nanoparticles are shown in Fig. 20. As shown in Fig. 20, the surface enhancement of Au nanoparticle coated magnetic microspheres is larger than that of Au nanoparticles 10^2 times which were prepared with the same procedure used to coat the surface of the microspheres, however, the measurements were not performed exactly in the same way. SER spectrum is measured from only one microsphere, however in case of Au nanoparticles; measurements were made from 100 μl of liquid containing R6G molecules in Au nanoparticle solution. Therefore, the number of molecules adsorbed on the surface of Au nanoparticles in solution phase is probably higher than on the surface of Au nanoparticle coated magnetic microspheres.

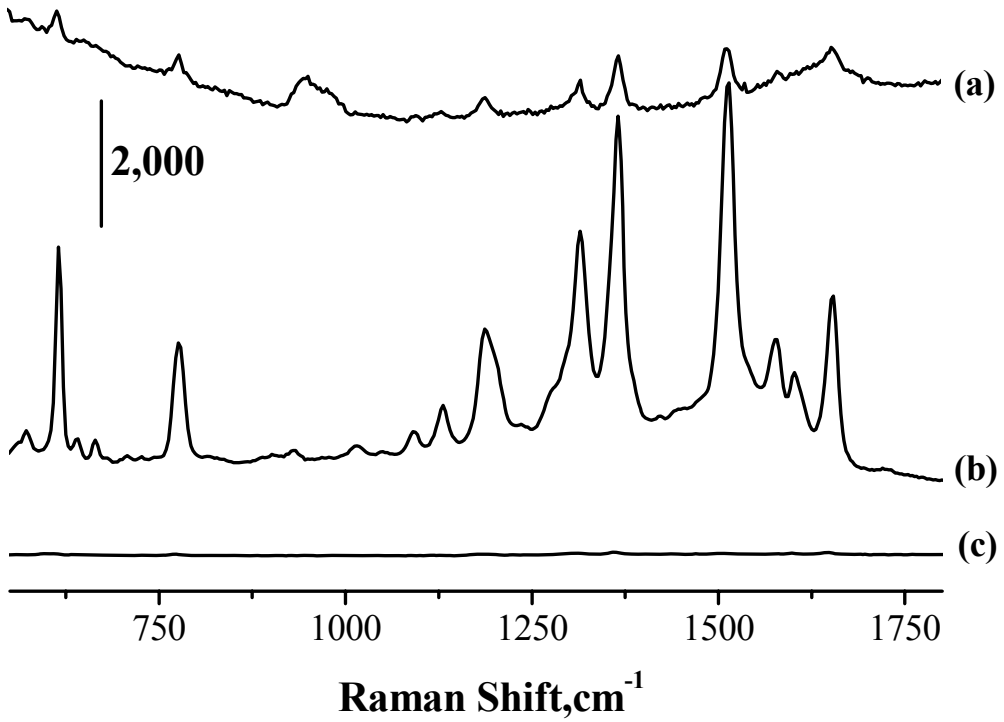

Figure 20. a) Raman spectrum of 1.0×10^{-4}M R6G and SERS spectra of 5.0×10^{-7} M R6G on **b)** Au nanoparticle coated magnetic microspheres and **c)** in Au nanoparticles. Integration time was 100 s for spectrum (a) and 1 s for the others.

When we use hydroxylamine as reducing agent to deposit Au nanoparticles onto magnetic microsphere we did not observe the formation of Au nanoparticles in the solution phase which is an indication of reduction of Au nanoparticles on the surface of the microparticles or no nucleation center in the solution phase. However, with the use of $NaBH_4$ as reducing agent, the bulk of the solution color was wine red after the introduction of $NaBH_4$ to the solution. This reveals that Au nanoparticles were also formed in the solution phase. Since hydroxylamine is a milder reducing agent than sodium borohydride, bulk reaction probably can not take place, however, it can reduce gold ions which were attached to the surface of the microparticles.

4.1.3.2.2 Coating Magnetic Microspheres with Ag Nanoparticles

Ag nanoparticles were coated on the surface of magnetic microspheres in two ways: hydroxylamine and sodium borohydrate reduction methods. In hydroxylamine reduction method, Ag^+ ions are aggregated as AgCl due to presence of Cl^- ions originating from the hydroxylamine salt (hydroxylamine hydrochloride). Therefore, Ag nanoparticle coating on magnetic microspheres by hydroxylamine reduction method was not successful.

Ag nanoparticles were coated on magnetic microspheres similar to the coating of Au nanoparticle procedure using $NaBH_4$ reduction method. Five sets of experiments were carried out to optimize the Ag nanoparticle coating on magnetic microspheres. Various concentrations of Ag^+ and $NaBH_4$ and were used and the final product was characterized using Raman spectrometer and SEM. EDX elemental plots for Ag on magnetic microspheres which were taken after coating the surface of the microspheres with various concentrations of Ag^+ and $NaBH_4$ were shown in Fig. 21. The Ag nanoparticle distribution on the particles is more uniform with the increase of residing period from 1 to 24 h as shown in Fig. 21a and 21b and the SERS activity of 24 h soaked microspheres in Ag^+ solution showed better SERS activity. The increase of Ag^+ concentration from $1.0x10^{-3}$ M to $5.0x10^{-3}$ M by keeping the $NaBH_4$ concentration constant yielded better coating with an increase in SERS signals as shown in Fig. 21b and 21c. It can be concluded that the $NaBH_4$ concentration was more than sufficient in the solution medium when we increased the concentration of Ag^+ resulted in a better coating with a better SERS activity. Increasing or decreasing the concentration of $NaBH_4$ by 50% makes the coating poorer as shown in Fig 21d and 21e. As a result, the best SERS activity was obtained from the coating using

$5.0x10^{-3}$ M Ag^{+} and $2.0x10^{-3}$ M $NaBH_4$ concentrations (Fig. 21c) using which further experiments were performed.

The chemical composition of Ag nanoparticle coated magnetic microspheres was analysed using an EDX spectrometer attached to the SEM. The EDX spectrum (Fig. 22) shows the presence of silver on the surface of two microspheres analyzed.

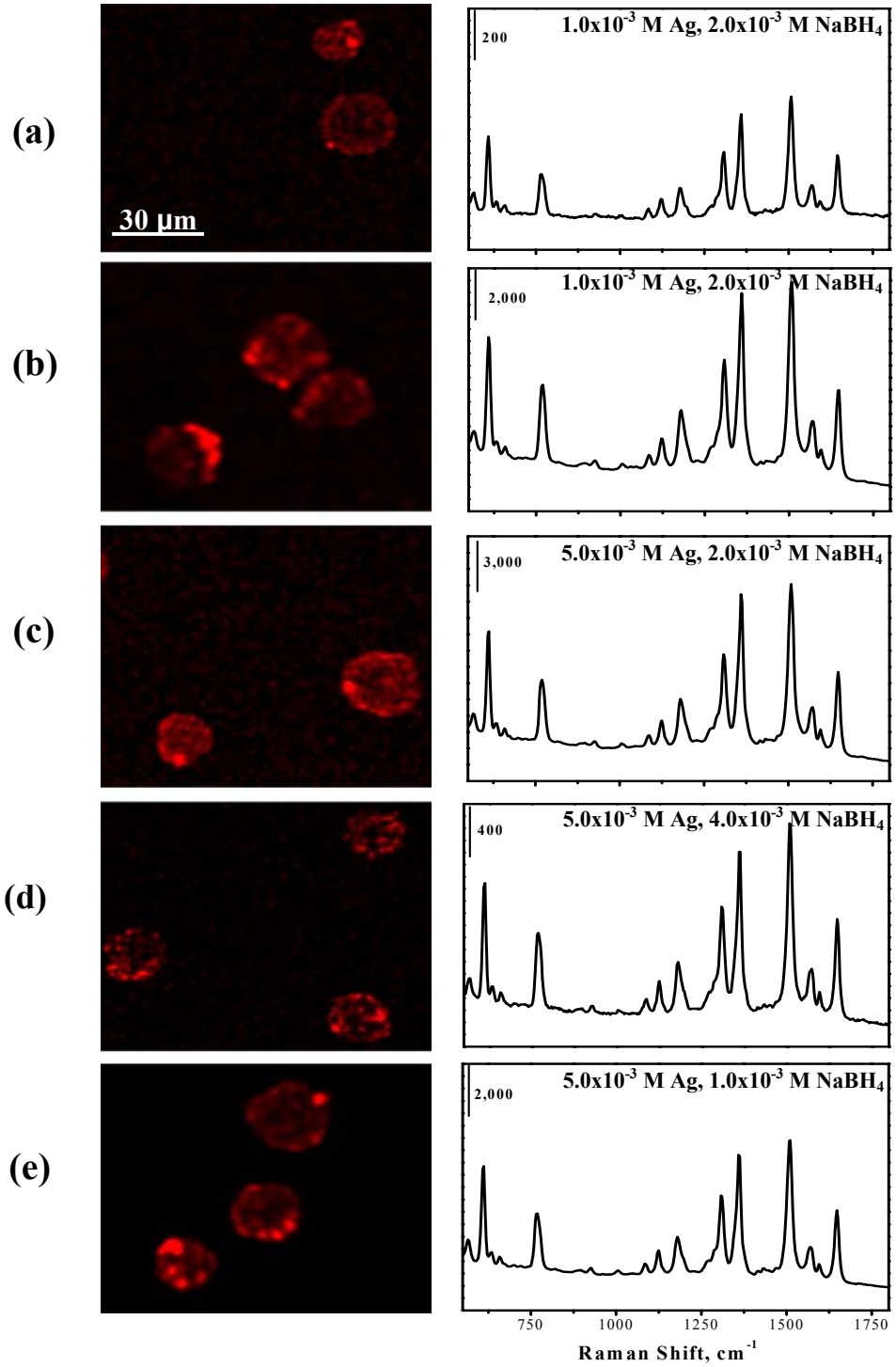

Figure 21. EDX element plot for Ag on Ag nanoparticle coated magnetic microspheres prepared by the reduction of Ag^+ with $NaBH_4$ at various Ag and $NaBH_4$ Red color shows silver spots. The spectrum next to each EDX elemental plot shows the SER spectrum of $5.0x10^{-7}$ M R6G in presence of Ag nanoparticle coated magnetic microspheres. Magnetic microspheres were soaked in Ag^+ solution for 24 h in each experiment except for a (1 hr). Integration time was 1s for each SER spectra.

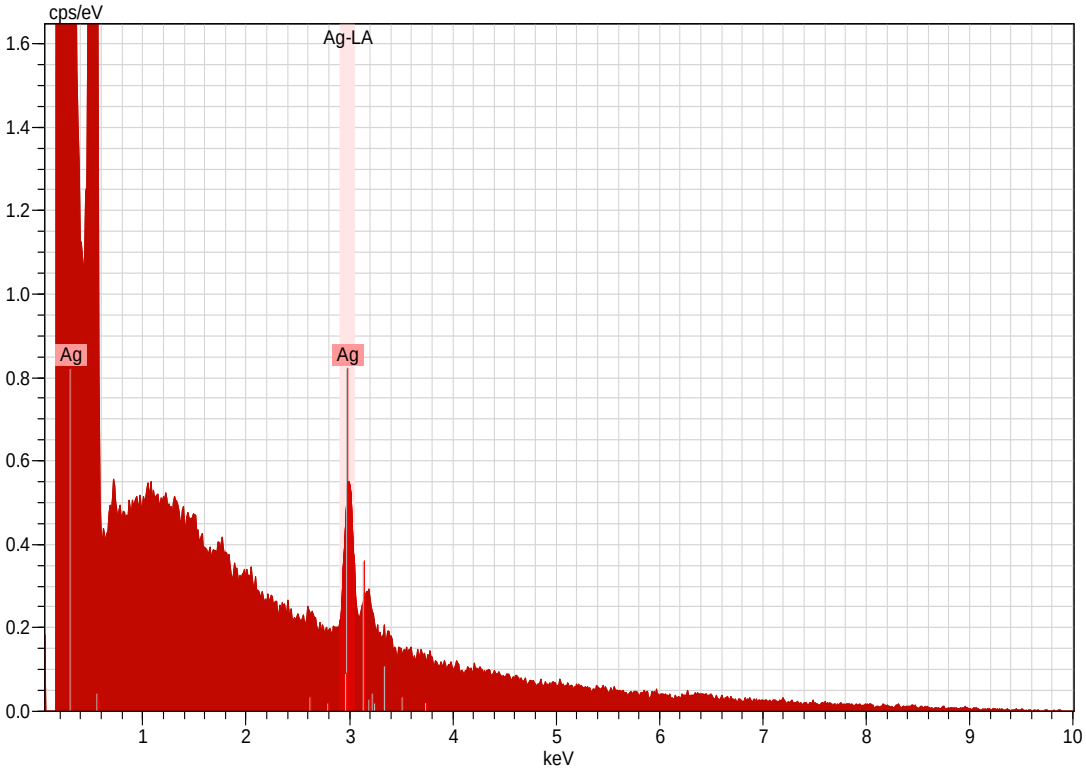

Figure 22. EDX spectrum of Ag nanoparticle coated magnetic microspheres.

Fig. 23 shows the Raman spectrum of free R6G molecules, magnetic microspheres, magnetic microspheres in R6G solution, Ag nanoparticle coated magnetic microspheres and Ag nanoparticle coated magnetic microspheres in R6G solution. As can be seen from Fig. 23, in the absence of Ag nanoparticle coated magnetic microspheres, no signal from R6G was measured and the blank signals from magnetic microspheres alone or coated with Ag nanoparticles are negligible compared to SERS signals from R6G molecules.

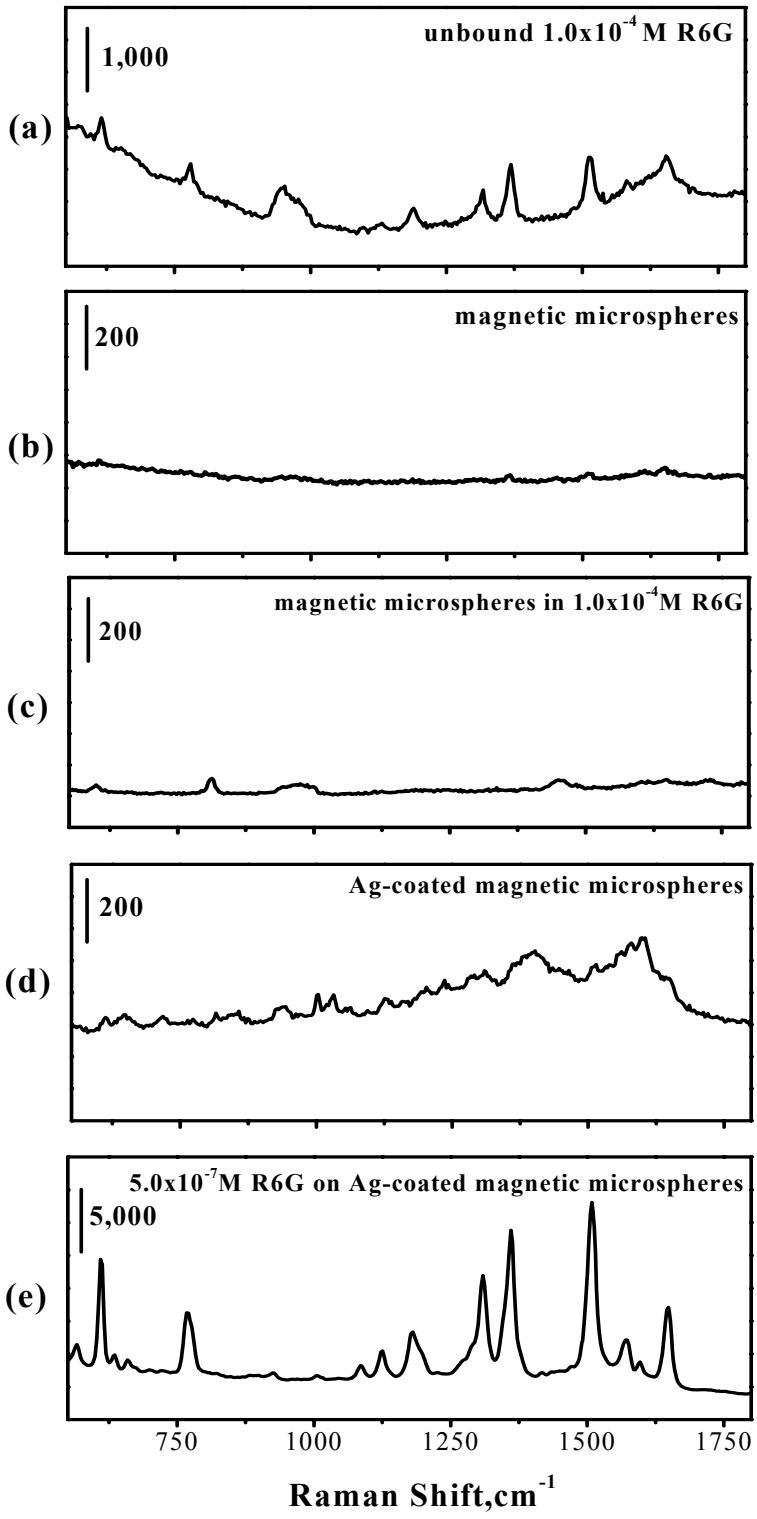

Figure 23. Raman spectrum of **a)** 1.0×10^{-4}M R6G, **b)** magnetic microspheres in deionized water, **c)** magnetic microspheres in 1.0×10^{-4}M R6G, **d)** Ag coated magnetic microspheres SER spectrum of **e)** 5.0×10^{-7}M R6G on Ag nanoparticle coated magnetic microspheres. Integration time was 100 sec for spectrum (a) and for others were 1 sec.

SER spectra of $5.0x10^{-7}$ M R6G on the surface of three different Ag nanoparticle coated magnetic microspheres were shown in Fig. 24. The relative standard deviations (RSD %) for three measurements were around 10 %. With the knowledge that the recorded Raman spectra are consistent and reproducible, it is possible to measure different aspects of the SERS process.

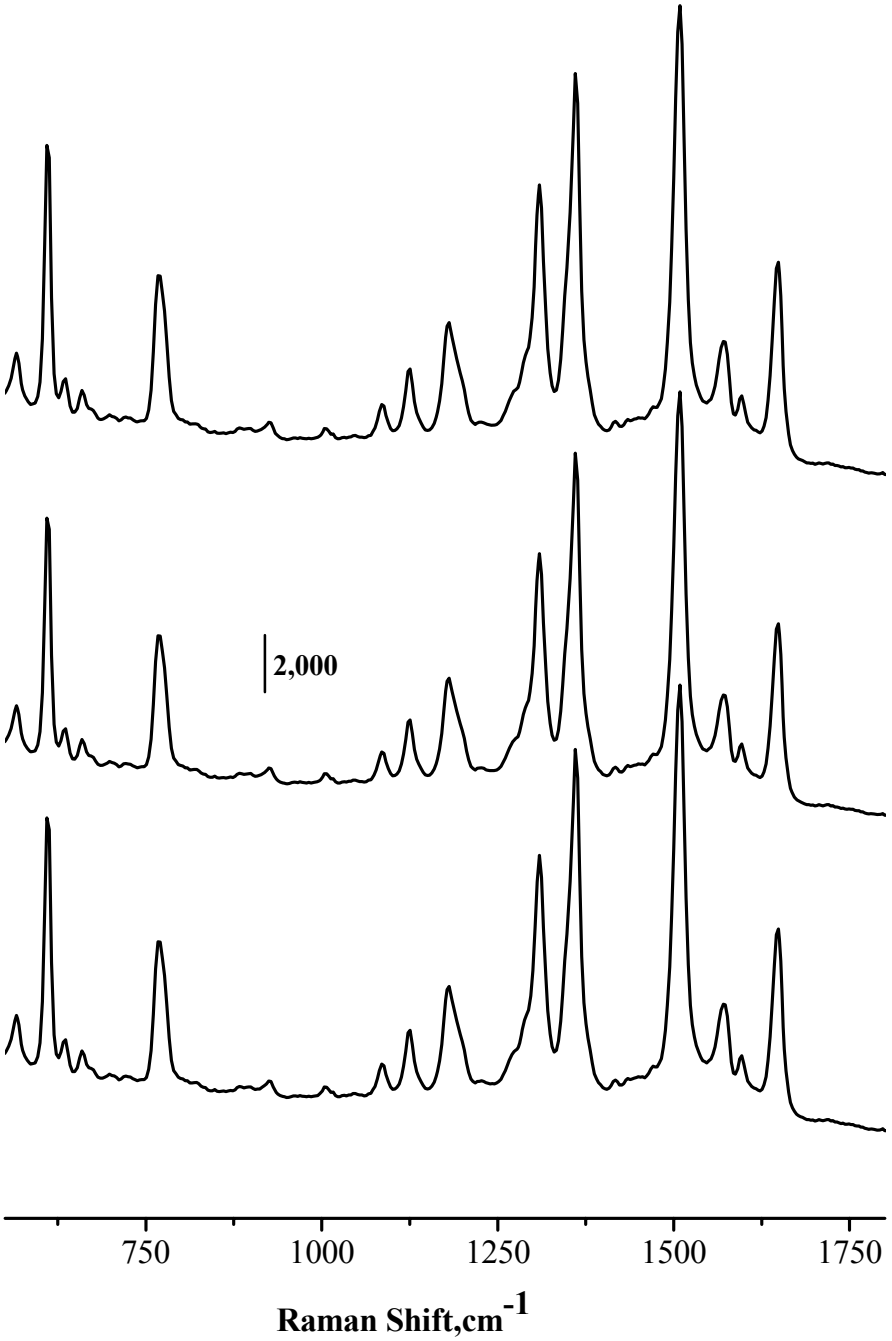

Figure 24. SERS spectra of three replicates of 5.0×10^{-7} M R6G on Ag nanoparticle coated magnetic microsphere. Integration time was 1 sec.

The SERS spectra of R6G aqueous solutions having concentrations between 1.0×10^{-8} M and 1.0×10^{-10} M are shown in Fig 25. The Raman spectrum of 1.0×10^{-4} M R6G in deionized water (Fig. 25a) is included for comparison purposes. The high

sensitivity of the SERS substrates allowed the spectra to be measured with an analytical-grade Raman system with a 1 s acquisition time as seen from Fig. 25 at a concentration level of $1.0x10^{-8}$ M. Fig. 26 displays the background corrected intensities of the peaks at 614, 776 and 1364 cm^{-1} vs. concentration of R6G corrected for their integration times. The quantitation limit achieved was $1.0x10^{-10}$ M as illustrated in Fig. 25 however, the signals from the microspheres at this concentration level start to be seen within the signals of R6G molecule. The signals from R6G molecule is represented with dots in Fig. 25. Enhancement factors were calculated by using the equation (3) and found as $4.2x10^{7}$, $8.7x10^{7}$, $6.1x10^{7}$ with respect to the peaks at 614, 776 and 1364 cm^{-1}, respectively.

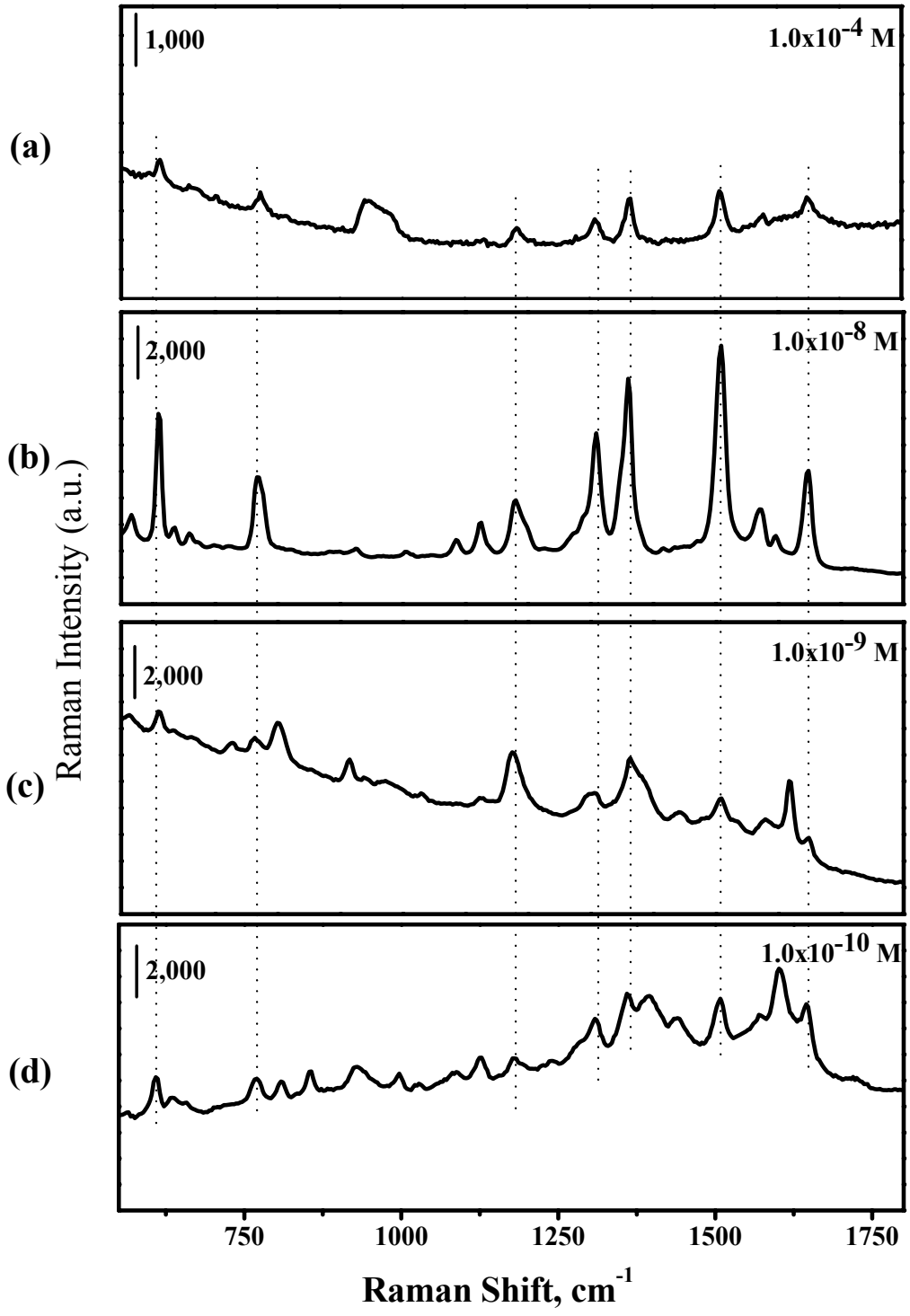

Figure 25. Raman spectrum of **a)**$1.0x10^{-4}$ M R6G and SERS of **b)**$1.0x10^{-8}$ M, **c)** $1.0x10^{-9}$ M and **d)** $1.0x10^{-10}$ M R6G on Ag nanoparticle coated magnetic microspheres. The spectra were acquired with a 100 s exposure for a, 0.5 sec for b, 5 s for c and 10 sec for d.

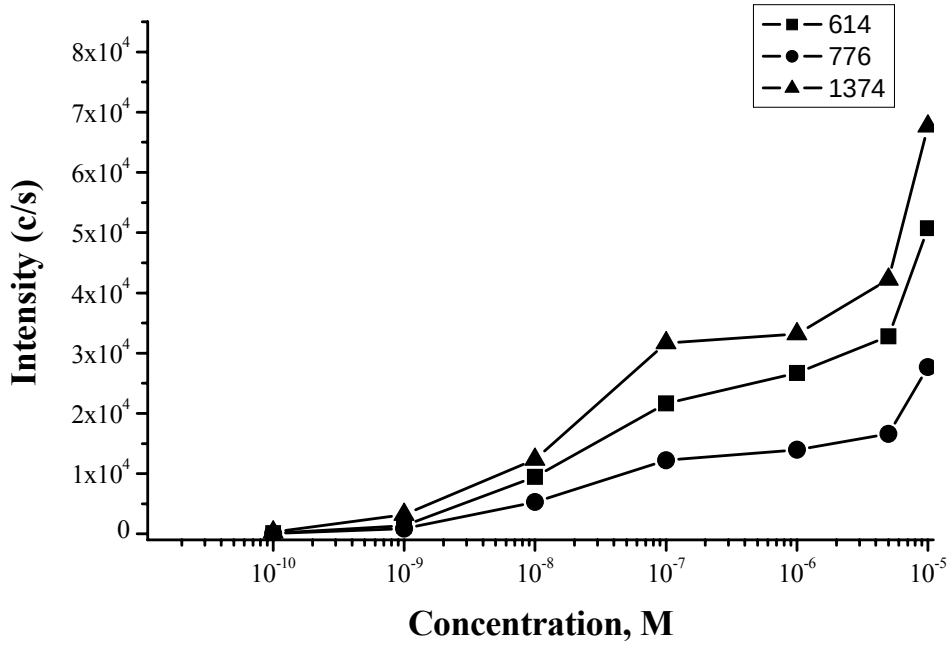

Figure 26. Peak height vs. concentration graph of 614, 776 and 1364 cm^{-1} peaks.

The SER spectra of R6G in Ag nanoparticles and on the surface of magnetic microparticles are shown in Fig. 27 to compare the SERS activity of these two SERS substrates in solution phase and after coated onto microspheres. Enhancement factors were calculated with respect to the peaks at 614, 776 and 1364 cm^{-1} as $1.7x10^3$, $2.0x10^3$ and $1.7x10^3$ using Ag nanoparticles as SERS substrate, respectively. The enhancement factor is around 10^7 when the Ag nanoparticle coated microspheres were used as SERS substrate. In conclusion, the SERS activity of Ag nanoparticles as SERS substrate on the surface of microspheres is 10^4 times better compared to that in Ag nanoparticles in solution.

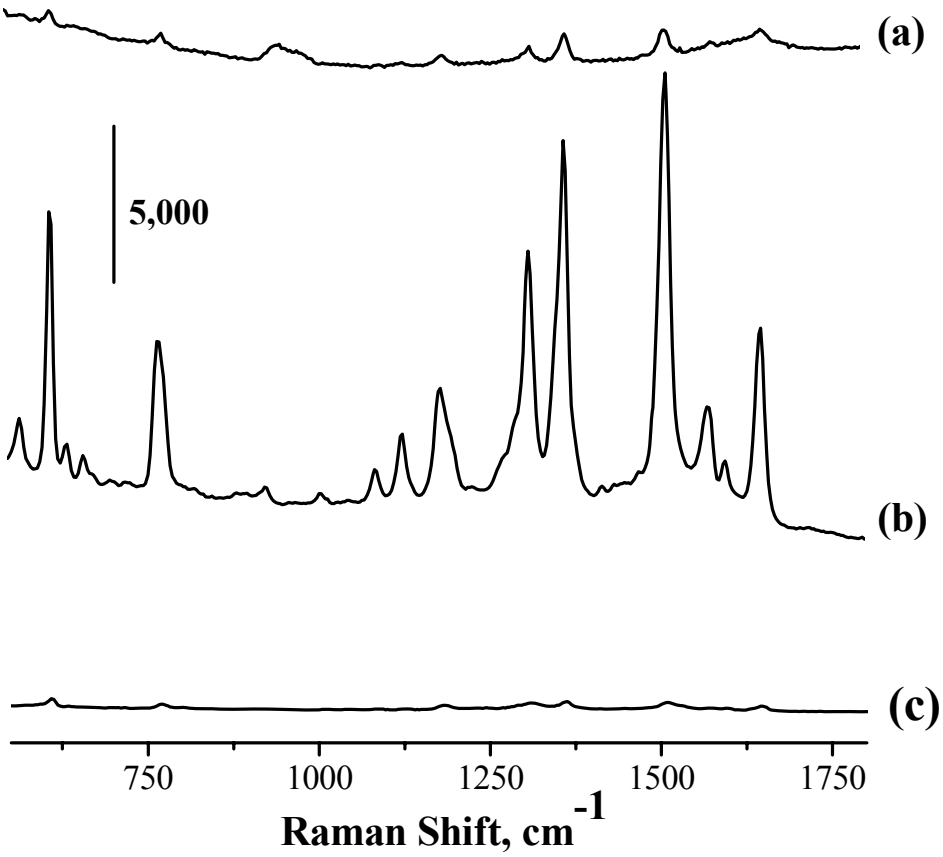

Figure 27. a) Raman spectrum of 1.0×10^{-4} M R6G and SER spectra of 5.0×10^{-7} M R6G on **b)** Ag nanoparticle coated magnetic microspheres and **c)** in Ag nanoparticles solution. Integration time was for 100 s for spectrum a and 1 s for the others.

4.2 Immobilization of Au nanoparticles on Spherotech Amine Functionalized Magnetic Microspheres

In literature Au nanoparticles have been immobilized onto commercially available amine functionalized magnetic microparticles via their amine functional groups and used as a SERS substrate for the first time using naphthalene as SERS probe.[41] In order to compare the nanoparticle coated magnetic microspheres proposed in our study as SERS substrate, Au nanoparticles were immobilized onto Spherotech magnetic microparticles via amine groups on the surface of Spherotech microparticles and SER spectrum is illustrated in Fig. 28. The enhancement factor was calculated as ~200 with respect to the peak at 614 cm^{-1}. Therefore, the enhancement factor was smaller when it was compared with the enhancement factor obtained from Au nanoparticles coated on magnetic microparticles reported in the current work.

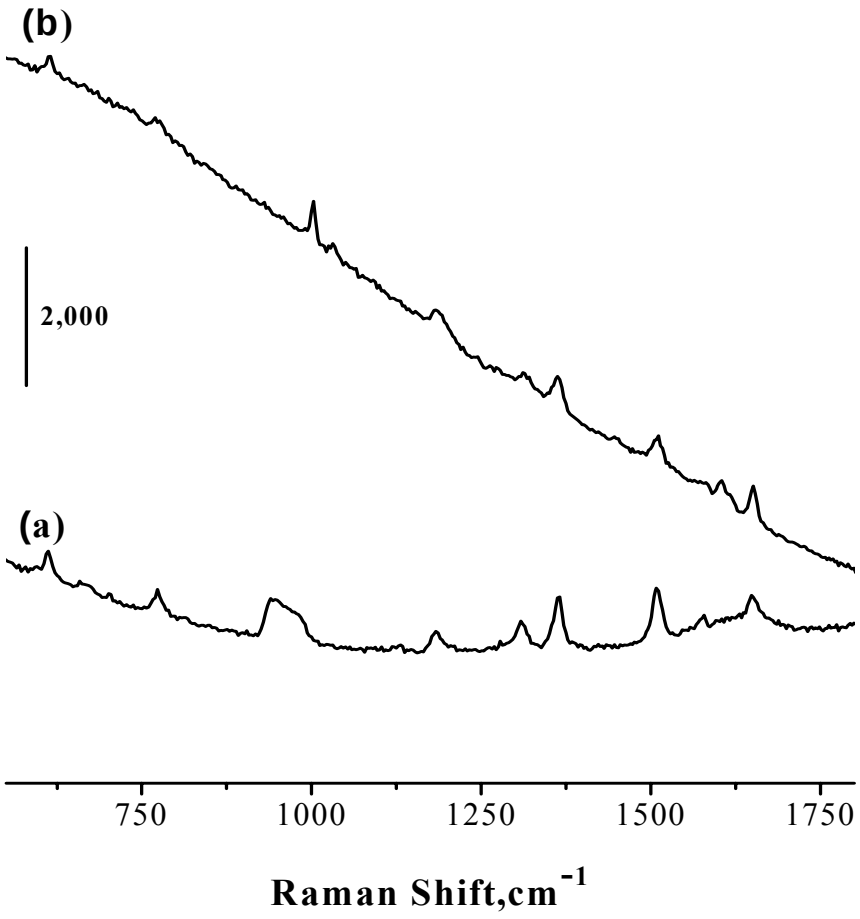

Figure 28. Raman spectrum of **a)** 1.0×10^{-4}M R6G and SER spectrum of **b)** 5.0×10^{-5}M R6G adsorbed on Au nanoparticle immobilized on Spherotech magnetic microspheres. Integration time for Raman spectrum was 100 s and SER spectrum was 10 s.

4.3 Analysis of Aspartic Acid by SERS using Au and Ag Nanoparticles as SERS Substrates

In this section we will investigate the interaction of aspartic acid with Au and Ag nanoparticles depending on the pH of the solution.

4.3.1 Aspartic Acid

Raman studies of amino acids adsorbed on metal surface yield basic and guiding information for Raman studies of biopolymers adsorbed on metal surfaces. pKa values for aspartic acid are as follows: for α-carboxylic acid 2.10, side chain carboxylic acid 3.86 and α-amino 9.82. [25] These pKa values indicate that below pH 2.10, both carboxylic groups are protonated, between pH 2.10 and 3.86 α-carboxylic acid is deprotonated, above pH 3.86 side chain carboxylic acid is deprotonated. α-amino group is protonated below pH 9.82 and deprotonated above pH 9.82. In this study, in order to better understand the interaction of aspartic acid with the metal surface in different forms due to the pH changes, SER spectra of aspartic acid were studied at various pH values depending on which amino and carboxyl groups were protonated and deprotonated.

It is not possible to compare the Raman versus the SERS signal of aspartic acid because the Raman signal is limited with the solubility of aspartic acid which is 0.45g/100 ml in water (3.0×10^{-2} M). Therefore, it is not possible to report an enhancement factor or to make a comment on the enhancement mechanism for aspartic acid on Au or Ag metal surfaces. For reference purposes, Raman spectrum of

solid aspartic acid as powder form was taken as shown in Fig. 29 and the peak assignments of selected peaks are written in Table 7.

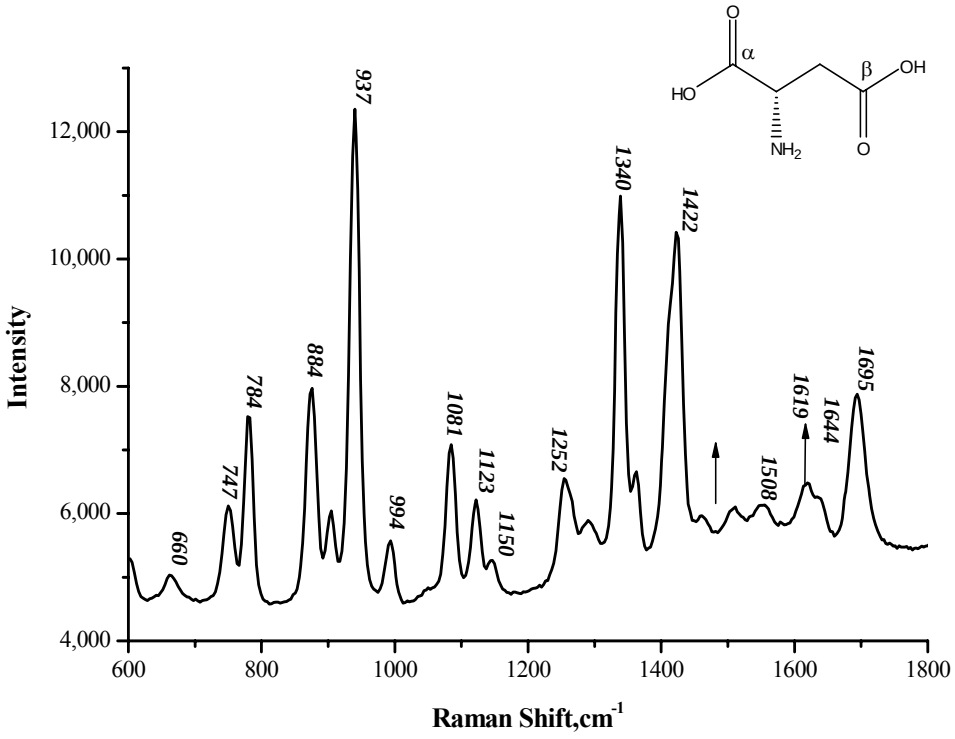

Figure 29. Raman spectrum of solid aspartic acid. Integration time was 100 s.

Table 7. Selected Raman bands of solid aspartic acid and their assignments. [109]

Raman Band (cm^{-1})	Assignment
1695	C=O stretching
1644	NH_3^+ asymmetric in-plane bending
1619	COO^- asymmetric stretching
1508	NH_3^+ symmetric in-plane bending
1422	COO^- symmetric stretching
1340	CH in-plane bending
1252	CO stretching+ OH in-plane bending
1150	NH_3^+ rocking
1123	NH_3^+ rocking
1081	CN stretching
994	CC stretching
937	OH out of plane bending
874	CH_2 rocking
780	OCO^- out of plane bending
747	COO^- in-plane bending
660	COOH in-plane bending
603	COO^- in-plane bending

In these experiments, two laser sources was used for SERS measurements, 632 nm and 532 nm because specifically, the strongest SERS enhancement occurs under conditions where the incident and Raman scattered photons are both strongly enhanced. SERS signals of aspartic acid on Ag nanoparticles using 532 nm as an excitation source resulted in a better signal intensity than that measured using 632 nm laser as excitation source. This is probably due to the fact that surface plasmon of Ag nanoparticles is closer to the wavelength of the excitation source when 532 nm diode laser was used as the source and electromagnetic enhancement theory states that once the wavelength of the incident light is close to the LSPR of metallic surface, with the molecules adsorbed or close to the surface yield a large electromagnetic field which is responsible for the enhancement in Raman signal. The experimental evidence of these arguments will be represented in further sections of this thesis. Besides, the results are in agreement with the studies in literature in which SERS using colloidal Ag resulted better spectra with 532 nm excitation source than 632 nm or Near-Infrared Region (NIR) excitation sources.[110-112]

It should be noted that interpreting SER spectra is difficult, since SER spectra includes both the vibrational bands and their interaction with the surface which results shift in the peak position of this band. Moreover, all vibrational bands are not enhanced in the SERS.

4.3.2 Aspartic Acid Adsorbed on Ag Nanoparticles

In literature amine group related bands are named as either amide I, amide II and amide III depending on the peak positions around 1620, 1510 and 1290 cm^{-1}, [28, 29,

[42, 45] or symmetric NH_3^+ deformation, asymmetric NH_3^+ deformation and NH bending, respectively.[25, 43, 46, 113] In this study, we will use amide nomenclature for peak assignments corresponding to these bands.

When aspartic acid was mixed with Ag nanoparticles, SER spectra of aspartic acid adsorbed on Ag nanoparticles were recorded at various pH values and are displayed in Fig. 30. Ag nanoparticle solution was mixed with aspartic acid solution with a ratio of (v/v) 10:1 and the pH of the solutions was adjusted either with 0.010 M HCl or 0.050 M NaOH solutions.

The initial pH of the solution was 3.95 when Ag nanoparticles were mixed with aspartic acid solution. At pH 3.95 the peak at 1374 cm^{-1} was attributed to the symmetric stretching of $-COO^-$ group and there was no identification of the C=O vibration of carboxyl group which supposed to be at ~1630 cm^{-1} [43] Asymmetric stretching of COO^- was attributed as 1582 cm^{-1}[20, 29]. When pH of the solution was adjusted to pH 1.74, asymmetric stretching of COO^- at 1582 cm^{-1} vanished probably due to the protonation of carboxylate group to carboxyl group. Protonation of carboxylate group caused decreasing in the intensity of symmetric stretching at 1374 cm^{-1} and shifted to higher frequency, 1384 cm^{-1} which can be explained by assuming change in the proximity of carboxyl group to Ag nanoparticles.[92] Also a new peak appeared at 1635 cm^{-1} which belongs to the C=O stretching of the carboxyl group. At pH 3.95, the strong band at 1173 cm^{-1} and its shoulder at 1121 cm^{-1} are possibly due to NH_2 twisting or NH_3^+ rocking, [43] respectively. These two peaks were assigned as NH_3^+ rocking because the SER spectra at higher pH values where NH_3^+ transformed to NH_2 and 1173 cm^{-1} and 1121 cm^{-1} peaks were disappeared. However, at lower pH (pH 1.74) these two peaks were still present in the spectrum. Moreover, the peak at 1615 cm^{-1} was attributed to amide I band since at pH 11.27 this peak mostly vanished

which indicates that NH_3^+ was converted to NH_2 by deprotanation. Moreover, at pH 1.74 the peak at 1003 cm^{-1} in Fig. 30 was attributed to –CN stretching which can be explained by assuming that amino group was adsorbed on the surface. Also at pH 1.74 the presence of peak at 2965 cm^{-1} as shown in Fig. 31 explained as the presence of NH_3^+ groups and this band was assigned as NH_3^+ stretching vibration by Moskovists et. al.[43] Furthermore, at pH 1.74 and 3.95, amide III band was assigned to the positions at 1295 cm^{-1} and amide II band was detected only at pH 1.74 at 1503 cm^{-1} position which confirms that amino group was close to the Ag surface at low pH values. Moreover, at pH 3.95 carboxylate group originated bands below 1000 cm^{-1} were measured and these bands are C-COO^- at 911 cm^{-1}[43] and COO^- deformation at 726 cm^{-1}, whereas symmetric stretching of CNC is at 800 cm^{-1}.[114] It should be noted that the presence of CH_2 bending at 1441 cm^{-1} indicates that aliphatic chain of aspartic acid was close to the surface.

SERS of aspartic acid on Ag nanoparticles has been studied by Castro et al.[26] and Arenas et al.[25] Arenas et al. reported that when the pH is higher than 9.82, both amino and carboxylate groups interacted with the surface and at pH 7 NH_2 group was far from the surface which indicates that aspartic acid interacted via its carboxyl groups to the Ag surface. Castro et al. reported that aspartic acid interacts through its carboxylate groups at all pH values. In this study, we concluded that aspartic acid interacts through its amino and carboxylate groups with the Ag surface due to the presence of both amino and carboxylate related bands in the SERS spectra. Arenas et al. and Castro et al. prepared Ag nanoparticles by $NaBH_4$ reduction method and reported that Ag nanoparticles had the maximum absorption at 390 nm which were smaller in size compared to Ag nanoparticles we prepared. The differences in the

interaction of Ag nanoparticles with aspartic acid in these two studies and in our study can be the result of having different nanoparticle sizes.

Fig. 32 displays the pH dependent UV–VIS absorption spectra of the silver nanoparticles in the presence of aspartic acid. Addition of aspartic acid to Ag nanoparticles decreased the absorbance of Ag nanoparticles, along with an increment in the signal of the tail of the peak between 500-800 nm probably due to the aggregation of Ag nanoparticles as shown in Fig. 32a and 32c. As the pH of the solution was adjusted to lower pH values, agglomeration of Ag nanoparticles increases and the SPR band of Ag nanoparticles disappears as shown in Fig. 32b.

Fig. 33 displays the SER spectra of aspartic acid adsorbed on Ag nanoparticles at various pH values investigated with 632 nm excitation source. As it is expected, the same bands with varying intensities were obtained with 632 nm laser source at the same pH values compared to 532 nm laser source. However, the signal intensities are better with 532 nm laser than that using 632 nm laser as it is expected with respect to EM theory. Surface plasmon of Ag nanoparticles are close to the wavelength of the excitation source and the EM theory states that once the wavelength of the incident light is close to the LSPR of metallic surface, followed by the molecules adsorbed or close to the surface yield a large electromagnetic field.

Fig. 35 displays the pH dependent UV–VIS absorption spectra of the silver nanoparticles in the presence of aspartic acid used for SERS experiments using 632 nm source.

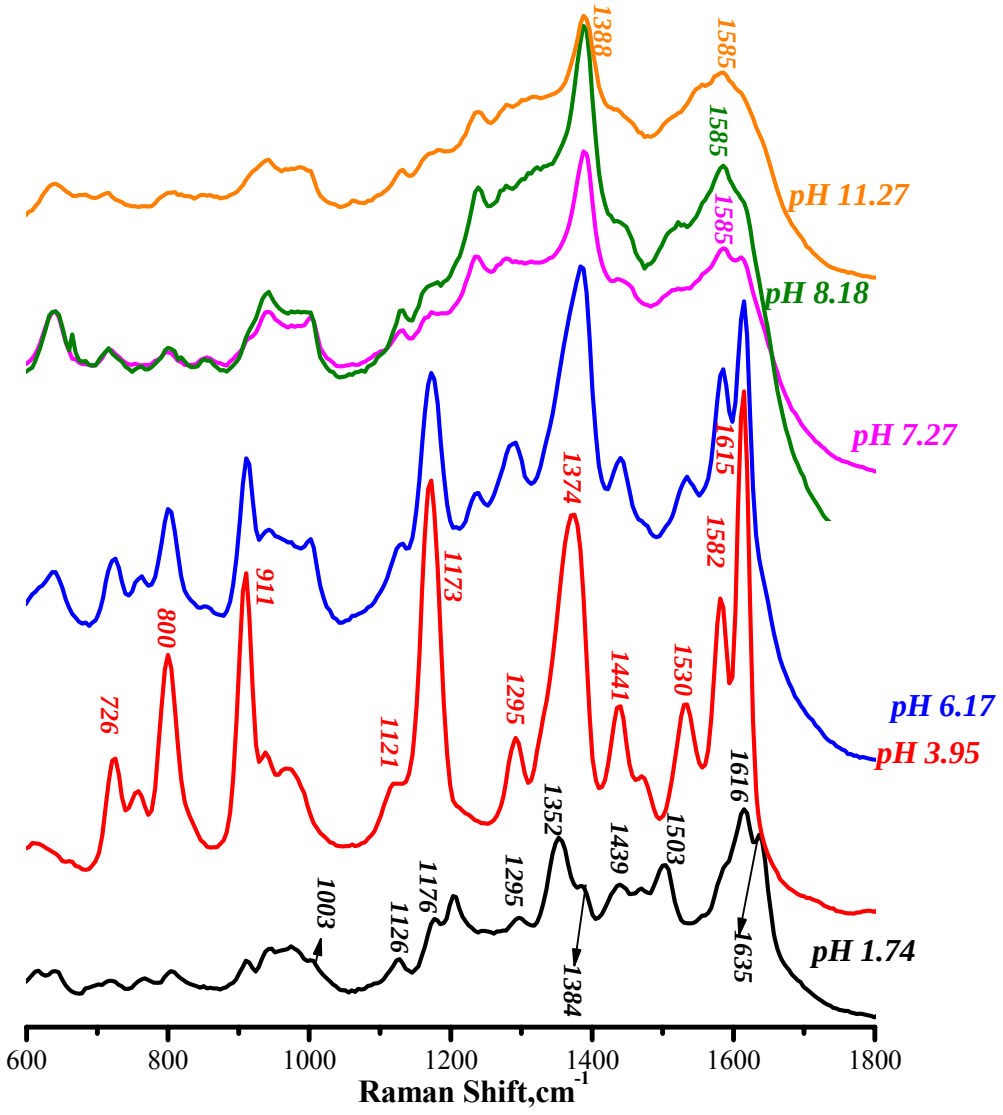

Figure 28. 600-1800 cm^{-1} region of SER spectra of $1.0x10^{-3}$ M aspartic acid adsorbed on Ag nanoparticles in aqueous solutions of various pH values using *532 nm* excitation source. For SER spectrum at pH 3.95 integration time was 5 s, for SER spectra of all other pH's integration time was 30 s.

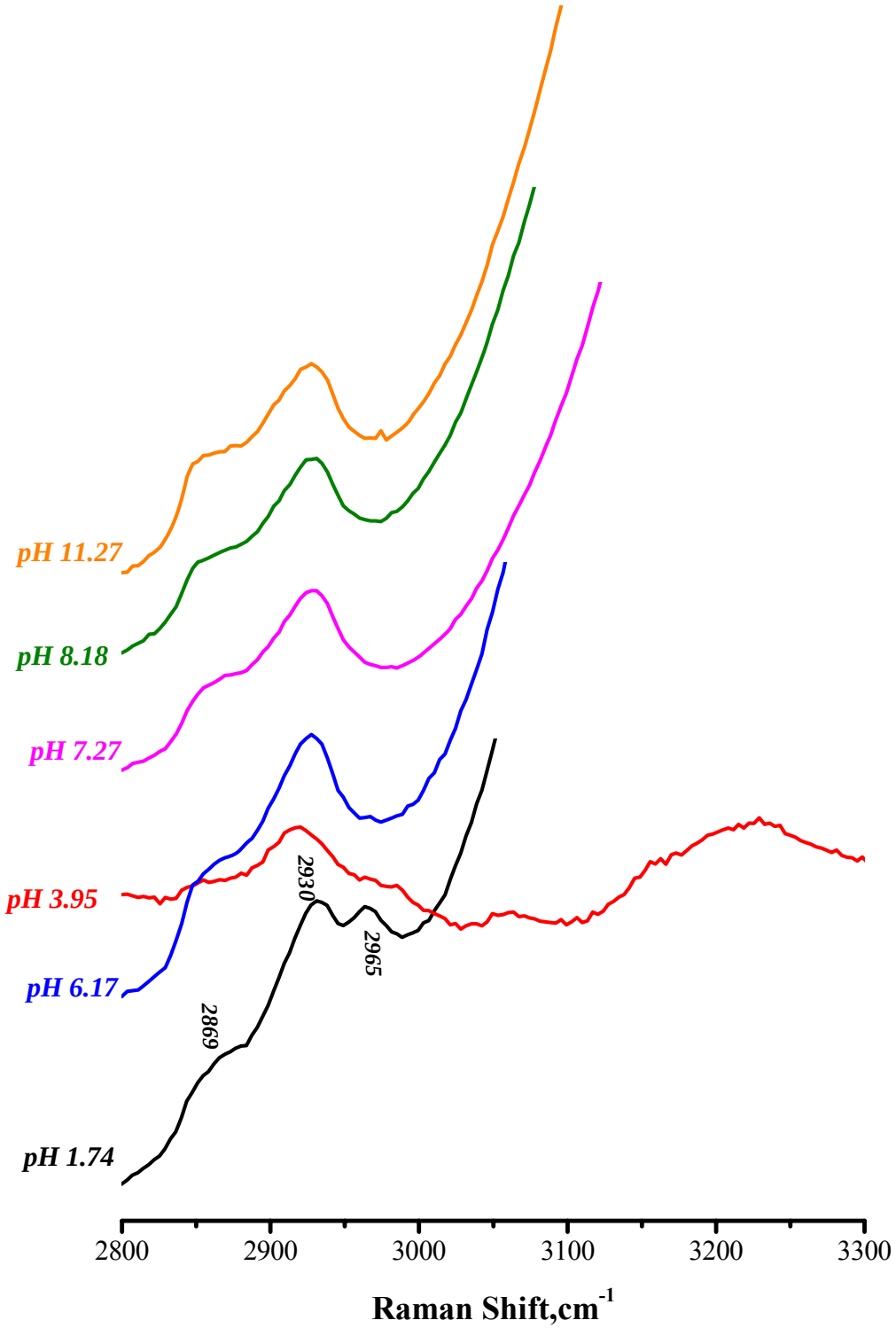

Figure 29. 2800-3300 cm^{-1} region of SER spectra of $1.0x10^{-3}$ M aspartic acid adsorbed on Ag nanoparticles in aqueous solutions of various pH values using ***532 nm*** excitation source. For SER spectrum at pH 3.81 integration time was 5 s, for SER spectra at the other pH integration time was 30 s.

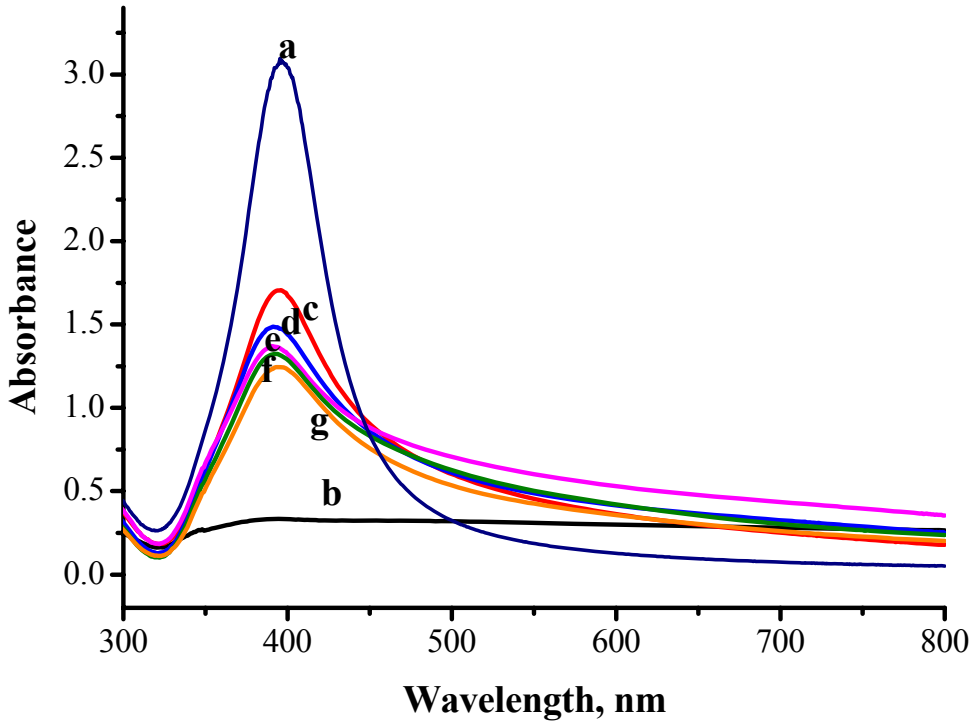

Figure30. UV-Vis spectra of **a)** Ag nanoparticles and aspartic acid adsorbed on Ag nanoparticles SER spectra of which are shown in Fig. 30 at various pH values **b)** pH 1.74 **c)** pH 3.95 **d)** pH6.17 **e)** pH 7.27 **f)** pH 8.18 **g)** pH 11.27

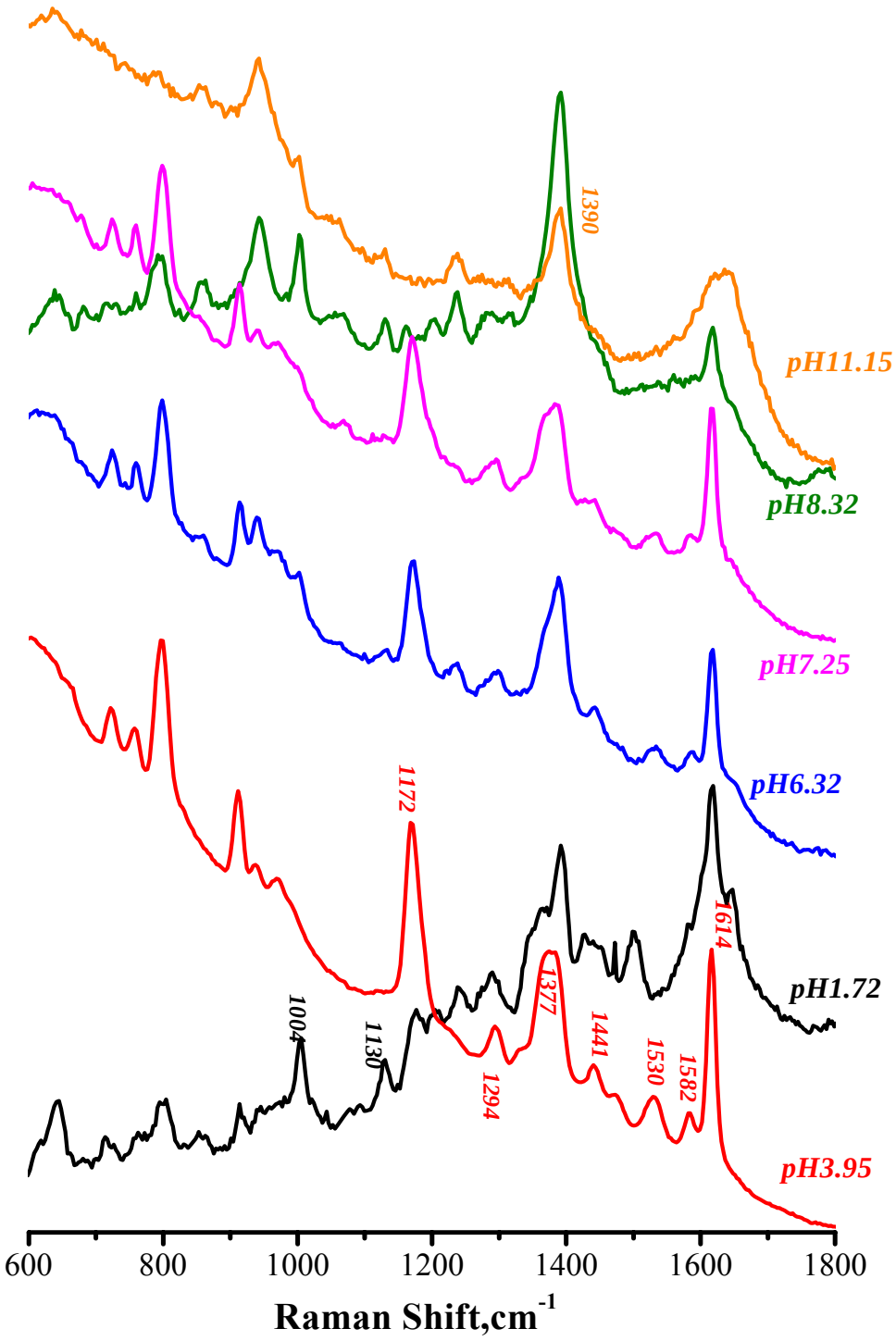

Figure 31. 600-1800 cm^{-1} region of SER spectra of $1.0x10^{-3}$ M aspartic acid adsorbed on Ag nanoparticles in aqueous solutions of various pH using ***632 nm*** excitation source. For SER spectrum at pH 3.95 and pH 6.32 integration times were 30 se, at pH 11.15 integration time was 100 s for SER spectra at the other pH integration time was 60 s.

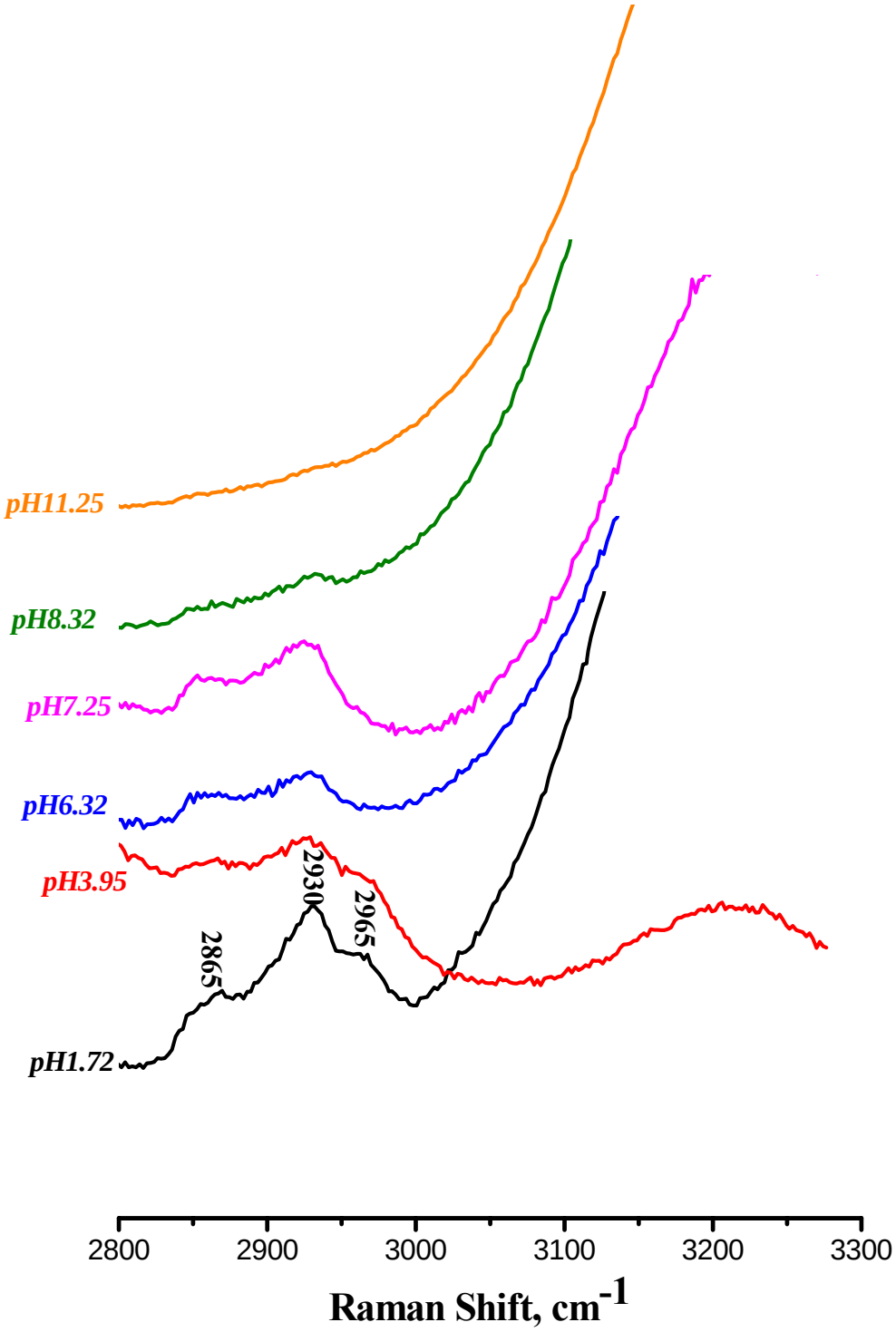

Figure 32. 2800-3300 cm^{-1} region of SER spectra of $1.0x10^{-3}$ M aspartic acid adsorbed on Ag nanoparticles in aqueous solutions of various pH with ***632 nm*** excitation source. For SER spectrum at pH 3.95 and pH 6.32 integration times were 30 s, at pH 11.15 integration time was 100 s for SER spectra at the other pH integration time was 60 s

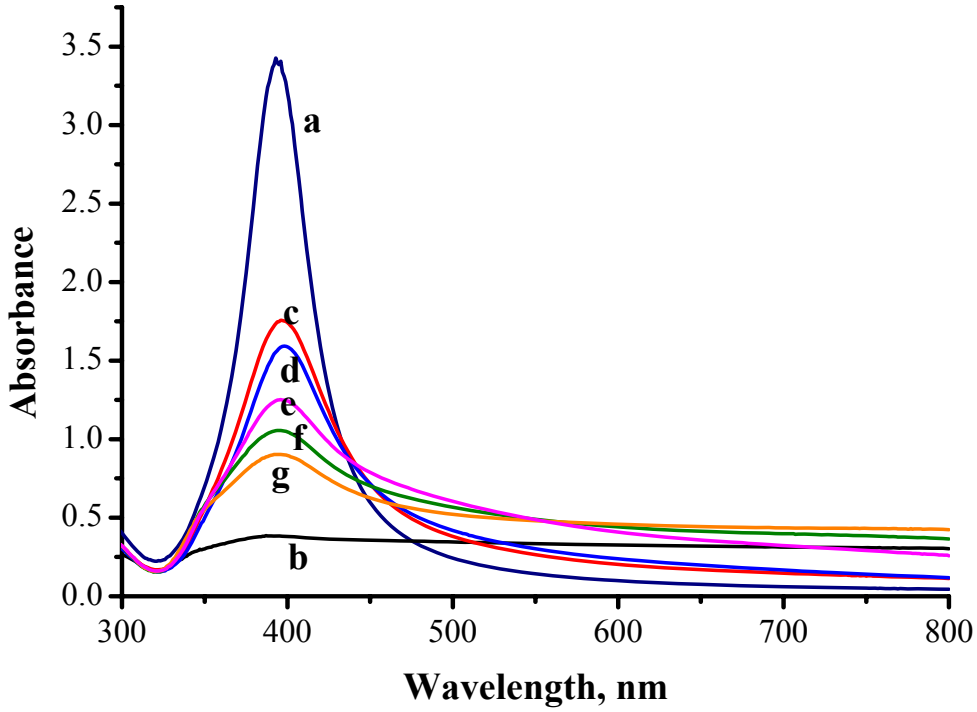

Figure 33. UV-Vis spectra of **a)** Ag nanoparticles and aspartic acid adsorbed on Ag nanoparticles at **b)** pH 1.72, **c)** pH 3.95, **d)** pH 6.32, **e)** pH 7.25, **f)** pH 8.32 and **g)** pH 11.15.

4.3.3 Aspartic Acid Adsorbed on Au Nanoparticles

$1.0x10^{-2}$ M aspartic acid was mixed with citrate capped Au nanoparticles in 1:10 ratio and SER spectra as a function of pH are displayed in Fig. 36. After mixing Au nanoparticles and aspartic acid, initial pH of the solution was 5.12 and then, pH of the solution was adjusted either with 0.010M HCl and 0.050 M NaOH. At pH 5.12, the peak at 1640 cm^{-1} was attributed to amide I band.[29] The peaks at 1530 and 1374 cm^{-1} were assigned to asymmetric deformation of NH_3^+ [24] and symmetric stretching of $-COO^-$group.[43] At pH 3.07, a new peak belonged to asymmetric stretching of $-COO^-$ group appeared at 1585 cm^{-1}. At pH 1.23, the peak at 1640 cm^{-1} was attributed to amide I band and 1245 cm^{-1} was assigned to amide III band which is combination of

N-H in-plane bending and C-N stretching vibrations,[100] respectively. Amide II band was measured at pH 1.23 at 1495 cm^{-1}. The peaks at 1013 and 1074 cm^{-1} could be assigned to C-N stretching.[29] Moreover, NH_3^+ rocking mode is observed at 1129 cm^{-1}[143]. On the other hand, symmetric stretching of –COO- was at a higher wavenumber for pH 1.23 with respect to pH 5.12, which indicates that carboxyl groups are not as close to the Au surface as at pH 5.12. The presence of both amino and carboxyl originated bands indicates that aspartic acid interacts through both functional groups to the Au surface at pH 1.23. The bands at 716 and 843 cm^{-1} were attributed to deformation of COO- and symmetric CCN stretching.[114] At pH values from 5.12 to 8.54 SER spectra of aspartic acid did not change very much in terms of peak positions. However, pH 11.27 at which NH_3^+ is converted to NH_2 by deprotonation, the spectrum changed dramatically. Amide I peak disappeared and asymmetric and symmetric stretching of $-COO^-$ was observed at 1560 and 1363 cm^{-1}, respectively. NH_2 rocking and amide III bands existed at 1156 and 1238 cm^{-1}. Moreover, the peak at 1445 was attributed to CH_2 bending indicating that aliphatic chain of aspartic acid was close to the Au surface at pH 11.27. The presence of both amino and carboxyl related bands indicates that aspartic acid interacts through both functional groups with the Au surface at pH 11.27.

The behavior of aspartic acid on Au surface similar to the results obtained by Dou et al.[19] and by Sabur et al.[24] for glycine adsorbed on Au nanoparticles. They proposed that protonated amino groups interact preferentially with negatively charged Au nanoparticles.

When we compare the interaction of aspartic acid with Au and Ag nanoparticles, the SER signals of aspartic acid indicates that aspartic acid interacts better and/or close in proximity to Ag nanoparticles than Au nanoparticles. Moreover,

aspartic acid interacts with Ag nanoparticles via its carboxyl groups at high pH values. However, at low pH values, interaction is through amine and carboxyl groups. In the case of Au nanoparticles, interaction is through both carboxyl and amine functional groups at all pH values studied.

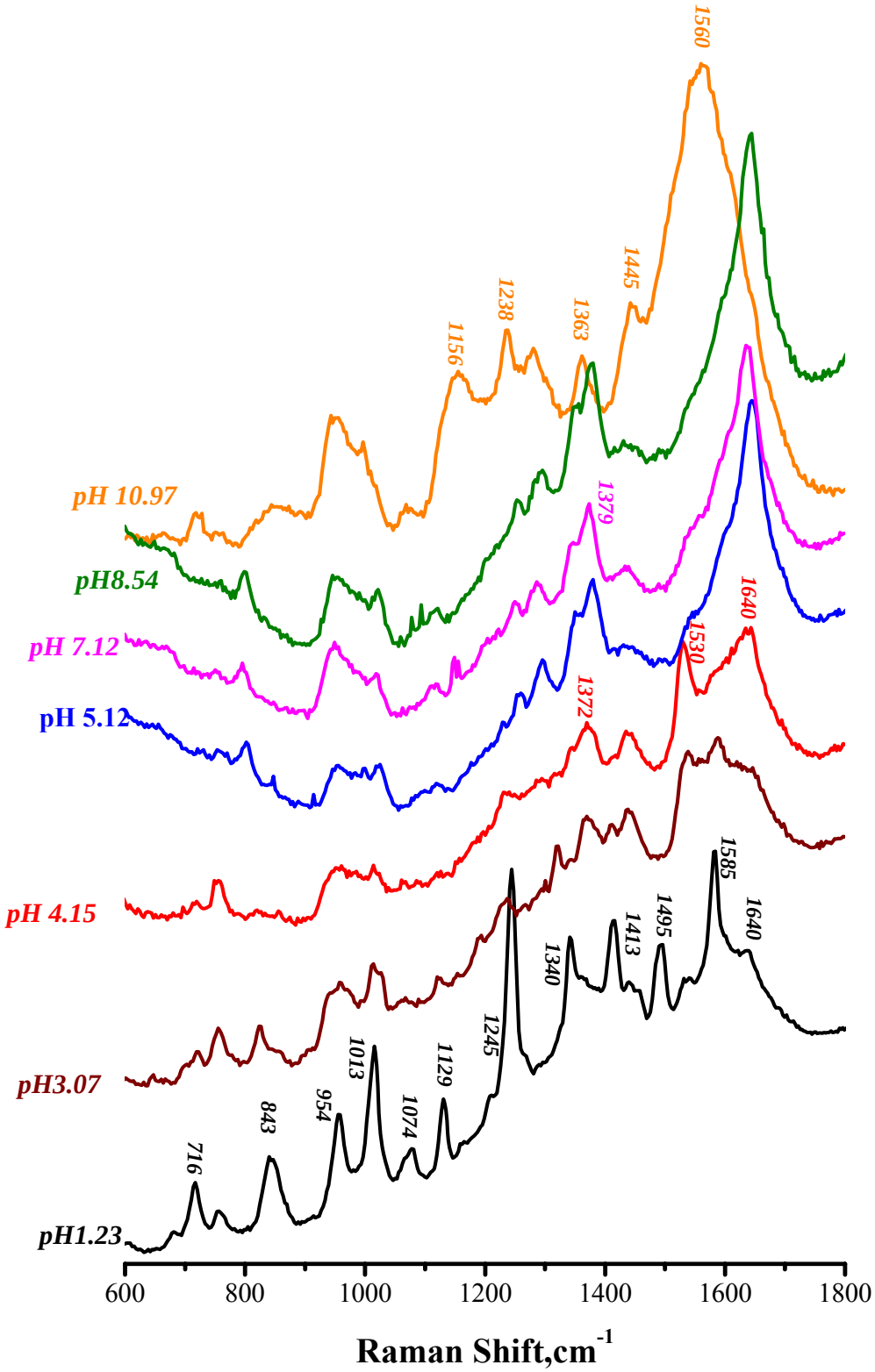

Figure 34.SER spectra of 1.0x10^{-3}M aspartic acid adsorbed on Au nanoparticle in aqueous solution at various pH with ***632 nm*** excitation source. Integration time for SER spectra are 200 s.

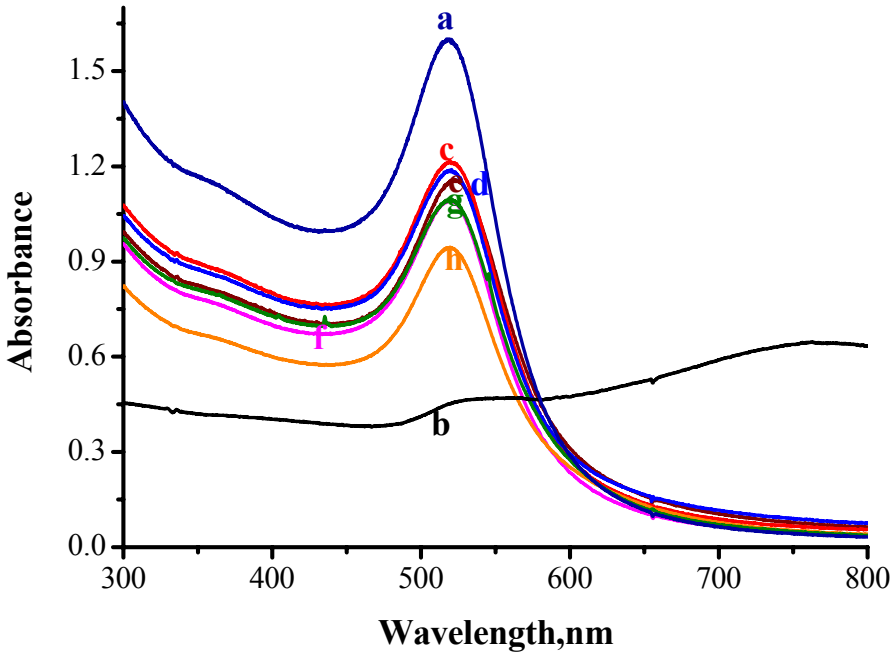

Figure 35. UV-Vis spectra of **a)** Au nanoparticles and aspartic acid adsorbed Au nanoparticles at pH **b)** 1.23, **c)** 4.15, **d)** 5.12, **e)** 3.07, **f)** 7.12, **g)** 8.54 and **h)** 10.97

SERS of aspartic acid on colloidal Au were tried to measure with 532 nm excitation source, but no signals were able to be detected. Similarly Dou et al. [19] did not obtain any SERS signal from glycine and lysine on Au nanoparticles with 514.5 nm excitation source.

5. CONCLUSIONS

In this thesis, in first part we have examined whether micrometer sized magnetic microspheres can be applied as SERS substrates in molecular recognition. The preparation and characterization of oleic acid capped magnetite nanoparticles were presented. Oleic acid was found to bind Fe atoms by chelating bidentate. Oleic acid coated magnetite nanoparticles were encapsulated in PMMA-DVB by a modified suspension polymerization method. Magnetic microspheres were prepared in a relatively narrow size distribution with mean diameter 22 μm and classified as ***nearly monodisperse*** according to the PDI value calculated. Au and Ag nanoparticles were coated onto magnetic microspheres by different reduction processes. Au nanoparticles were coated onto magnetic microspheres with hydroxylamine and borohydrate reduction methods and Ag nanoparticles were coated with borohydrate reduction method. Enhancement factors were for Au nanoparticles coated magnetic microspheres by hydroxylamine reduction and by $NaBH_4$ reduction methods as 10^5 and for Ag nanoparticles coated magnetic microspheres as 10^7. Limit of quantitation of R6G molecule using Ag nanoparticle coated magnetic microspheres was found to be $1.0x10^{-10}$ M. Considering that the usual SERS substrates such as on electrochemically roughed electrodes and colloidal solutions are lacking in stability and/or reproducibility, the usage of magnetic microspheres are not only stable but also highly effective for SERS characterization of molecular adsorbates reproducibly is an obvious merit of our work.

In the second part of the thesis, interaction of aspartic acid with colloidal Ag and Au are followed by SERS. Aspartic acid interacts with Ag nanoparticles at low pH through its amine and carboxyl groups, and at high pH via its carboxyl functional

group. On the other hand, interaction of aspartic acid with Au nanoparticles is through its amine and carboxyl functional groups at both low and high pH values. When the interactions of aspartic acid with Au and Ag surfaces are compared, aspartic acid interacts better or is closer to Ag surface than Au surface. SERS of aspartic acid on Au nanoparticles is reported for the first time in this study. The interaction of aspartic acid with Au and Ag nanoparticles are followed as a function of pH in detail to understand the affect of pH on the interaction. pH experiments and its affect on the interaction is an obvious value of our work.

Studies are currently under way to use these magnetic microspheres to detect other analytes classes such as amino acids and long chain homopeptides. Why are we interested in using amino acid chains?

Considerable effort has been directed toward the development of surface-immobilized chemical reagents for the preconcentration and isolation of metal ions from solution. The extraction of metal ions from aqueous samples is critical to environmental clean-up initiatives, metal recovery, and preconcentration of metal ions for ultra trace-level determinations. The immobilization of selective ligands onto high-surface-area supports is the basis of most of these studies. The understanding of the chemistry of these materials, as well as the assessment of their capacity, preconcentration efficiency, and breakthrough characteristics, has generally relied on detection of metal ions eluted from a packed column. Detailed knowledge of the chemistry of metal-ion binding to surface-immobilized ligands is critical to their successful application. However, little is known about the structure of surface complexes and how these compare to those formed in homogeneous solution. This lack of information relates to the challenge of developing *in situ* spectroscopic methods that are capable of detecting metal-ion complexes with surface-bound

ligands. Therefore, the goal of our research is to develop rapid, simple and accurate methods for the preconcentration and/or determination of trace amounts of heavy metals in drinking water, groundwater, and fresh surface water. Our research will focus on metal binding by immobilized amino acids as well as short chain polypeptides on nanoparticles which are bound to the surface of magnetic microparticles. SERS will be used for the detection of metal ions and this technique can also provide the information about the sites responsible for metal binding. Using SERS for the detection and characterization of metals bound to peptide chains has not been reported in the literature so far. The information obtained from SERS spectra can be used to build a wide variety of interesting chelators which may have the desired characteristics of specificity and have the added side benefit of being nontoxic when discarded.

6. REFERENCES

1. Kneipp, K.; Kneipp, H.; Itzkan, I.; Dasari, R. R.; Feld, M. S., Surface-enhanced Raman scattering and biophysics. *Journal of Physics-Condensed Matter* **2002,** 14, (18), R597-R624.

2. Shafer-Peltier, K. E.; Haynes, C. L.; Glucksberg, M. R.; Van Duyne, R. P., Toward a glucose biosensor based on surface-enhanced Raman scattering. *Journal of the American Chemical Society* **2003,** 125, (2), 588-593.

3. Gu, W.; Choi, H.; Kim, K., A quantum mechanical theory for single molecule-single nanoparticle surface enhanced Raman scattering. *Journal of Physical Chemistry A* **2007,** 111, (33), 8121-8125.

4. Laserna, J. J., *Modern Techniques in Raman Spectroscopy*. John Wiley &Sons: 1996.

5. Fleischmann, M.; Hendra, P.; McQuillan, A. J., *Chemical Physics Letters* **1974,** 26, 163.

6. Jeanmaire, D. L.; R.P., V. D., *J. Electroanal. Chem.* **1977,** 84, 1.

7. Albrecht, M. G.; Creighton, J. A., *Journal of American Chemical Society* **1977,** 99, 5215.

8. Campion, A.; Kambhampati, P., Surface-enhanced Raman scattering. *Chemical Society Reviews* **1998,** 27, (4), 241-250.

9. Schatz, G. C.; Young, M. A.; Van Duyne, R. P., *Electromagnetic mechanism of SERS*. 2006; Vol. 103, p 19-45.

10. Moskovits, M., Surface-enhanced Spectroscopy. *Reviews of Modern Physics* **1985,** 57, (3), 783-826.

11. Petry, R.; Schmitt, M.; Popp, J., Raman Spectroscopy - A prospective tool in the life sciences. *Chemphyschem* **2003,** 4, (1), 14-30.

12. Weaver, M. J.; Zou, S. Z.; Chan, H. Y. H., The new interfacial ubiquity of surface-enhanced Raman spectroscopy. *Analytical Chemistry* **2000,** 72, (1), 38A-47A.

13. Arenas, J. F.; Woolley, M. S.; Tocon, I. L.; Otero, J. C.; Marcos, J. I., Complete analysis of the surface-enhanced Raman scattering of pyrazine on the silver electrode on the basis of a resonant charge transfer mechanism involving three states. *Journal of Chemical Physics* **2000,** 112, (17), 7669-7683.

14. Jiang, J. D.; Burstein, E.; Kobayashi, H., Resonan Raman Scattering by Crystal-Violet Molecules Adsorbed on a Smooth Gold Surface: Evidence for a Charge-Transfer Excitation. *Physical Review Letters* **1986,** 57, (14), 1793-1796.

15. Campion, A.; Ivanecky, J. E.; Child, C. M.; Foster, M., On the Mechanism of Chemical Enhancement in Surface-Enhanced Raman-Scattering. *Journal of the American Chemical Society* **1995,** 117, (47), 11807-11808.

16. Kambhampati, P.; Child, C. M.; Foster, M. C.; Campion, A., On the chemical mechanism of surface enhanced Raman scattering: Experiment and theory. *Journal of Chemical Physics* **1998,** 108, (12), 5013-5026.

17. Otto, A., Theory of first layer and single molecule surface enhanced Raman scattering (SERS). *Physica Status Solidi a-Applied Research* **2001,** 188, (4), 1455-1470.

18. Nabiev, I. R.; Sokolov, K. V.; Manfait, M., *Biomolecular spectroscopy,'Surface-enhanced Raman Spectroscopy and its Biomedical Applications'*. Chichester-Wiley 1993; p 267-338.

19. Dou, X. M.; Jung, Y. M.; Yamamoto, H.; Doi, S.; Ozaki, Y., Near-infrared excited surface-enhanced Raman scattering of biological molecules on gold colloid I: Effects of pH of the solutions of amino acids and of their polymerization. *Applied Spectroscopy* **1999,** 53, (2), 133-138.

20. Ooka, A. A.; Kuhar, K. A.; Cho, N. J.; Garrell, R. L., Surface interactions of a homologous series of alpha,omega-amino acids on colloidal silver and gold. *Biospectroscopy* **1999,** 5, (1), 9-17.

21. Schwartzberg, A. M.; Grant, C. D.; Wolcott, A.; Talley, C. E.; Huser, T. R.; Bogomolni, R.; Zhang, J. Z., Unique gold nanoparticle aggregates as a highly active surface-enhanced Raman scattering substrate. *Journal of Physical Chemistry B* **2004,** 108, (50), 19191-19197.

22. Zhao, H. Y.; Yuan, B.; Don, X. M., The effects of electrostatic interaction between biological nano-metal colloid molecules and on near-infrared surface-enhanced Raman scattering. *Journal of Optics a-Pure and Applied Optics* **2004,** 6, (9), 900-905.

23. Joo, S. W.; Chung, T. D.; Jang, W. C.; Gong, M. S.; Geum, N.; Kim, K., Surface-enhanced Raman scattering of 4-cyanobiphenyl on gold and silver nanoparticle surfaces. *Langmuir* **2002,** 18, (23), 8813-8816.

24. Sabur, A.; Havel, M.; Gogotsi, Y., SERS intensity optimization by controlling the size and shape of faceted gold nanoparticles. *Journal of Raman Spectroscopy* **2008,** 39, (1), 61-67.

25. Arenas, J. F.; Castro, J. L.; Otero, J. C.; Marcos, J. I., Study of interaction between aspartic acid and silver by surface-enhanced Raman scattering on H2O and D2O sols. *Biopolymers* **2001,** 62, (5), 241-248.

26. Castro, J. L.; Montanez, M. A.; Otero, J. C.; Marcos, J. I., SERS and Vibrational Spectra of Aspartic Acid. *Journal of Molecular Structure* **1995,** 349, 113-116.

27. Herne, T. M.; Ahern, A. M.; Garrell, R. L., Surface-Enhanced Raman-Spectroscopy of Peptides - Preferential N-terminal Adsorption on Colloidal Silver. *Journal of the American Chemical Society* **1991,** 113, (3), 846-854.

28. Stewart, S.; Fredericks, P. M., Surface-enhanced Raman spectroscopy of peptides and proteins adsorbed on an electrochemically prepared silver surface. *Spectrochimica Acta Part a-Molecular and Biomolecular Spectroscopy* **1999,** 55, (7-8), 1615-1640.

29. Stewart, S.; Fredericks, P. M., Surface-enhanced Raman spectroscopy of amino acids adsorbed on an electrochemically prepared silver surface. *Spectrochimica Acta Part a-Molecular and Biomolecular Spectroscopy* **1999,** 55, (7-8), 1641-1660.

30. Shin, K. S., Effect of surface morphology on surface-enhanced Raman scattering of 4-aminobenzenethiol adsorbed on gold substrates. *Journal of Raman Spectroscopy* **2008,** 39, (4), 468-473.

31. Szafranski, C. A.; Tanner, W.; Laibinis, P. E.; Garrell, R. L., Surface-enhanced Raman spectroscopy of Aromatic Thiols and Disulfides on Gold Electrodes. *Langmuir* **1998,** 14, (13), 3570-3579.

32. Suzuki, M.; Niidome, Y.; Kuwahara, Y.; Terasaki, N.; Inoue, K.; Yamada, S., Surface-enhanced nonresonance Raman scattering from size- and morphology-controlled gold nanoparticle films. *Journal of Physical Chemistry B* **2004,** 108, (31), 11660-11665.

33. Bryant, M. A.; Pemberton, J. E., Surface Raman-Scattering of Self-Assembled Monolayers Formed from 1-alkanethiols - Behavior of Films at Au and Comparison to Films at Ag. *Journal of the American Chemical Society* **1991,** 113, (22), 8284-8293.

34. Vanduyne, R. P.; Hulteen, J. C.; Treichel, D. A., Atomic-Force Microscopy and Surface-Enhanced Raman-Spectroscopy .1. Ag Island Films and Ag Film over Polymer Nanosphere Surfaces supported on Glass. *Journal of Chemical Physics* **1993,** 99, (3), 2101-2115.

35. Chen, J. N.; Martensson, T.; Dick, K. A.; Deppert, K.; Xu, H. Q.; Samuelson, L.; Xu, H. X., Surface-enhanced Raman scattering of rhodamine 6G on nanowire arrays decorated with gold nanoparticles. *Nanotechnology* **2008,** 19, (27), 1-5.

36. Freeman, R. G.; Grabar, K. C.; Allison, K. J.; Bright, R. M.; Davis, J. A.; Guthrie, A. P.; Hommer, M. B.; Jackson, M. A.; Smith, P. C.; Walter, D. G.; Natan, M. J., Self-Assembled Metal Colloid Monolayers-An Approach to SERS Substrates. *Science* **1995,** 267, (5204), 1629-1632.

37. Grabar, K. C.; Freeman, R. G.; Hommer, M. B.; Natan, M. J., Preparation and Characterization of Au Colloid Monolayers. *Analytical Chemistry* **1995,** 67, (4), 735-743.

38. Oldenburg, S. J.; Westcott, S. L.; Averitt, R. D.; Halas, N. J., Surface enhanced Raman scattering in the near infrared using metal nanoshell substrates. *Journal of Chemical Physics* **1999,** 111, (10), 4729-4735.

39. Akbarian, F.; Dunn, B. S.; Zink, J. I., Porous sol-gel silicates containing gold particles as matrices for surface-enhanced Raman spectroscopy. *Journal of Raman Spectroscopy* **1996,** 27, (10), 775-783.

40. Kim, J. H.; Kim, J. S.; Choi, H.; Lee, S. M.; Jun, B. H.; Yu, K. N.; Kuk, E.; Kim, Y. K.; Jeong, D. H.; Cho, M. H.; Lee, Y. S., Nanoparticle probes with surface enhanced Raman spectroscopic tags for cellular cancer targeting. *Analytical Chemistry* **2006,** 78, (19), 6967-6973.

41. Mosier-Boss, P. A.; Lieberman, S. H., Surface-enhanced Raman spectroscopy substrate composed of chemically modified gold colloid particles immobilized on magnetic microparticles. *Analytical Chemistry* **2005,** 77, (4), 1031-1037.

42. Podstawka, E.; Ozaki, Y.; Proniewicz, L. M., Part I: Surface-enhanced Raman spectroscopy investigation of amino acids and their homodipeptides adsorbed on colloidal silver. *Applied Spectroscopy* **2004,** 58, (5), 570-580.

43. Suh, J. S.; Moskovits, M., Surface-Enhanced Raman Spectroscopy of Amino Acids and Nucleotide Bases Adsorbed on Silver. *Journal of the American Chemical Society* **1986,** 108, (16), 4711-4718.

44. Podstawka, E.; Ozaki, Y.; Proniewicz, L. M., Part III: Surface-enhanced Raman scattering of amino acids and their homodipeptide monolayers deposited onto colloidal gold surface. *Applied Spectroscopy* **2005,** 59, (12), 1516-1526.

45. Podstawka, E.; Ozaki, Y.; Proniewicz, L. M., Part II: Surface-enhanced Raman spectroscopy investigation of methionine containing fleterodipeptides adsorbed on colloidal silver. *Applied Spectroscopy* **2004,** 58, (5), 581-590.

46. Castro, J. L.; SanchezCortes, S.; Ramos, J. V. G.; Otero, J. C.; Marcos, J. I., Surface-enhanced Raman spectroscopy of gamma-aminobutyric acid on silver colloid surfaces. *Biospectroscopy* **1997,** 3, (6), 449-455.

47. Mikhaylova, M.; Kim, D. K.; Berry, C. C.; Zagorodni, A.; Toprak, M.; Curtis, A. S. G.; Muhammed, M., BSA immobilization on amine-functionalized superparamagnetic iron oxide nanoparticles. *Chemistry of Materials* **2004,** 16, (12), 2344-2354.

48. Liu, Z. L.; Yang, X. B.; Yao, K. L.; Du, G. H.; Liu, Z. S., Preparation and characterization of magnetic P(St-co-MAA-co-AM) microspheres. *Journal of Magnetism and Magnetic Materials* **2006,** 302, (2), 529-535.

49. Liu, Z. L.; Ding, Z. H.; Yao, K. L.; Tao, J.; Du, G. H.; Lu, Q. H.; Wang, X.; Gong, F. L.; Chen, X., Preparation and characterization of polymer-coated core-shell structured magnetic microbeads. *Journal of Magnetism and Magnetic Materials* **2003,** 265, (1), 98-105.

50. Zeng, L.; Luo, K. K.; Gong, Y. F., Preparation and characterization of dendritic composite magnetic particles as a novel enzyme immobilization carrier. *Journal of Molecular Catalysis B-Enzymatic* **2006,** 38, (1), 24-30.

51. Yamaura, M.; Camilo, R. L.; Felinto, M., Synthesis and performance of organic-coated magnetite particles. *Journal of Alloys and Compounds* **2002,** 344, (1-2), 152-156.

52. Koneracka, M.; Kopcansky, P.; Timko, M.; Ramchand, C. N., Direct binding procedure of proteins and enzymes to fine magnetic particles. *Journal of Magnetism and Magnetic Materials* **2002,** 252, (1-3), 409-411.

53. Bergemann, C.; Muller-Schulte, D.; Oster, J.; a Brassard, L.; Lubbe, A. S., Magnetic ion-exchange nano- and microparticles for medical, biochemical and molecular biological applications. *Journal of Magnetism and Magnetic Materials* **1999,** 194, (1-3), 45-52.

54. Zhang, C. C.; Li, X.; Pang, J. X., Synthesis and adsorption properties of magnetic resin microbeads with amine and mercaptan as chelating groups. *Journal of Applied Polymer Science* **2001,** 82, (7), 1587-1592.

55. Landfester, K.; Ramirez, L. P., Encapsulated magnetite particles for biomedical application. *Journal of Physics-Condensed Matter* **2003,** 15, (15), S1345-S1361.

56. Tada, D. B.; Vono, L. L. R.; Duarte, E. L.; Itri, R.; Kiyohara, P. K.; Baptista, M. S.; Rossi, L. M., Methylene blue-containing silica-coated magnetic particles: A potential magnetic carrier for photodynamic therapy. *Langmuir* **2007,** 23, (15), 8194-8199.

57. Goodwin, S. C.; Bittner, C. A.; Peterson, C. L.; Wong, G., Single-dose toxicity study of hepatic intra-arterial infusion of doxorubicin coupled to a novel magnetically targeted drug carrier. *Toxicological Sciences* **2001,** 60, (1), 177-183.

58. Berry, C. C.; Curtis, A. S. G., Functionalisation of magnetic nanoparticles for applications in biomedicine. *Journal of Physics D-Applied Physics* **2003,** 36, (13), R198-R206.

59. Wu, Z. J.; Wu, J. H.; Xiang, H.; Chun, M. S.; Lee, K., Organosilane-functionalized Fe3O4 composite particles as effective magnetic assisted adsorbents. *Colloids and Surfaces a-Physicochemical and Engineering Aspects* **2006,** 279, (1-3), 167-174.

60. Nunez, L.; Buchholz, B. A.; Vandegrift, G. F., Waste Remediation Using In-Situ Magnetically Assisted Chemical-Separation. *Separation Science and Technology* **1995,** 30, (7-9), 1455-1471.

61. Nunez, L.; Buchholz, B. A.; Kaminski, M.; Aase, S. B.; Brown, N. R.; Vandegrift, G. F., Actinide separation of high-level waste using solvent extractants on magnetic microparticles. *Separation Science and Technology* **1996,** 31, (10), 1393-1407.

62. Horak, D.; Semenyuk, N.; Lednicky, F., Effect of the reaction parameters on the particle size in the dispersion polymerization of 2-hydroxyethyl and glycidyl

methacrylate in the presence of a ferrofluid. *Journal of Polymer Science Part a-Polymer Chemistry* **2003,** 41, (12), 1848-1863.

63. Liu, X. Q.; Guan, Y. P.; Shen, R.; Liu, H. Z., Immobilization of lipase onto micron-size magnetic beads. *Journal of Chromatography B-Analytical Technologies in the Biomedical and Life Sciences* **2005,** 822, (1-2), 91-97.

64. Horak, D.; Lednicky, F.; Petrovsky, E.; Kapicka, A., Magnetic characteristics of ferrimagnetic microspheres prepared by dispersion polymerization. *Macromolecular Materials and Engineering* **2004,** 289, (4), 341-348.

65. Ma, Z. Y.; Guan, Y. P.; Liu, X. Q.; Liu, H. Z., Preparation and characterization of micron-sized non-porous magnetic polymer microspheres with immobilized metal affinity ligands by modified suspension polymerization. *Journal of Applied Polymer Science* **2005,** 96, (6), 2174-2180.

66. Horak, D.; Petrovsky, E.; Kapicka, A.; Frederichs, T., Synthesis and characterization of magnetic poly(glycidyl methacrylate) microspheres. *Journal of Magnetism and Magnetic Materials* **2007,** 311, (2), 500-506.

67. Ma, Z. Y.; Guan, Y. P.; Liu, H. Z., Synthesis and characterization of micron-sized monodisperse superparamagnetic polymer particles with amino groups. *Journal of Polymer Science Part a-Polymer Chemistry* **2005,** 43, (15), 3433-3439.

68. Li, X. H.; Sun, Z. G., Synthesis of Magnetic Polymer Microspheres and Application for Immobilization of Proteinase Of Balillus-Sublitis. *Journal of Applied Polymer Science* **1995,** 58, (11), 1991-1997.

69. Shang, H.; Chang, W. S.; Kan, S.; Majetich, S. A.; Lee, G. U., Synthesis and characterization of paramagnetic microparticles through emulsion-templated free radical polymerization. *Langmuir* **2006,** 22, (6), 2516-2522.

70. Gou, M. L.; Qian, Z. Y.; Wang, H.; Tang, Y. B.; Huang, M. J.; Kan, B.; Wen, Y. J.; Dai, M.; Li, X. Y.; Gong, C. Y.; Tu, M. J., Preparation and characterization of magnetic poly(epsilon-caprolactone)-poly(ethylene glycol)-poly(epsilon-caprolactone) microspheres. *Journal of Materials Science-Materials in Medicine* **2008,** 19, (3), 1033-1041.

71. Lee, Y.; Rho, J.; Jung, B., Preparation of magnetic ion-exchange resins by the suspension polymerization of styrene with magnetite. *Journal of Applied Polymer Science* **2003,** 89, (8), 2058-2067.

72. Yang, C. L.; Guan, Y. P.; Xing, J. M.; Liu, J. G.; Shan, G. B.; An, Z. T.; Liu, H. Z., Preparation of magnetic polystyrene microspheres with a narrow size distribution. *Aiche Journal* **2005,** 51, (7), 2011-2015.

73. Massart, R., Preparation of Aqueous Magnetic Liquids in Alkaline and Acidic Media. *IEEE Transactions on Magnetics* **1981,** 17, (2), 1247-1248.

74. Korolev, V. V.; Ramazanova, A. G.; Blinov, A. V., Adsorption of surfactants on superfine magnetite. *Russian Chemical Bulletin* **2002,** 51, (11), 2044-2049.

75. Zhang, L.; He, R.; Gu, H. C., Oleic acid coating on the monodisperse magnetite nanoparticles. *Applied Surface Science* **2006,** 253, (5), 2611-2617.

76. Kataby, G.; Cojocaru, M.; Prozorov, R.; Gedanken, A., Coating carboxylic acids on amorphous iron nanoparticles. *Langmuir* **1999,** 15, (5), 1703-1708.

77. Bica, D.; Vekas, L.; Rasa, M., Preparation and magnetic properties of concentrated magnetic fluids on alcohol and water carrier liquids. *Journal of Magnetism and Magnetic Materials* **2002,** 252, (1-3), 10-12.

78. Fried, T.; Shemer, G.; Markovich, G., Ordered two-dimensional arrays of ferrite nanoparticles. *Advanced Materials* **2001,** 13, (15), 1158-+.

79. Williams, D. N.; Gold, K. A.; Holoman, T. R. P.; Ehrman, S. H.; Wilson, O. C., Surface modification of magnetic nanoparticles using gum arabic. *Journal of Nanoparticle Research* **2006,** 8, (5), 749-753.

80. Hong, M. K.; Park, B. J.; Choi, H. J., Preparation and physical characterization of polyacrylamide coated magnetite particles. *Physica Status Solidi a-Applications and Materials Science* **2007,** 204, (12), 4182-4185.

81. Cocker, T. M.; Fee, C. J.; Evans, R. A., Preparation of magnetically susceptible polyacrylamide/magnetite beads for use in magnetically stabilized fluidized bed chromatography. *Biotechnology and Bioengineering* **1997,** 53, (1), 79-87.

82. Maria, L.; Leite, M.; Costa, M. A. S.; Ribeiro, J. M. S.; Senna, L. F.; Silva, M. R., Characterization of magnetic microspheres based on network styrene and divinylbenzene copolymers. *Materials Letters* **2004,** 58, (24), 3001-3006.

83. Arshady, R., Suspension, emulsion, and dispersion polymerization – A methodological survey. *Colloid and Polymer Science* **1992,** 270, (8), 717-732.

84. Choi, J.; Kwak, S. Y.; Kang, S.; Lee, S. S.; Park, M.; Lim, S.; Kim, J.; Choe, C. R.; Hong, S. I., Synthesis of highly crosslinked monodisperse polymer particles: Effect of reaction parameters on the size and size distribution. *Journal of Polymer Science Part a-Polymer Chemistry* **2002,** 40, (23), 4368-4377.

85. Dowding, P. J.; Goodwin, J. W.; Vincent, B., Production of porous suspension polymers using a continuous tubular reactor. *Colloid and Polymer Science* **2000,** 278, (4), 346-351.

86. Maggioris, D.; Goulas, A.; Alexopoulos, A. H.; Chatzi, E. G.; Kiparissides, C., Prediction of particle size distribution in suspension polymerization reactors: effect of turbulence nonhomogeneity. *Chemical Engineering Science* **2000,** 55, (20), 4611-4627.

87. Brown, K. R.; Natan, M. J., Hydroxylamine seeding of colloidal Au nanoparticles in solution and on surfaces. *Langmuir* **1998,** 14, (4), 726-728.

88. Hildebrandt, P.; Stockburger, M., Surface-Enhanced Resonance Raman-Spectroscopy of Rhodamine-6G Adsorbed On Colloidal Silver. *Journal of Physical Chemistry* **1984,** 88, (24), 5935-5944.

89. Michaels, A. M.; Nirmal, M.; Brus, L. E., Surface enhanced Raman spectroscopy of individual rhodamine 6G molecules on large Ag nanocrystals. *Journal of the American Chemical Society* **1999,** 121, (43), 9932-9939.

90. Michaels, A. M.; Jiang, J.; Brus, L., Ag nanocrystal junctions as the site for surface-enhanced Raman scattering of single Rhodamine 6G molecules. *Journal of Physical Chemistry B* **2000,** 104, (50), 11965-11971.

91. Tian, Z. Q.; Ren, B.; Wu, D. Y., Surface-enhanced Raman scattering: From noble to transition metals and from rough surfaces to ordered nanostructures. *Journal of Physical Chemistry B* **2002,** 106, (37), 9463-9483.

92. Singha, A.; Dasgupta, S.; Roy, A., Comparison of metal-amino acid interaction in Phe-Ag and Tyr-Ag complexes by spectroscopic measurements. *Biophysical Chemistry* **2006,** 120, (3), 215-224.

93. Dresco, P. A.; Zaitsev, V. S.; Gambino, R. J.; Chu, B., Preparation and properties of magnetite and polymer magnetite nanoparticles. *Langmuir* **1999,** 15, (6), 1945-1951.

94. Liu, X. Q.; Kaminski, M. D.; Guan, Y. P.; Chen, H. T.; Liu, H. Z.; Rosengart, A. J., Preparation and characterization of hydrophobic superparamagnetic magnetite gel. *Journal of Magnetism and Magnetic Materials* **2006,** 306, (2), 248-253.

95. Liu, X. Q.; Ma, Z. Y.; Xing, J. M.; Liu, H. Z., Preparation and characterization of amino-silane modified superparamagnetic silica nanospheres. *Journal of Magnetism and Magnetic Materials* **2004,** 270, (1-2), 1-6.

96. Deng, J. G.; He, C. L.; Peng, Y. X.; Wang, J. H.; Long, X. P.; Li, P.; Chan, A. S. C., Magnetic and conductive Fe3O4-polyaniline nanoparticles with core-shell structure. *Synthetic Metals* **2003,** 139, (2), 295-301.

97. Wu, N. Q.; Fu, L.; Su, M.; Aslam, M.; Wong, K. C.; Dravid, V. P., Interaction of fatty acid monolayers with cobalt nanoparticles. *Nano Letters* **2004,** 4, (2), 383-386.

98. Lee, S. G.; Lyoo, W. S., Preparation of monodisperse poly(vinyl alcohol) microspheres by heterogeneous surface saponification and iodine complex formation. *Journal of Applied Polymer Science* **2008,** 107, (3), 1701-1709.

99. Capek, I.; Riza, M.; Akashi, M., On The Kinetics of Polymerization And Copolymerization of Poly(Oxyethylene) Macromonomers and Styrene. *Makromolekulare Chemie-Macromolecular Chemistry and Physics* **1992,** 193, (11), 2843-2860.

100. Cai, S. W.; Singh, B. R., Identification of beta-turn and random coil amide III infrared bands for secondary structure estimation of proteins. *Biophysical Chemistry* **1999,** 80, (1), 7-20.

101. Xu, X. S.; Ming, H.; Zhang, Q. J.; Zhang, Y. S., Properties of Raman spectra and laser-induced birefringence in polymethyl methacrylate optical fibres. *Journal of Optics a-Pure and Applied Optics* **2002,** 4, (3), 237-242.

102. Thomas, K. J.; Sheeba, M.; Nampoori, V. P. N.; Vallabhan, C. P. G.; Radhakrishnan, P., Raman spectra of polymethylmethacrylate optical fibres excited by a 532 nm diode pumped solid state laser. *Journal of Optics a-Pure and Applied Optics* **2008,** 10.

103. Kimling, J.; Maier, M.; Okenve, B.; Kotaidis, V.; Ballot, H.; Plech, A., Turkevich method for gold nanoparticle synthesis revisited. *Journal of Physical Chemistry B* **2006,** 110, (32), 15700-15707.

104. Astilean, S.; Bolboaca, M.; Maniu, D.; Iliescu, T., Ordered Metallic Nanostructure for Surface Enhanced Raman Spectroscopy. *Romanian Reports in Physics* **2004,** 56, (3), 346-351.

105. Sung, Y. E.; Thomas, A.; Gamboaaldeco, M.; Franaszczuk, K.; Wieckowski, A., Adsorption Characteristics by A Radiochemical Method on Smooth Electrode Surfaces. *Journal of Electroanalytical Chemistry* **1994,** 378, (1-2), 131-142.

106. Zhu, Z. H.; Zhu, T.; Liu, Z. F., Raman scattering enhancement contributed from individual gold nanoparticles and interparticle coupling. *Nanotechnology* **2004,** 15, (3), 357-364.

107. Yu, H. Z.; Zhang, J.; Zhang, H. L.; Liu, Z. F., Surface-enhanced Raman scattering (SERS) from azobenzene self-assembled "sandwiches". *Langmuir* **1999,** 15, (1), 16-19.

108. Chaney, S. B.; Shanmukh, S.; Dluhy, R. A.; Zhao, Y. P., Aligned silver nanorod arrays produce high sensitivity surface-enhanced Raman spectroscopy substrates. *Applied Physics Letters* **2005,** 87, (3).

109. Navarrete, J. T. L.; Hernandez, V.; Ramirez, F. J., IR and Raman Spectra of L-Aspartic Acid and Isotopic Derivatives. *Biopolymers* **1994,** 34, (8), 1065-1077.

110. Pajchrowski, G.; Abdali, S.; Norbygaard, T., Stilbazolium merocyanine dye determination in different solutions, concentrations and colloids using SERS. *Journal of Raman Spectroscopy* **2007,** 38, (2), 154-158.

111. Haes, A. J.; Haynes, C. L.; McFarland, A. D.; Schatz, G. C.; Van Duyne, R. R.; Zou, S. L., Plasmonic materials for surface-enhanced sensing and spectroscopy. *Mrs Bulletin* **2005,** 30, (5), 368-375.

112. Istvan, K.; Keresztury, G.; Szep, A., Normal Raman and surface enhanced Raman spectroscopic experiments with thin layer chromatography spots of essential amino acids using different laser excitation sources. *Spectrochimica Acta Part a-Molecular and Biomolecular Spectroscopy* **2003,** 59, (8), 1709-1723.

113. Navarrete, J. T. L.; Hernandez, V.; Ramirez, F. J., Vibrational Study of Aspartic-Acid And Glutamic-Acid Dipeptides. *Journal of Molecular Structure* **1995,** 348, 249-252.

114. Socrates, G., *Infrared and Raman Characteristic Group Frequencies Tables and Charts*. Third ed.; Wiley: 2001.

7. LIST OF ABBREVIATIONS

AES: Auger Electron Spectroscopy

ATR-IR: Attenuated Total Reflectance Infrared Spectroscopy

BPO: Benzoyl peroxide

CM: Chemical Mechanism

DLATGS: Deuterated L-alanine. doped triglycene sulphate

DMF: Dimethyl formamide

DVB: Divinyl benzene

EDA: Ethylene diamine

EDX: Energy Dispersive X-Ray Spectroscopy

EELS: Electron Energy Loss Spectroscopy

EM: Electromagnetic Mechanism

FTIR: Fourier Transform Infrared Spectroscopy

LSPR: Localized Surface Plasmon

MMA: methyl methacrylate

PMMA: poly (methyl methacrylate)

PVA: poly (vinyl alcohol)

SEM : Scanning Electron Microscopy

SERS: Surface Enhanced Raman Scattering

UHV: Ultra High Vacuum

XPS: X-Ray Photoelectron Spectroscopy

XRD: X-Ray Diffraction